

**University of Alberta**

**Frost Heave Studies Using Digital Photographic Technique**

by

Dejun (Derek) Xia 

A thesis submitted to the Faculty of Graduate Studies and Research  
in partial fulfillment of the requirements for the degree of

**Master of Science**  
in  
**Geotechnical Engineering**

Department of Civil & Environmental Engineering

Edmonton, Alberta  
Spring 2006



Library and  
Archives Canada

Bibliothèque et  
Archives Canada

Published Heritage  
Branch

Direction du  
Patrimoine de l'édition

395 Wellington Street  
Ottawa ON K1A 0N4  
Canada

395, rue Wellington  
Ottawa ON K1A 0N4  
Canada

*Your file* *Votre référence*  
*ISBN: 0-494-13911-0*  
*Our file* *Notre référence*  
*ISBN: 0-494-13911-0*

#### NOTICE:

The author has granted a non-exclusive license allowing Library and Archives Canada to reproduce, publish, archive, preserve, conserve, communicate to the public by telecommunication or on the Internet, loan, distribute and sell theses worldwide, for commercial or non-commercial purposes, in microform, paper, electronic and/or any other formats.

The author retains copyright ownership and moral rights in this thesis. Neither the thesis nor substantial extracts from it may be printed or otherwise reproduced without the author's permission.

#### AVIS:

L'auteur a accordé une licence non exclusive permettant à la Bibliothèque et Archives Canada de reproduire, publier, archiver, sauvegarder, conserver, transmettre au public par télécommunication ou par l'Internet, prêter, distribuer et vendre des thèses partout dans le monde, à des fins commerciales ou autres, sur support microforme, papier, électronique et/ou autres formats.

L'auteur conserve la propriété du droit d'auteur et des droits moraux qui protègent cette thèse. Ni la thèse ni des extraits substantiels de celle-ci ne doivent être imprimés ou autrement reproduits sans son autorisation.

---

In compliance with the Canadian Privacy Act some supporting forms may have been removed from this thesis.

Conformément à la loi canadienne sur la protection de la vie privée, quelques formulaires secondaires ont été enlevés de cette thèse.

While these forms may be included in the document page count, their removal does not represent any loss of content from the thesis.

Bien que ces formulaires aient inclus dans la pagination, il n'y aura aucun contenu manquant.

  
**Canada**

*To*  
*my wife Kun Yang*  
*and my daughter Yuwei Xia*

## **Abstract**

When saturated fine grained soils undergo freezing, frost heave usually takes place. During subsequent thaw process, the soils can lose strength causing engineering problems. Furthermore, using artificial ground freezing adds importance to the effort to understand the details of how soil freezes.

A total of 12 laboratory freezing tests were carried out using Devon silt to study the effects of different temperature gradients, applied vertical pressures and pore water salinities on the freezing process, ice lens formation, and frost heave. A fluorescent tracer was used to follow the unfrozen water and the ice lens growth during freezing. Time-lapse photography allowed for a digital photo record to visually document and illustrate the various processes during actual tests. The results of these investigations confirmed most previous findings. However, additional water migration in the frozen zone above the final ice lens was further observed in these investigations, which has not been previously reported.

## **Acknowledgement**

I would like to thank my mentors Dr. Dave C. Segó, Dr. Lukas U. Arenson and Dr. Kevin W. Biggar for their guidance and support during this study, as well as the financial support through the NSERC Discovery Grants held by Dr. Kevin W. Biggar and Dr. Dave C. Segó. The technical contribution of Christine Hereygers and Steve Gamble of the University of Alberta Geotechnical Centre is highly appreciated.

## Table of Contents

1 Introduction .....	1
2 Literature review .....	4
3 Laboratory tests .....	13
3.1 Equipment and materials .....	14
3.2 Sample preparation .....	17
3.3 Freezing tests and data logging .....	22
3.4 Collection of data in the end of freezing tests .....	23
3.5 Image analysis .....	23
3.6 Moisture content and pore water salinity measuring .....	24
3.7 Limitations .....	25
4 Test results .....	26
4.1 General freezing of Devon silt .....	27
4.1.1 Frost penetration and frozen fringe development .....	31
4.1.2 Horizontal ice lens formation and development .....	34
4.1.3 Vertical ice lens formation .....	35
4.1.4 Heave and water intake .....	35
4.1.5 Water migration within frozen zone .....	36
4.1.6 Moisture content (MC) redistribution .....	38
4.1.7 Water balance calculation .....	39
4.1.8 Discussion .....	41
4.2 Effects of temperature gradient (Cooling rate) .....	50
4.2.1 Frost penetration and frozen fringe .....	54
4.2.2 Horizontal ice lens formation and growth .....	57
4.2.3 Heave and water intake .....	58
4.2.4 Moisture content redistribution .....	59

4.2.5 Discussion of the effects of temperature gradient.....	60
4.3 Effects of applied stress.....	64
4.3.1 Frost penetration.....	71
4.3.2 Horizontal ice lens formation and its development.....	73
4.3.3 Heave and water intake .....	75
4.3.4 Moisture content redistribution.....	76
4.3.5 Discussion of the effects of applied vertical stress.....	77
4.4 Effects of water salinity .....	82
4.4.1 Frost penetration during tests with saline pore fluid .....	93
4.4.2 Ice lens formation and development.....	95
4.4.3 Heave and water intake .....	98
4.4.4 Moisture content and redistribution, and salinity rejection .....	100
4.4.5 Discussion of the effects of pore water salinity .....	104
5 Summary and conclusions.....	108
6 Recommendations.....	114
7 Reference .....	116
Appendix A Temperature with time within each test.....	121
Appendix B Moisture content and salinity data of each test .....	137

## List of Tables

Table 3.1 Test overview.....	13
Table 4.1.1 Image locations for Figure 4.1.1 .....	30
Table 4.1.2 Water balance calculation .....	41
Table 4.1.3 The difference of Water amount of water balance calculation .....	49
Table 4.2.1 Image locations for Figure 4.2.1 .....	50
Table 4.2.2 Image locations for Figure 4.2.2 .....	54
Table 4.3.1 Image locations for Figure 4.3.1 .....	66
Table 4.3.2 Image locations for Figure 4.3.2 .....	68
Table 4.3.3 Image locations for Figure 4.3.3 .....	70
Table 4.3.4 Summary of the time for onset of heave and water expulsion.....	75
Table 4.3.5 Summary of final ice lens growth rate and SP at the onset of the final ice lens formation .....	80
Table 4.4.1 Image locations for Figure 4.4.1 .....	84
Table 4.4.2 Image locations for Figure 4.4.2 .....	86
Table 4.4.3 Image locations for Figure 4.4.3 .....	86
Table 4.4.4 Image locations for Figure 4.4.4 .....	90
Table 4.4.5 Image locations for Figure 4.4.5 .....	91
Table 4.4.6 Image locations for Figure 4.4.6 .....	92
Table 4.4.7 Starting time and total amount for water in take and frost heave for all the saline tests .....	98
Table 5.1 Summary of test conditions of each series of tests .....	109
Table 5.1 Freezing behaviour influenced by temperature gradient, stress and salinity.....	113

## List of Figures

Figure 2.1 Typical components of a frozen soil .....	5
Figure 2.2 Location of unfrozen water in coarse and fine grained frozen soils .....	7
Figure 2.3 Temperature profile and ice lens formation .....	9
Figure 3.1 The freezing cell.....	15
Figure 3.2 The schematic freezing system .....	16
Figure 3.3 Grain size distribution of Devon Silt .....	17
Figure 3.4 e-log (p) curve for Devon Silt .....	19
Figure 3.5 Compression curve ( $\sigma_c=25$ kPa).....	20
Figure 3.6 Compression curve ( $\sigma_c=50$ kPa).....	20
Figure 3.7 Compression curve ( $\sigma_c=100$ kPa).....	21
Figure 3.8 Compression curve ( $\sigma_c=200$ kPa).....	21
Figure 3.9 Image enhancement .....	24
Figure 3.10 Electrical conductivity meter calibration .....	25
Figure 4.1.1 Serial images of the freezing process of test #1 .....	30
Figure 4.1.2 Frost penetration with time in test #1 .....	32
Figure 4.1.3 Temperature profiles at different time in test #1 .....	32
Figure 4.1.4 Frozen fringe thickness with time in test #1 .....	33
Figure 4.1.5 Frozen fringe thickness at different height of sample in test #1 .....	33
Figure 4.1.6 Horizontal ice lens at different depth of the sample in test #1 .....	34
Figure 4.1.7 Final ice lens growth in test #1.....	35
Figure 4.1.8 Reticulate ice structure .....	36
Figure 4.1.9 Water-intake (WIT) during freezing in test #1.....	37
Figure 4.1.10 Heave of the top of the sample during freezing in test #1 .....	37
Figure 4.1.11 Thickness increasing of the ice lens above the final one in test #1 .....	38

Figure 4.1.12 Moisture content (MC) profile in test #1 .....	39
Figure 4.1.13 The temperature (left) compared to the cooling rate (right) of the warmest ice lens in test #1 .....	43
Figure 4.1.14 Typical unfrozen water contents.....	46
Figure 4.1.15 The growth of the ice lens right above the final one in test #1 .....	47
Figure 4.2.1 Serial images of the freezing process of test #2 .....	51
Figure 4.2.2 Serial images of the freezing process of test #3 .....	53
Figure 4.2.3 Frost penetration under different temperature gradients.....	55
Figure 4.2.4 Frozen fringe thickness changes with time under different temperature gradients.....	56
Figure 4.2.5 Frozen fringe thickness along the height of the sample in tests #1, #2 and #3.....	56
Figure 4.2.6 Final ice lens growth under different temperature gradient.....	58
Figure 4.2.7 Water intake in tests #1, #2 and #3.....	59
Figure 4.2.8 Frost heave in tests #1, #2 and #3.....	59
Figure 4.2.9 Moisture content ratio profile in tests #1, #2 and #3.....	60
Figure 4.2.10 Temperature profile and suction profile of freezing soil .....	63
Figure 4.3.1 Serial images of the freezing process of test #4 .....	66
Figure 4.3.2 Serial images of the freezing process of test #5 .....	68
Figure 4.3.3 Serial images of the freezing process of test #6 .....	70
Figure 4.3.4 Frost penetration under different vertical stress.....	72
Figure 4.3.5 Frozen fringe thickness changes with time under different vertical stresses .....	72
Figure 4.3.6 Frozen fringe thickness along the height of the sample under different vertical stresses .....	73
Figure 4.3.7 Final ice lens growth under different vertical stresses.....	75

Figure 4.3.8 Water intake under different vertical stresses .....	76
Figure 4.3.9 Frost heave under different vertical stresses .....	76
Figure 4.3.10 Moisture content (ratio) profile after frozen in tests #1, #4, #5 and #6 .....	77
Figure 4.3.11 The final ice lens growth rate at the onset of the final ice lens formation under different vertical stresses .....	80
Figure 4.3.12 The segregation potential (SP) at the onset of the final ice lens formation under different vertical tresses .....	81
Figure 4.4.1 Serial images of the freezing process of test #7 .....	84
Figure 4.4.2 Serial images of the freezing process of test #8 .....	86
Figure 4.4.3 Serial images of the freezing process of test #9 .....	87
Figure 4.4.4 Serial images of the freezing process of test #10 .....	89
Figure 4.4.5 Serial images of the freezing process of test #11.....	91
Figure 4.4.6 Serial images of the freezing process of test #12 .....	92
Figure 4.4.7 Frost penetration under different pore water salinities .....	94
Figure 4.4.8 Frozen fringe thicknesses with time with different pore water salinities .....	94
Figure 4.4.9 Frozen fringe thicknesses along the height of the samples with different pore water salinities .....	95
Figure 4.4.10 Location of the final ice lens with different pore water salinities .....	97
Figure 4.4.11 Final ice lens growth with different pore water salinities.....	97
Figure 4.4.12 Water intake with different pore water salinities .....	99
Figure 4.4.13 Frost heave with different pore water salinities .....	99
Figure 4.4.14 Water intake in tests #9, #10, #11 and #12 .....	100
Figure 4.4.15 Frost heave in tests #9, #10, #11 and #12 .....	100
Figure 4.4.16 Moisture content (ratio) profile after frozen in tests #1, #7,	

#8 and #9 .....	102
Figure 4.4.17 Moisture content (ratio) profile after frozen in tests #9, #10, #11 and #12 .....	102
Figure 4.4.18 Salinity (ratio) profile after frozen in tests #7, #8 and #9 .....	103
Figure 4.4.19 Salinity (ratio) profile after frozen in tests #9, #10, #11 and #12.....	103
Figure 4.4.20 Pore freezing point with different salinities.....	105
Figure 5.1 Schematic frozen sample and MC redistribution after freezing.....	111

# 1 INTRODUCTION

According to their response during freezing, soils can be classified into two groups, frost-susceptible soils and non-frost-susceptible soils (Jumikis, 1966). Coarse grained soils such as sands and gravels do not heave when they freeze, and the soil structure does not change, so they are called non-frost-susceptible soils. When saturated fine grained soils such as silt and clay undergo freezing, frost heave usually takes place with moisture migration forming segregated ice lenses changing the structure of the soil. Thus fine grained soils are called frost susceptible soils. When soil experiences a freeze-thaw cycle, the structure of a non-frost-susceptible soil does not change whereas the structure of a frost-susceptible soil changes, and during thaw the soil can lose strength, undergo excessive settlement and release moisture if excessive ice forms during freezing

The frost heave and subsequent thaw weakening can cause engineering problems for foundations, slopes and road pavements in zones that experience sub-zero conditions. For instance, in foundation engineering, the heave of the soil under the building due to frost can uplift the building. If the uplift is uneven, severe damage can take place. In addition, the ground will lose strength and thus bearing capacity when the ice thaws (Zhang et al., 1993). Other problems such as frost-jacking and thaw settlement, and weakened layers within slopes are also familiar to geotechnical engineers (Nidowicz and Shur, 1998). These problems can also be caused by some man-made facilities such as chilled gas pipelines and refrigerated cold storage facilities (Huang et al., 2004). Furthermore, using artificial ground freezing in civil, environmental, and mining engineering for the construction of temporary support structures, frozen soil barriers, and undisturbed

sampling of cohesionless soils adds importance to understand the details of how soil freeze (Sego et al. 1998; Sayles and Iskandar 1998; Hass and Seegers 2000).

Freezing in a frost-susceptible soil is a complicated process including both heat and mass transfer. The mass transfer, i.e. moisture migration is an important process during the freezing. Freezing and associated frost heave of a soil is influenced by factors such as grain size distribution, mineralogy of fines, availability and salinity of pore water, overburden stress, and rate of heat extraction (Taber 1929; Beskow 1935; Kaplar 1970; Anderson and Tice 1972; Penner 1972; Konrad and Morgenstern 1982; Konrad 1987, 1990). Most of these previous studies have contributed to discover the mechanisms involved in the freezing process. However, all of these previous studies used indirect measurements such as nuclear magnetic resonance, X-ray diffraction, heat capacity, differential thermal analysis to locate unfrozen water. Until today only the results of freezing but not the freezing process itself have been observed and documented. The theory of ice lens formation and frozen fringe development is built on assumptions and indirect data measured during laboratory freezing tests and field investigations associated with freezing. It is therefore desirable to find more direct evidence about the freezing process.

The investigations presented here present a visual documentation to observe and study the influence of temperature gradients, overburden pressures and pore water salinities on the freezing process. A fluorescent tracer was used to observe the unfrozen water and the ice lens growth during freezing. Time-lapse photography provide a digital photo record to visually document and illustrate the various processes during tests.

The objective of these investigations is to study the freezing process and frost heave correlated to moisture migration between frozen and unfrozen zone under different boundary conditions described above using equipments which can visually record and document the phenomena related to freezing soil. The effects of temperature gradients, overburden pressures and pore water salinities on ice lens formation and structure, moisture migration, frost penetration, frozen fringe and frost heave will be discussed in this thesis. The following chapters present these investigations of freezing on Devon silt. Chapter 2, literature review, introduces a background of freezing soils. Chapter 3, laboratory tests, details the test equipments, materials and procedure, and limitations of the tests. A consolidation test for determining the consolidation index is presented in this chapter as well. Chapter 4, test results, which is the most important and longest part of this thesis, provides all the results of the tests and the discussion of the results, including the images captured during each freezing test. The recommendations are provided in chapter 6 after chapter 5, the conclusions. Most temperature data are placed in the appendices.

## 2 LITERATURE REVIEW

A frozen soil consists of four phases, soil particles, ice crystals, unfrozen water and gas. When the temperature in a soil decreases below 0°C, the pore water starts to change its phase from liquid to solid. However, not all the water changes phase at this temperature (Bouyoucos, 1916; Lovell, 1957), which means that water and ice can coexist simultaneously in frozen soils (Figure 2.1). The amount of unfrozen water in a soil is governed by the temperature, the applied pressure, the particles' specific surface area, their mineralogical and chemical composition, the arrangement of the soil particles, the soil density, the solute concentration, and composition of the pore fluid (e.g. Vershinin et al., 1960; Nerseova and Tsytoich, 1963; Hoekstra, 1969; Anderson and Tice, 1972). The location of the unfrozen water is generally different within coarse-grained frozen soils and fine-grained soils (Jumikis, 1966; Arenson and Seg0, 2004). In coarse grained soils, the unfrozen water is in the middle of the pore space. This is due to the much higher thermal conductivity of the soil particles compared to the pore water, which induces faster heat removal through the soil skeleton than the pore water. Thus ice forms immediately surrounding the soil particles leaving unfrozen water in the void spaces between the soil particles coating with ice. Figure 2.2a is an example for the location of unfrozen water in poorly graded sand when frozen. In fine grained soils, the unfrozen water is immediately surrounding the soil particles as a strongly bonded water film between the soil particles and the ice (Figure 2.2b).

The behaviour related to freezing of these two classes of soils will be discussed in the following paragraphs.

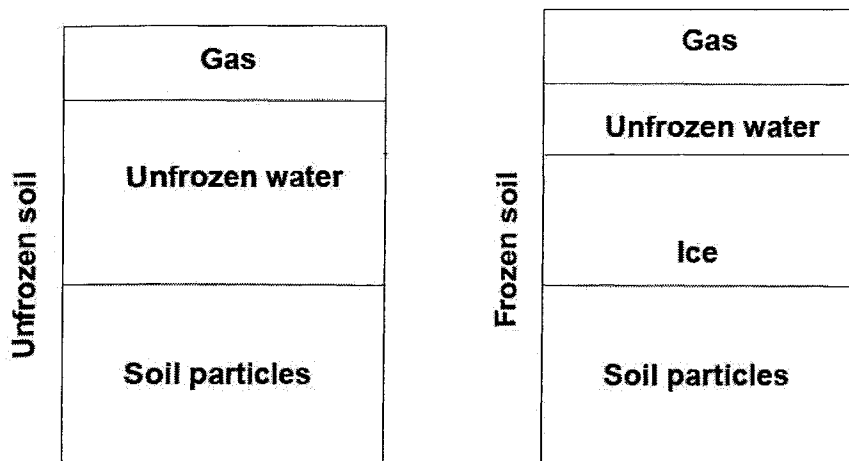


*Figure 2.1 Typical components of a frozen soil*

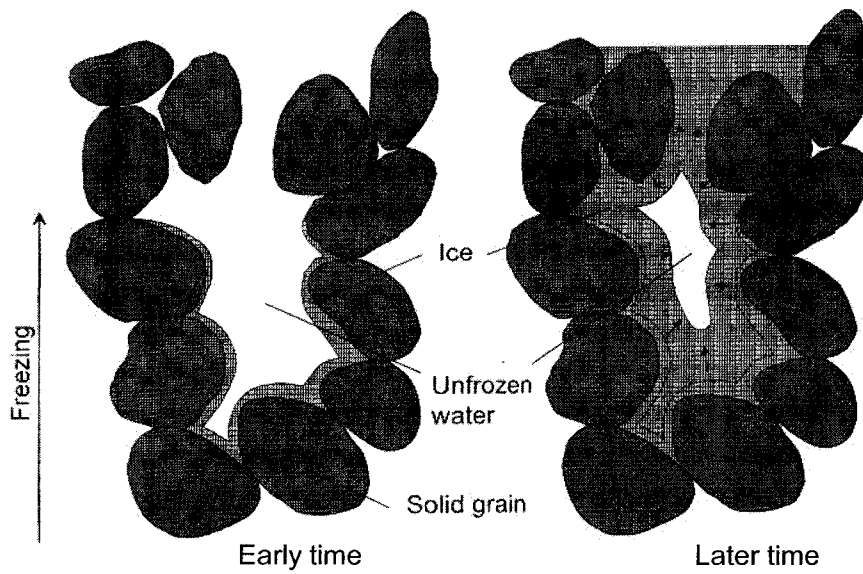
Coarse-grained soils are usually not frost-susceptible. When the soil freezes, if the freezing rate is slow enough, it does not change its structure since the 9% volume change pushes the unfrozen water away from the freezing front so does not change the voids in the soil. However, unfrozen water may still co-exist in the pores. This is especially in saline soils where the unfrozen water content is considerable due to freezing point depression of the saline pore water (Arenson and Seg0, 2004).

Fine-grained soils are usually frost-susceptible. When frost penetrates into a frost-susceptible soil, ice lenses form inducing frost heave. This requires the flow of water towards the frozen fringe and is unrelated to the fact that water expands upon freezing (Taber 1929, 1930). Freezing of a frost-susceptible soil is a complicated process, which includes both heat and mass transfer. Mass transfer via moisture migration, is an important mechanism during the freezing process. When a fine-grained soil freezes, not all the water within the soil pores changes phase at its normal freezing point (Bouyoucos, 1916; Lovell, 1957), i.e. pure water's freezing point is 0°C at atmosphere pressure. Soil water exists simultaneously as free water in bulk, capillary water, film water, and hygroscopic

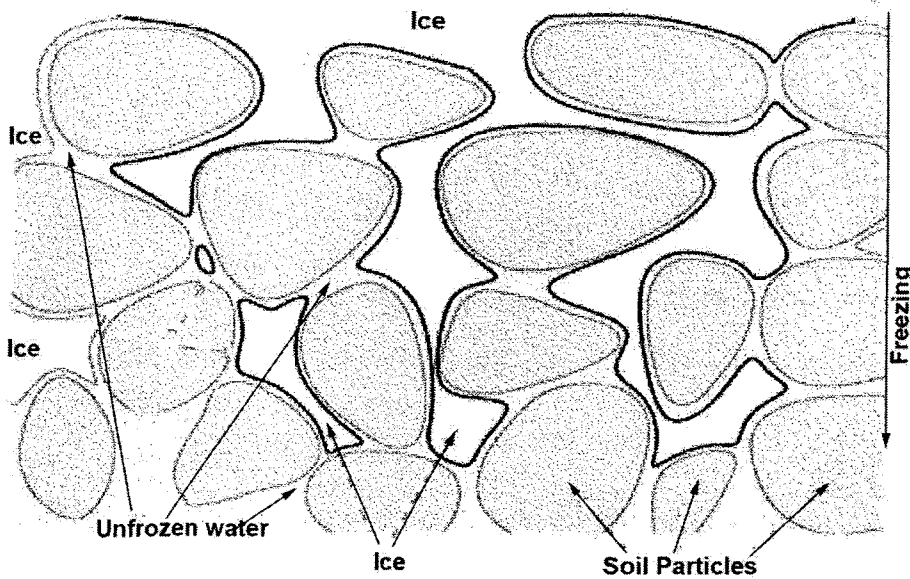
water, and each may have different freezing points (Jumikis, 1966). The free water in bulk filling the soil voids is the first to freeze, then the capillary water, the film water and finally the hygroscopic water due to different stresses and ionic constituents in the different kinds of water. When the bulk free water freezes as the sample is below 0°C, moisture migration within the soil mass may still occur through the unfrozen water, coexisting with ice as thin films of adsorbed water and as capillary water that lies outside the range of adsorption forces but fails to freeze because it occupies spaces too narrow to be penetrated by a curved ice-water interface. The zone through which free water is drawn from the unfrozen zone to the warmest ice lens is called frozen fringe (Miller, 1972) (Figure 2.3). The temperature gradient provokes a suction gradient which also induces water migration (Oliphant et al., 1983). When pressurized water is frozen, the bond between the soil particles and water breaks, so water molecules leave the particles and join the growing ice crystals. Additional other unfrozen water will be drawn in to repair the broken bonds (Jumikis, 1966). The rate of water flow is governed by Darcy's law and depends on the distribution of hydraulic gradient and hydraulic conductivity in the frozen soil.

Typically, one-dimensional laboratory freezing tests are used to study the freezing process and to determine the freezing characteristics of soils. For many years, two types of laboratory freezing tests have been established according to the boundary temperature: step-freezing, in which the temperature boundary condition is constant, and ramp-freezing, in which the temperature at the boundaries of a soil specimen is changed at a specified rate. According to the water supply, laboratory tests are differentiated into open system and closed system tests. In an open system test, free water in excess of that contained in the voids of the soil before freezing is as a source of water available to the frozen front. In a close system test, there is no external water source present, and the

soil may transfer water thus the soil may only redistribute water. The step-freezing and ramp-freezing tests discussed herein are both open system tests.



(a) In coarse grained soils (after Arenson and Seg0 2004).



(b) In fine grained soils (after Rempel et al., 2004).

Figure 2.2 Location of unfrozen water in coarse and fine grained frozen soils.

In many laboratory tests, heave of the sample surface, water intake, temperature profile during freezing, moisture content and salinity profile are monitored and measured to analyze the freezing process and heave mechanism (Konrad and Morgenstern, 1980; Mageau and Morgenstern, 1980; Konrad, 1990; Rempel et al., 2004).

In step-freezing tests, the cold plate and the warm plate are maintained at constant temperatures during freezing. The temperature profile along the sample height during transient heat flow is generally linear within both the frozen and unfrozen zone due to the small height of test specimen, which is caused by similar thermal conductivity within frozen or unfrozen zone (Konrad, 1994). The profile becomes linear along the whole sample height at thermal steady state. The final ice lens, the last one during the freezing, initiates when the thermal steady state is reached, i.e. the zero degree isotherm is stable. In ramp-freezing tests, the temperatures of the cold plate and the warm plate are reduced at a specific rate. This mode consists of a linear reduction with time of the cold and warm plate temperatures to produce a fairly constant rate of frost penetration and a fairly regular ice-soil structure (Figure 2.3 b). In general, frost heave rate increase with time and there is no final ice lens developed, since the frost front continuously advances in response to steadily changing temperature boundary conditions.

Step-freezing tests generate a stratified ice-soil structure shown in Figure 2.3a. At the beginning of testing, the soil is frozen with increasing ice enrichment but no visible ice lenses because of the rapid change of temperature across the sample. Then, as the frost front penetration slows down, very thin and barely visible ice lenses appear. Further reduction in frost penetration rate with a concomitant decrease in temperature gradient in the frozen soil as surface heave occurs with

time leads to increased thickness of ice lenses and increased spacing between consecutive ice lenses. As the thermal steady state is approached, the final ice lens is initiated and grows until the test is halted.

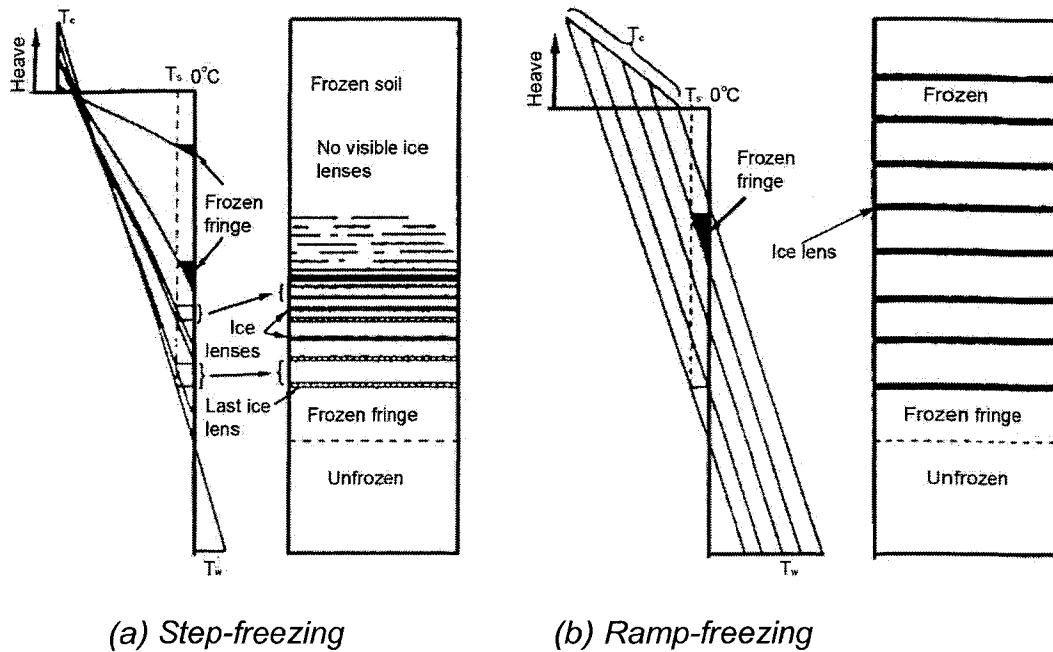


Figure 2.3 Temperature profile and ice lens formation (After Konrad 1994)

The freezing process and frost heave of a soil is influenced by factors such as grain size distribution, mineralogy of fines, availability and salinity of pore water, overburden stress, and rate of heat extraction (Taber, 1929; Beskow, 1935; Kaplar, 1970; Anderson and Tice, 1972; Penner, 1972; Konrad and Morgenstern, 1982; Konrad 1987, 1990).

For the same soil, a larger temperature gradient induces a higher cooling rate during freezing. The cooling rate influences the ice lens formation and the frost heave as described below. During transient heat flow, an ice lens stops growing when its temperature drops down to the temperature for which the hydraulic conductivity of the frozen soil beneath the ice lens is too low to permit water

movement, forcing a new ice lens to initiate in the warmer zone of the frozen fringe (Konrad, 1988). Small rates of cooling permit the growth of the current ice lens as long as its temperature does not exceed the limit temperature. The temperature of ice lens formation is dependent upon the cooling rate of the frozen fringe. The temperature at which the active ice lens stops growing also depends upon rate of cooling, and increases with decreasing rate of cooling (Konrad, 1994). The difference, between the temperature of ice lens initiation and the temperature at the end of the same ice lens growth, increases with decreasing rate of cooling.

Segregational frost heave, which is induced by the water migration (Taber, 1929), can be inhibited by the applied pressure on the soil subject to open-system freezing. According to the Clapeyron equation (Lewis and Randall, 1961), the suction at the warm side of the active ice lens decreases with increasing stress in the ice lens. Furthermore the pressure also influences the temperature of ice lens formation by narrowing the space between soil particles. The temperature of ice lens formation decreases as the pressure increases (Konrad and Morgenstern, 1982).

The salinity of the pore water depresses the freezing point of the pore water, and when the pore water is frozen, the solutes may be excluded from the ice matrix. Laboratory studies (Konrad and McCammon 1990) suggested that there is a threshold rate of cooling of  $3^{\circ}\text{C}/\text{day}$  above which no solutes are rejected from the ice matrix. For rates of cooling smaller than  $0.1^{\circ}\text{C}/\text{day}$ , more than 90% of the solutes are rejected from the ice. During freezing, final ice lens formation and rate of frost heave are influenced by the salinity of pore water. The rate of frost heave decreases with increasing pore water salinity (Konrad, 1990).

Konrad and Morgenstern (1980) introduced the concept of segregation potential

(SP), which is defined as the ratio of water intake rate and temperature gradient in the frozen fringe. The effects of factors such as vertical pressure and soil type on SP at the formation of the final ice lens can be accounted for using the equation below: (Konrad and Morgenstern 1982)

$$SP = SP_0 e^{-aP_e}$$

Where  $SP_0$  is the segregation potential obtained with no applied load,

$P_e$  is the vertical pressure,

$a$  is a soil parameter.

The SP can also be used for interpretation of frost heave of saline freezing (Konrad, 1990)

When a fine-grained soil is frozen under a temperature gradient, not only are the horizontal ice lenses formed but the vertical ice lenses may form as well. The ice lenses form a three-dimensional reticulate ice vein network. There are at least three theories to explain the origin of the reticulate ice veins in permafrost. Popov (1967) has suggested that the growth of horizontal ice lenses was accompanied by dehydration and vertical cracking of the underlying unfrozen sediments, with water migration to the vertical cracks in an open system where it froze to form the vertical ice lenses. Danilov (1969) and Katasonov (1960, 1961, 1967) have interpreted the inclined ice veins of lake and marine clays as being formed subparallel to a correspondingly inclined permafrost surface in a shallow water body, with freezing being directed upwards in an open sub-aquatic groundwater system. Mackay (1974) believed that the vertical and horizontal ice veins grew in shrinkage cracks with much of the water being derived from the adjoining clay.

Theories and practices on freezing soils have been well developed. Many phenomena correlated to freezing soils have been explained by researchers via

laboratory tests and site investigations. However, most explanations and theories were built on some assumptions and indirect measures such as site investigation, and standard laboratory freezing tests, which give the results of freezing but not the freezing process itself. In addition, some disagreements still exist in some aspects, e.g. the formation of vertical ice veins. To give direct evidences and explanations to the mechanism to freezing soils, investigations different from the traditional ones are necessary. Utilizing of digital image equipments and special materials makes it possible to visually document and illustrate the freezing processes. In these investigations presented hereafter, a fluorescent tracer was used to observe the unfrozen water and the ice lens growth during freezing. Time-lapse photography provided a digital photo record to visually document and illustrate the various processes during actual tests, which will be discussed in detail in the following chapters.

### 3 LABORATORY TESTS

Standard laboratory freezing tests do not directly show the frost penetration, the change of the frozen fringe and the ice lens formation during freezing processes. To better understand these phenomena, a special experimental apparatus was developed. The materials used and the detailed test procedure are discussed in this chapter.

A total of 12 one-dimensional open system (access to water) step-freezing laboratory tests were carried out using Devon silt under different boundary conditions of temperature gradients, vertical pressures and pore water salinities (Table 3.1). The effective conditions are shown in brackets if different from the nominal ones. The effective salinities were determined from the samples, which were taken from the slurry mixture before the de-aeration process to determine the initial moisture content.

Table 3.1 Test overview.

Test No.	Temperature		Salinity S (g/L)	Pressure	
	Top (°C)	Bottom (°C)		$\sigma_c$ (kPa)	$\sigma_f$ (kPa)
1	-5	2	0	100	0
2	-2	2	0	100	0
3	-15 (-14.5)	2	0	100	0
4	-5	2	0	100	100
5	-5	2	0	200	200
6	-5	2	0	400	400
7	-5	2	5 (5.9)	100	0
8	-5	2	10 (10.2)	100	0
9	-5	2	25 (25.7)	100	0
10	-15 (-14.5)	2	25 (23.6)	100	0
11	-5	2	25 (24.4)	200	200
12	-2.5	2	25 (24.7)	100	0

Note:  $\sigma_c$ : Consolidation pressure;  $\sigma_f$ : vertical pressure during freezing.

### 3.1 Equipment and materials

A cylindrical freezing cell with an inner diameter of 100 mm was used for the laboratory tests (Figure 3.1). Figure 3.2 is a schematic diagram of the freezing system. This freezing cell was composed of two parts. The upper one was used for applying pressure on the sample, and controlling the temperature of the top plate connected to a constant cold bath during freezing. The lower section contains the soil sample for consolidation and freezing. The temperature of the bottom of the soil sample was controlled via the bottom plate, which was connected to a second constant cold bath. Drainage of the sample occurred through the bottom plate for the open system freezing tests. The perspex wall of the cell allowed use of a high-resolution digital camera (Canon EOS Rebel with 6.3M pixel resolution) with a macro lens (Canon MP-E 65 mm f/2.8 1-5x Macro Photo) to record digital images of the frost penetration and ice-lens formation process. The thick perspex wall (about 20mm) of the cell and additional insulation around the cell guaranteed one-dimensional freezing process because of the lower thermal conductivity of the perspex cell which allowed vertical heat flow through the sample.

Four thermistors were used to monitor the temperature along the height of the sample. One was mounted on the bottom plate, another was on the top of the sample and the remaining two were placed along the height of the sample at equal spacing of 41mm. Another thermistor was exposed in the air to monitor the environment temperature around the freezing cell. Air pressure transducer and linear potentiometer (LP) were used to monitor and record the vertical pressure (air pressure) and top plate displacement during the consolidation and freezing phase of each test.

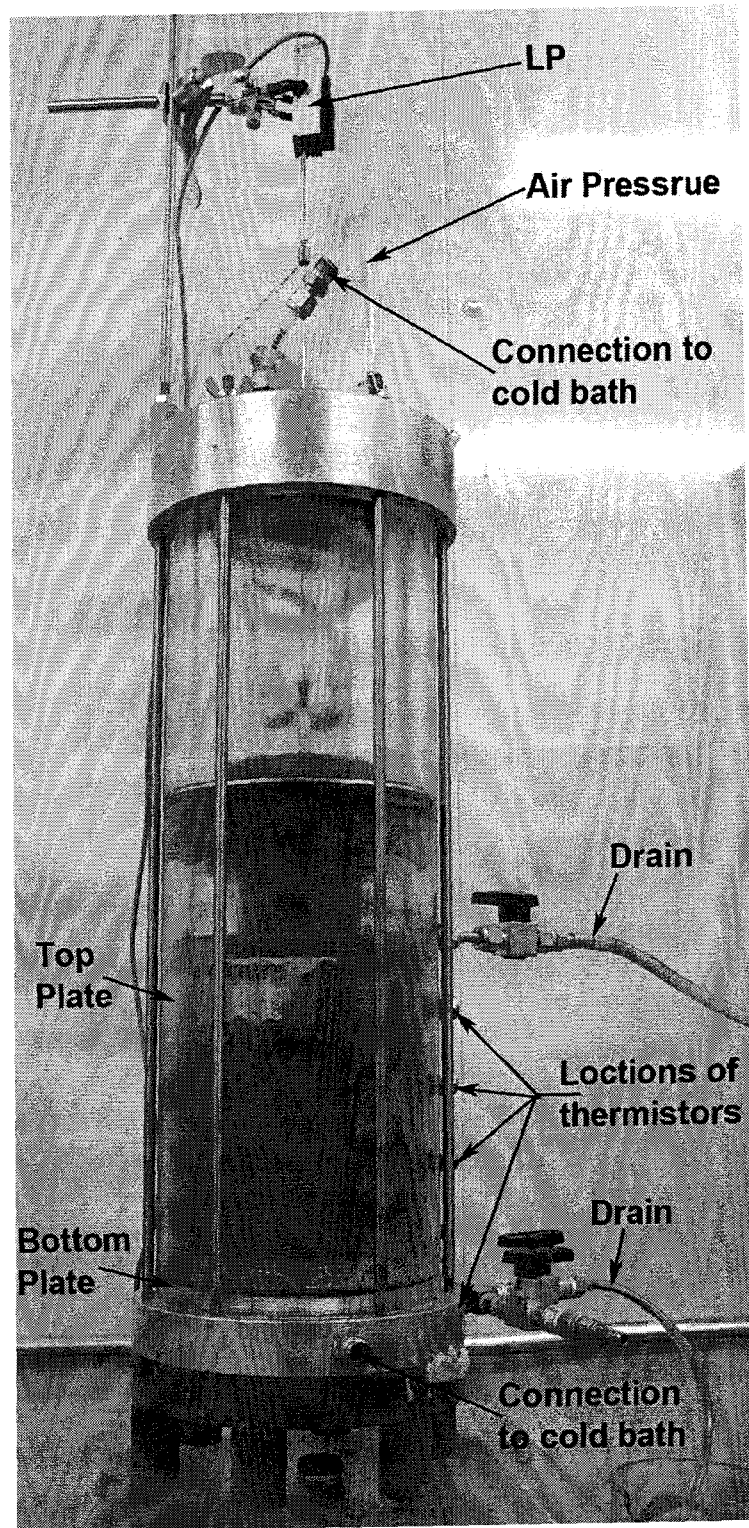


Figure 3.1 The freezing cell

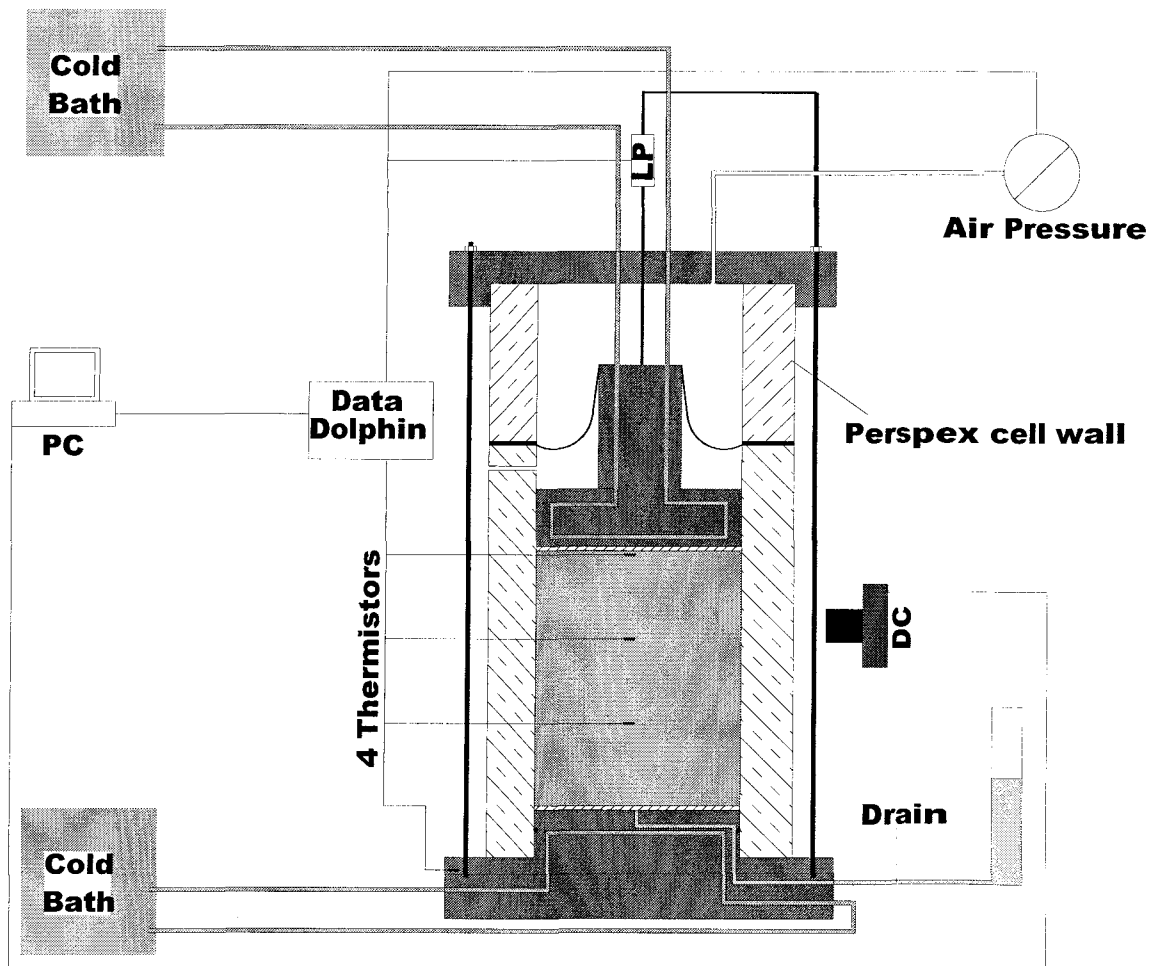


Figure 3.2 The schematic freezing system

A frost-susceptible soil, Devon silt (Figure 3.3) with a liquid limit of 32%, plastic limit of 20% and specific gravity of 2.65 was chosen for these investigations. In Figure 3.3, curves A and B represent two characteristic samples of Devon silt, used in these investigations. The Devon silt has 25% clay size particles. Several research results of frost susceptibility of this soil are available (Konrad and Morgenstern 1981; Konrad and Morgenstern 1982; Konrad 1990). A fluorescent tracer ( $C_{20}H_{12}O_5$ ) was used to observe the frozen and unfrozen zones within the sample and the ice lenses during freezing. This tracer appears green in an unfrozen state under ultra violet light and does not alter the freezing point when dissolved in unfrozen water (Arenson and Seg0, 2004). When the solution freezes,

the tracer is rejected from the ice, which makes the ice colorless under the UV light. These properties of the tracer guarantee that the unfrozen water in the soil sample is visible under UV light, and the freezing process remains unchanged by the tracer. The salts used for salinity tests were NaCl.

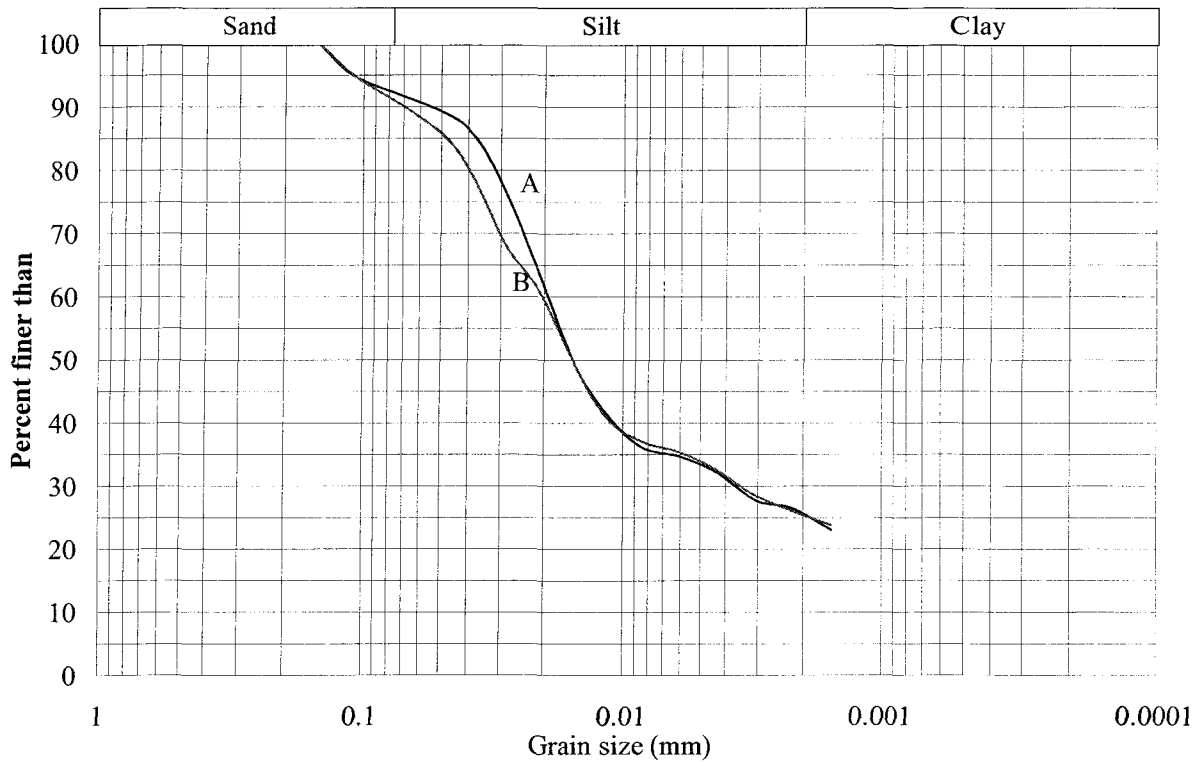


Figure 3.3 Grain size distribution of Devon Silt.

### 3.2 Sample preparation

The sample was prepared as a slurry with a gravimetric moisture content of 50% to 60%, which is about 1.5 times its liquid limit, by mixing the dry soil and distilled water with 5 g/liter of fluorescein. The total amount of slurry for each freezing test was determined by using the results of an independent consolidation test discussed below. Water with desired salinity (Table 3.1) was used for tests #7 to

#12. The slurry was prepared by mixing it for 1 hour after the ingredients sat in a mixing bowl for about 12 hours. It was then poured into the freezing cell and de-aerated by applying a vacuum on a shaking table as recommended by Konrad (1980). Small soil samples were taken to determine the initial moisture content and pore water salinity before de-aeration. This de-aeration process was divided into 3 stages. One third of the slurry was poured into the cell and de-aerated for 30 minutes. Then the next volume was added and the procedure repeated.

The slurry was then consolidated in the freezing cell using the consolidation pressure shown in Table 3.1 in the cold room at an ambient temperature of 1°C as used for freezing phase of each test. An independent consolidation test on the same soil in a freezing cell was carried out initially to determine the consolidation index,  $C_c=0.257$  (Figure 3.4). The height of sample before applying 25 kPa of consolidation stress was 127.8mm. The time for primary consolidation for each consolidation pressure ( $\sigma_c$ ) of 25, 50, 100, 200 kPa, is about 40 hours (Figure 3.5 to 3.8). These results were used to determine the amount of slurry and the end for primary consolidation of the sample prior to each freezing test. Air pressure was used to apply consolidation pressure according to the value in Table 3.1. The height of each sample was approximately 120 mm after consolidation with some difference depending on the initial moisture content, volume of the slurry added to the cell, and consolidation pressure.

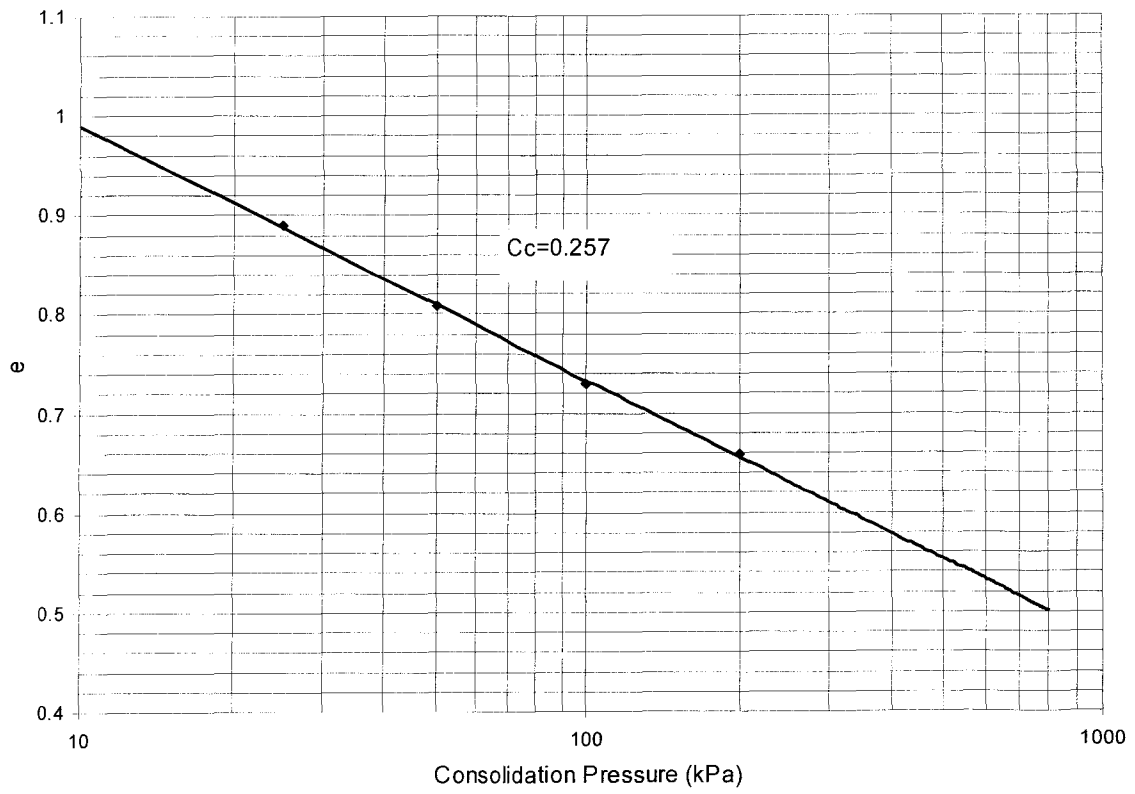


Figure 3.4  $e$ - $\log(p)$  curve for Devon Silt ( $e$ : void ratio;  $p$ : consolidation pressure)

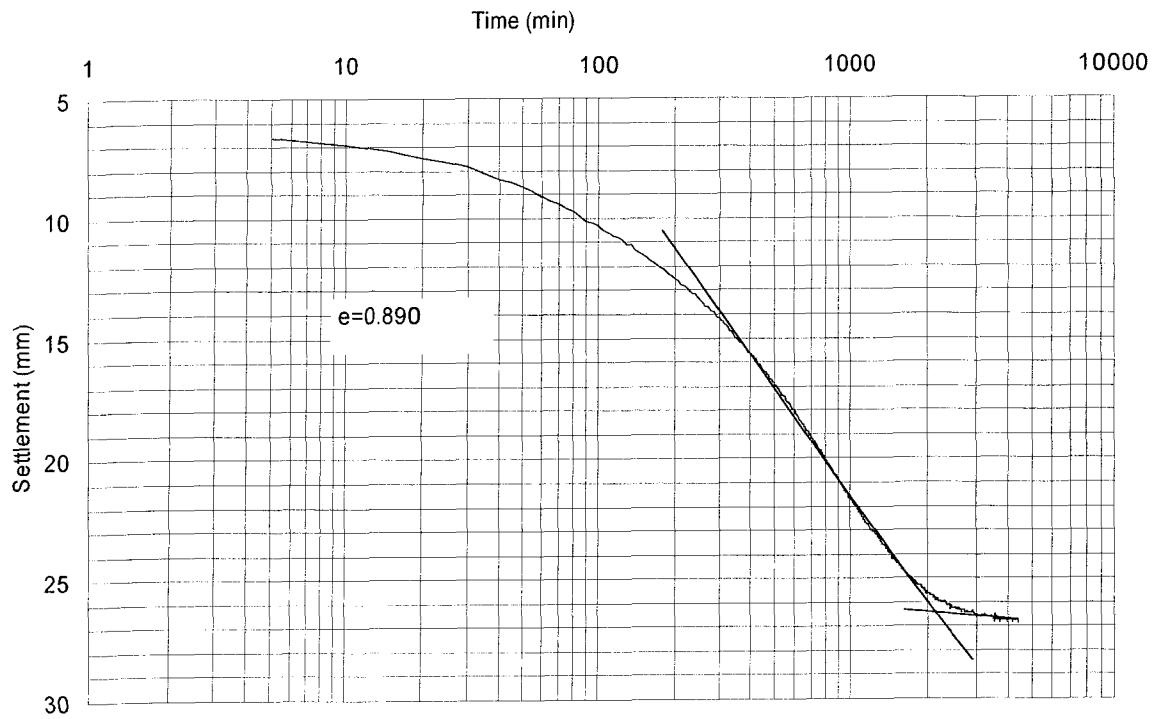


Figure 3.5 Compression curve ( $\sigma_c=25$  kPa) (Sample height before this consolidation is 127.8mm)

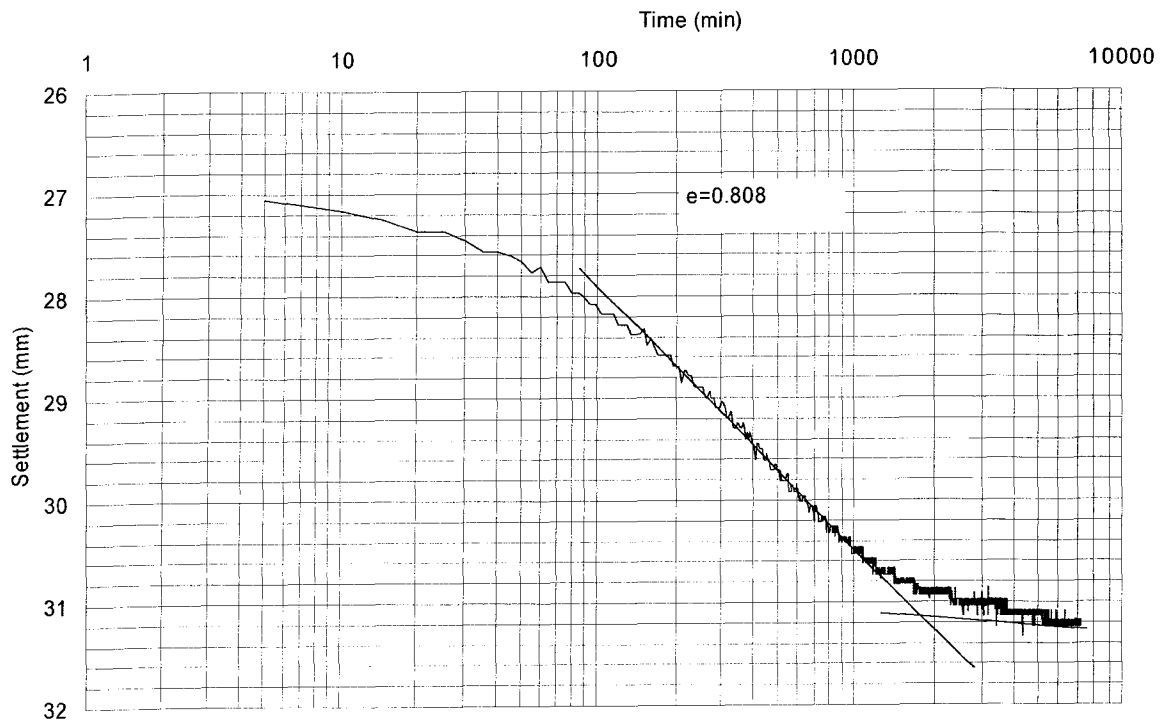


Figure 3.6 Compression curve ( $\sigma_c=50$  kPa)

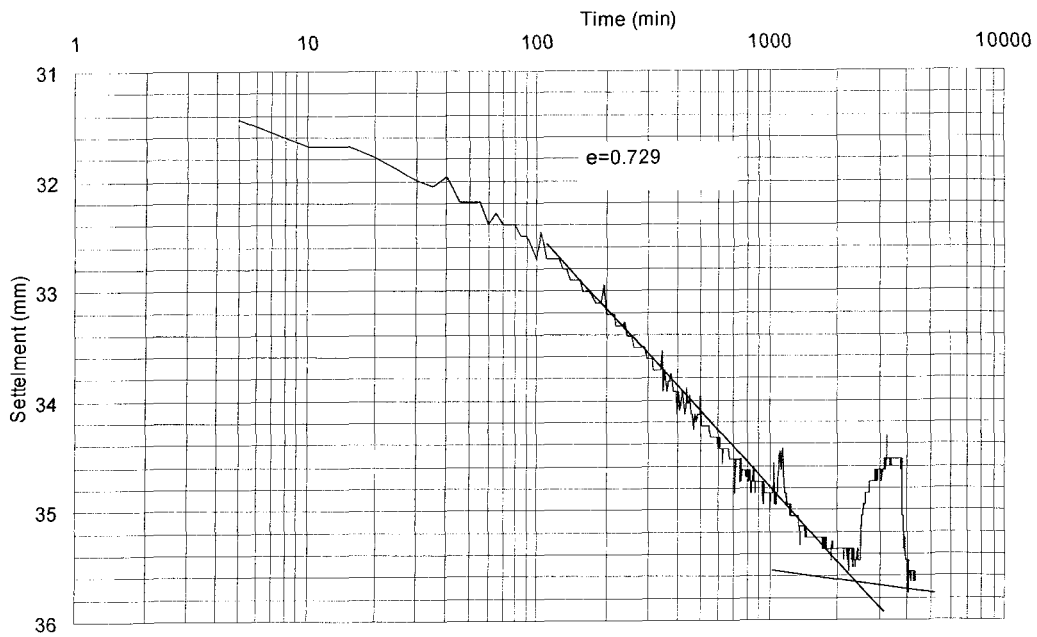


Figure 3.7 Compression curve ( $\sigma_c=100$  kPa)

NOTE: The air pressure was accidentally shut off for 1 hour when the sample was being consolidated, which resulted in a rebound

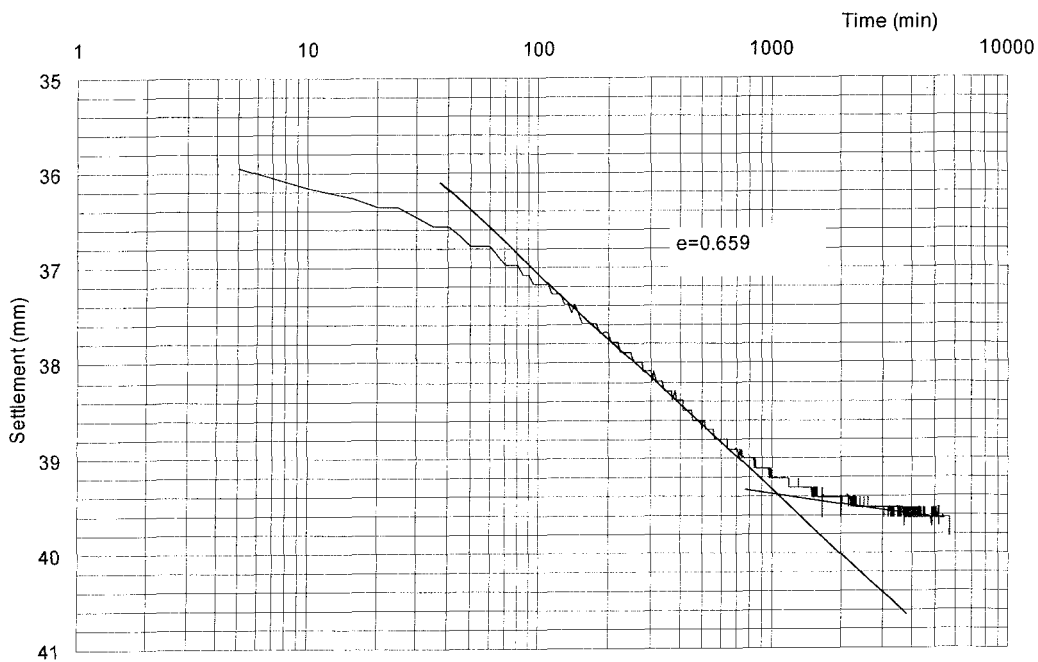


Figure 3.8 Compression curve ( $\sigma_c=200$  kPa)

### 3.3 Freezing tests and data logging

After consolidation, the air pressure applied for consolidation was removed from the cell to allow the thermistors to be installed in the sample. In tests #4, #5, #6 and #11, which were the freezing tests with vertical applied pressures of 100, 200, 400, and 200 kPa, the pressure was then re-applied for approximately 12 hours prior to the start of freezing until the end of each test. The 12-hour-period was necessary to insure the vertical effective stress in the sample was equal to the applied pressure. The digital camera, drainage, and LP were set up as shown in Figure 3.2. Insulation was wrapped around the cell with an opening left for photographing the sample during freezing. Glycol from two constant temperature baths was circulated through the top and bottom plates to initiate one-dimensional freezing of the sample. A sub-zero temperature was applied to the top plate and +2°C was applied to the bottom plate, which caused frost to penetrate from the top down. The temperature gradient within the sample was varied by changing the temperature of the top plate.

Before the start of freezing, the height of the sample was determined. During freezing, the volume of water drawn into or expelled by the sample was recorded manually using the graduated cylinder, and the heave was recorded automatically via the LP. In addition, high resolution digital images under UV light were captured with the digital camera at regular time intervals (2 minutes at the start then increased to 1 hour after a day). These pictures were used to visually observe the frost penetration, ice-lens formation and unfrozen water migration through the test.

### **3.4 Collection of data in the end of freezing tests**

At the end of each test, the frozen sample was taken out of the cell and segmented into 24 sections along its height to obtain the moisture content and the salinity profile for saline tests. In most tests except test #9, only part of each section was sampled for the moisture content and salinity tests. This caused some inaccuracy in the moisture content determination, which will be discussed below (Section 3.6).

### **3.5 Image analysis**

All images captured by the digital camera during freezing were digitally enhanced using inverted colouring to show the important information more clearly (Figure 3.9). In the modified image, the darker portion indicates the unfrozen zone of the sample while the lighter part shows the frozen zone. The bright lines are ice lenses. The frozen fringe, the zone between the lowest ice lens and the frost front, appears at a lighter color than the unfrozen zone but darker than the frozen zone. The scale beside the image, which is placed on the inside of the cell wall, is in millimeters.

The photos show the frost front location, frozen zone, frozen fringe, unfrozen zone, and ice lenses. The thickness of the frozen fringe, the thickness and density of the ice lenses can also be measured from the photos. Furthermore, frost penetration, the change of the thickness in the frozen fringe, and the thickness increase of the final ice lens with time can be determined from a series of photos. These will be discussed in Chapter 4.

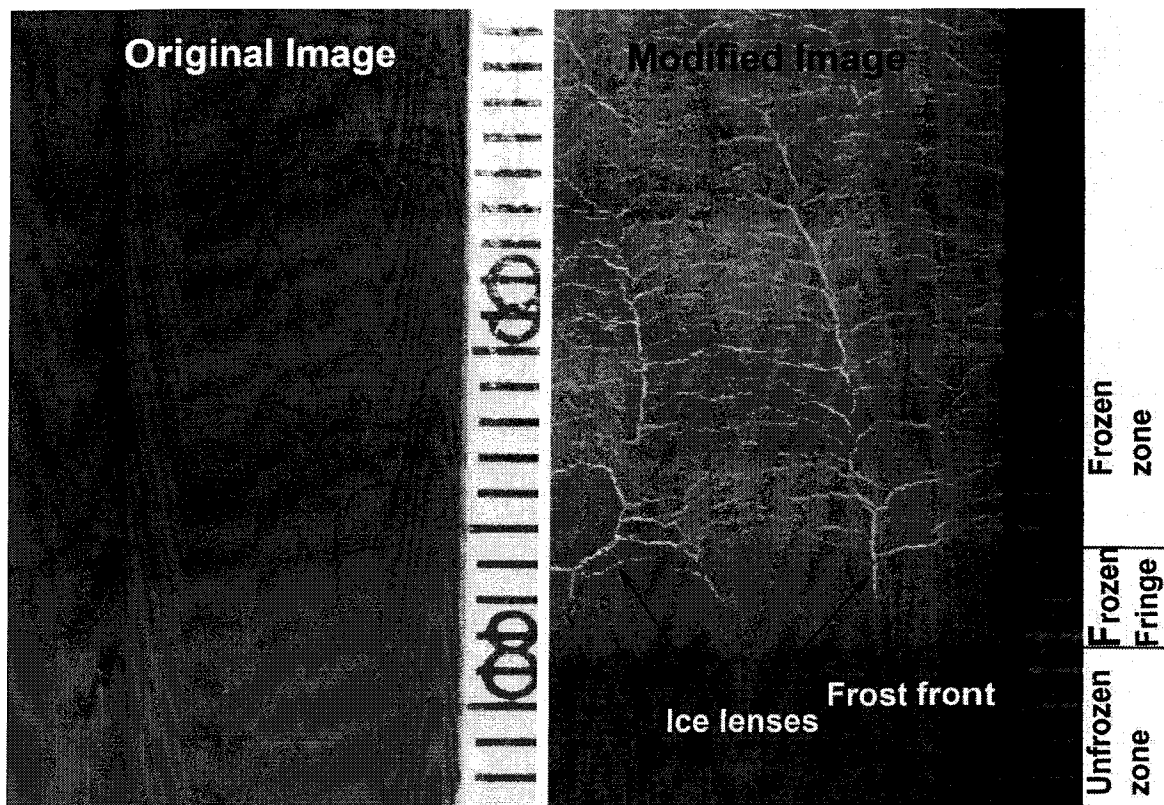


Figure 3.9 Image enhancement

### 3.6 Moisture content and pore water salinity measuring

In each test, soil samples were oven-dried for 24 hours to determine the initial moisture content before de-aeration and the moisture content profile after the freezing test. The moisture content samples were also used for salinity determination in saline freezing test. The oven-dried soils were subsequently soaked in distilled water in plastic bottles for 4 hours. The bottles were shaken for 1 minute to distribute the soil evenly in the water. The bottles were then left for 20 hours to allow most soil particles in the bottles to settle. An electrical conductivity meter (EC meter) was used to measure the salinity of the water in each of the bottles. The salinity was determined using the calibrations shown as Figure 3.10. In Figure 3.10,  $x$  and  $y$  represent the salinity measured by EC meter and the salinity calculated from the amount of salt and water in the solution, respectively.

The three curves (A, B, and C) represent the calibrations for different salinity ranges. For the measured salinity from 0.1g/L to 0.5g/L, calibration C was used; for the measured salinity from 0.5g/L to 2.5g/L, B was used; for the measured salinity from 2.5g/L to 15g/L, A was used. After calibration, the initial salinity of each sample can be calculated by multiplying the calibrated salinity with the ratio of the amount of added water to initial water content of the prepared sample.

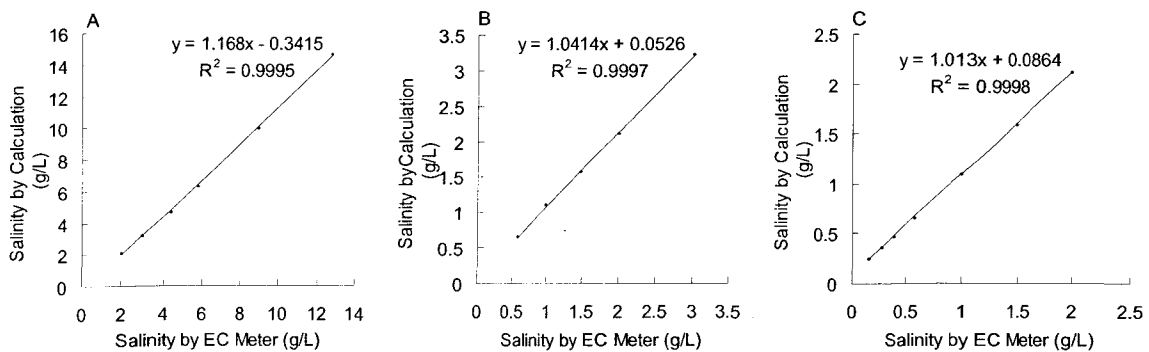


Figure 3.10 Electrical conductivity meter calibration

### 3.7 Limitations

Several limitations may affect the accuracy of these investigations. In these laboratory tests, the height of the sample before and after consolidation in each test was measured with a tape measure scaled in millimeters outside the cell wall. This will influence the accuracy of moisture content calculation after consolidation since the heights of the sample measured before and after consolidation may not be accurate. During freezing, the water drawn into or expelled from the cell was monitored visually reading the graduated cylinder scaled in milliliters. In addition, not the whole cross section of the sample was used for moisture content determination after freezing, which may influence on the moisture content profile. This will also be reflected in the water balance calculations.

Even though insulation was used, lateral heat flow exists in the freezing tests.

However, the lateral heat flow was neglected comparing to the vertical flow because the thermal conductivity of the cell wall and the insulation was much smaller than that of the soil sample. The friction between the inside of the cell wall and the frozen part of the soil influences the frost heave, which will be discussed in Chapter 4. During the freezing of the soil sample in each test, the position of the reservoir, connected with the drainage to the freezing cell, was not adjusted. Thus the hydraulic pressure at the bottom of the soil sample changes when the water surface level in the reservoir changed, which was caused by the water migration due to the freezing process. This change may influence the water migration. However, due to the small changes in the water level, this influence is not significant.

Even though the factors discussed above have some influences on the accuracy of the results, they only have a minor impact on the freezing process, which will be discussed in detail in the next chapter.

## **4 TEST RESULTS**

The results of the investigations are presented and discussed in this chapter. A total of 12 tests divided into 3 groups to study the effects of the temperature gradient, the applied stress and the pore-water salinity on the freezing process were carried out. Test #1 is the fundamental one, serving as a reference to be compared with others. Test #2 and test #3 were performed under the same boundary conditions as test #1 except for different temperature conditions to study the influence of the temperature gradient on frost penetration, ice lens formation, frost heave and water intake. Tests #4, #5, and #6 had non-saline pore water and the same temperature boundary condition as test #1. The vertical stresses during freezing were 100 kPa, 200 kPa and 400 kPa in this series to

study the influence of applied stress. Tests #7, through #12 had saline pore water. Tests #7, #8, and #9 were frozen under the same boundary conditions in terms of temperature and vertical stress as test #1 but with pore water salinities of 5 g/L, 10 g/L and 25 g/L. The 25 g/L of pore-water salinity, close to that of sea water, was used in test #9, #10, #11, and #12 while varying other boundary conditions (temperature and applied vertical stress).

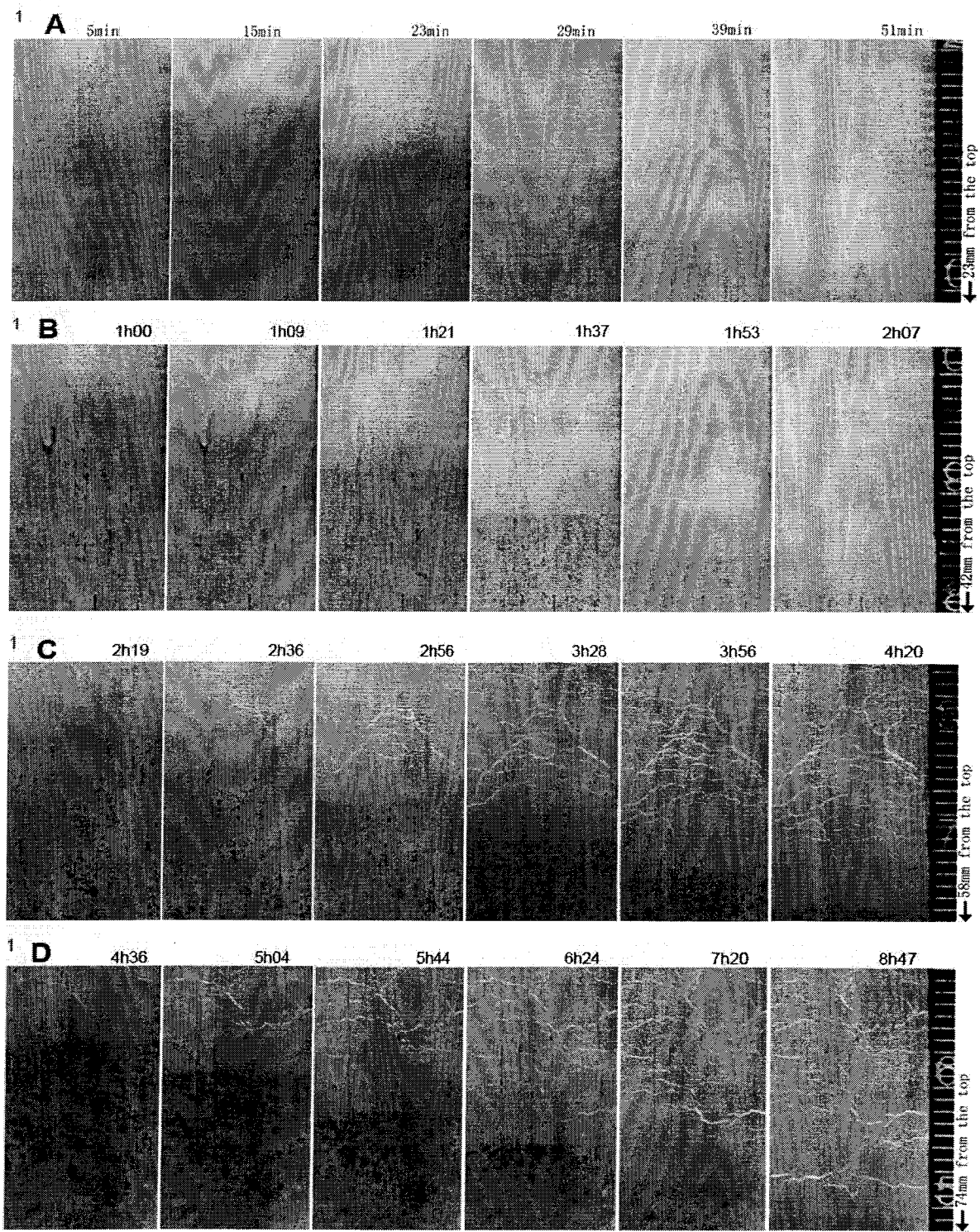
#### **4.1 General freezing of Devon silt**

In this section, most of the results were obtained from test #1 to illustrate and understand the freezing process of Devon silt. Figure 4.1.1 shows a series of images taken at different times during freezing of test #1. It illustrates the freezing process under the condition of no applied vertical stress with  $-5^{\circ}\text{C}$  on the top plate and  $2^{\circ}\text{C}$  on the bottom plate, with non-saline pore water. Each row of the images, downward from A to E, represents a different elevation in the sample (Table 4.1.1). Each row shows a increase in time as the  $0^{\circ}\text{C}$  isotherm progress downward into the sample. Figure 4.1.1.F, which is at the same elevation as Figure 4.1.1.E, illustrates the growth of the final ice lens.

In these color enhanced images, the dark zone indicates unfrozen material while the light zone indicates the freezing and frozen zone. The bright white lines are visible ice lenses and the zone between the lowest ice lens and the top of the dark zone is the frozen fringe, whose brightness is between the frozen zone and unfrozen zone (Konrad 1980). The top of the unfrozen zone is the freezing front, approximately  $0^{\circ}\text{C}$  isotherm.

Several phenomena are illustrated in these images. At the beginning of freezing, fine and closely spaced ice lenses were formed (Figure 4.1.1.A and Figure

4.1.1.B). As the freezing time elapses, the individual ice lenses grow thicker and the distance between adjacent ice lenses increases while the frost penetration rate slows (Figure 4.1.1.C to Figure 4.1.1.E). The frost penetration stops when the final ice lens initiates. The freezing front remained at the same elevation during growth of the final ice lens until the test was stopped (Figure 4.1.1.F).



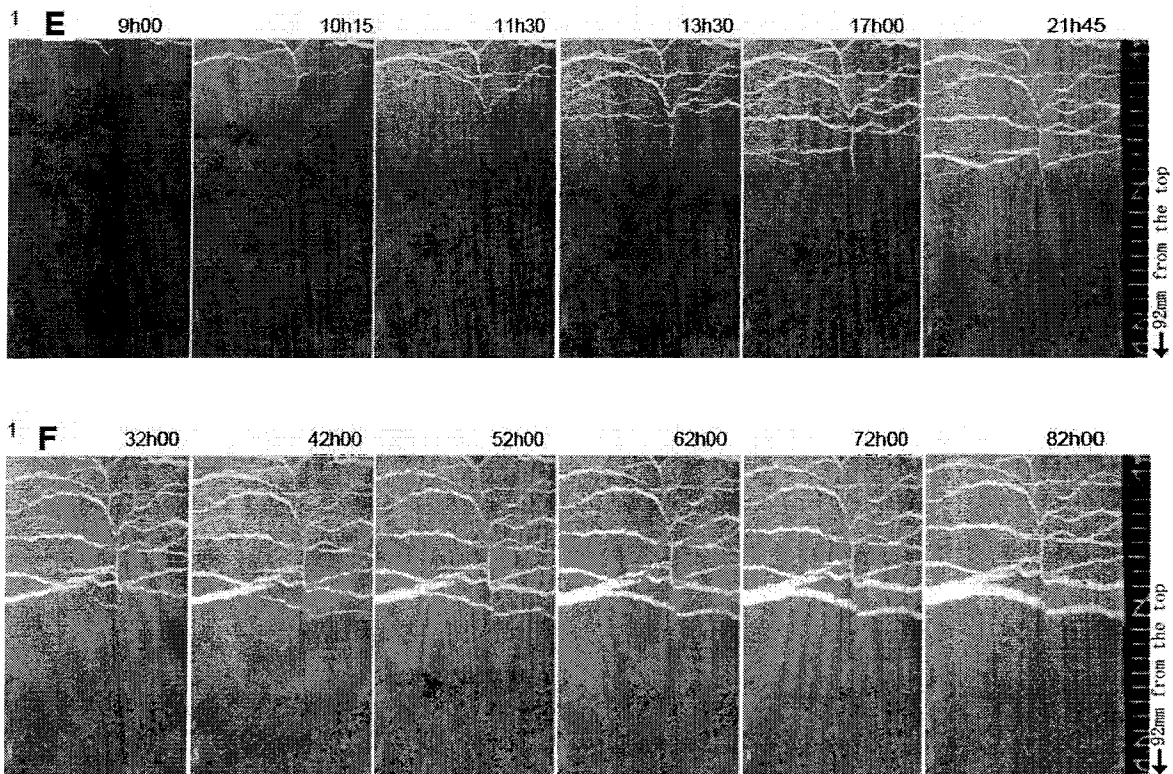


Figure 4.1.1 Serial images of the freezing process of test #1 (scale in millimeter).

Table 4.1.1 Image locations for Figure 4.1.1.

Row #	Distance for the top of the sample *	
	Top edge(mm)	Bottom edge (mm)
A	1	23
B	20	42
C	36	58
D	52	74
E	70	92
F	70	92

\* the top of the sample is the top of the sample after consolidation

#### **4.1.1 Frost penetration and frozen fringe development**

In Test #1, the frost penetrated into the soil sample at a fast rate at the beginning and then decreases. Figure 4.1.2 shows the frost penetration from the top of the sample at 122 mm. The elevation of the bottom is at 0 mm. The solid curve in Figure 4.1.2 represents the frost penetration. The steeper the slope, the faster the frost penetration. When the freezing process approached thermal steady state, the freezing front remained stationary within the sample. The position of the last ice lens was always above the elevation of the freezing front, and its location was congruent with the frost penetration. The distance between these two curves at a particular time represents the thickness of the frozen fringe, which grows thicker with time. Figure 4.1.3 shows the temperature profiles at different elapsed times during the freezing in test sample #1.

The frozen fringe thickness increased with time nearly linearly in the beginning (Figure 4.1.4) and varied with time, and the rate of growth of the average thickness decreases. The thickness of the frozen fringe also increased linearly with the frost penetration depth for the first 40 mm and then it varied during the next 40 mm of penetration (Figure 4.1.5).

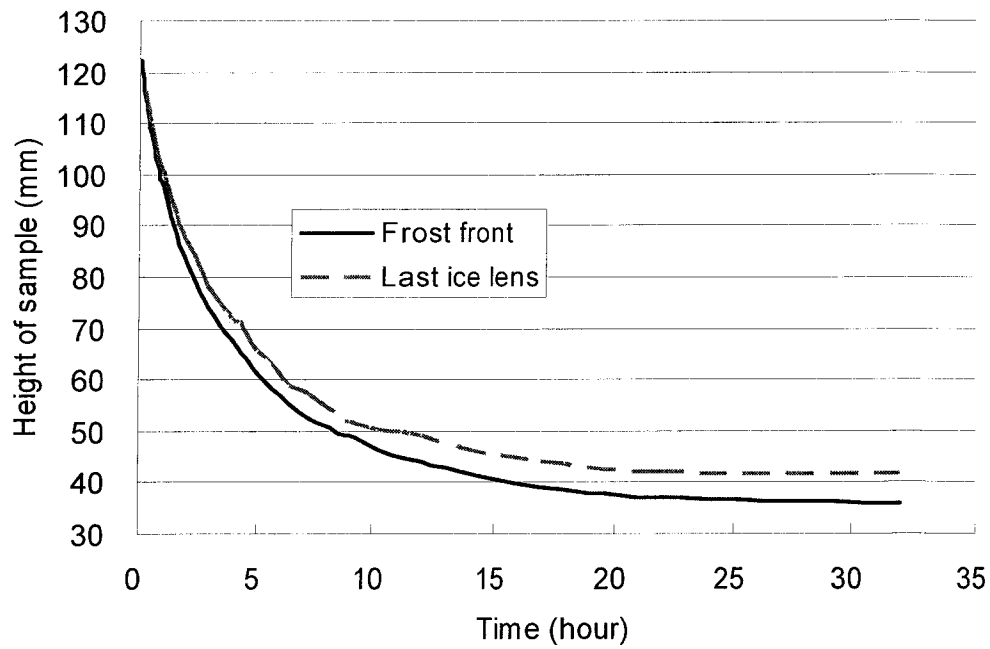


Figure 4.1.2 Frost penetration with time in test #1.

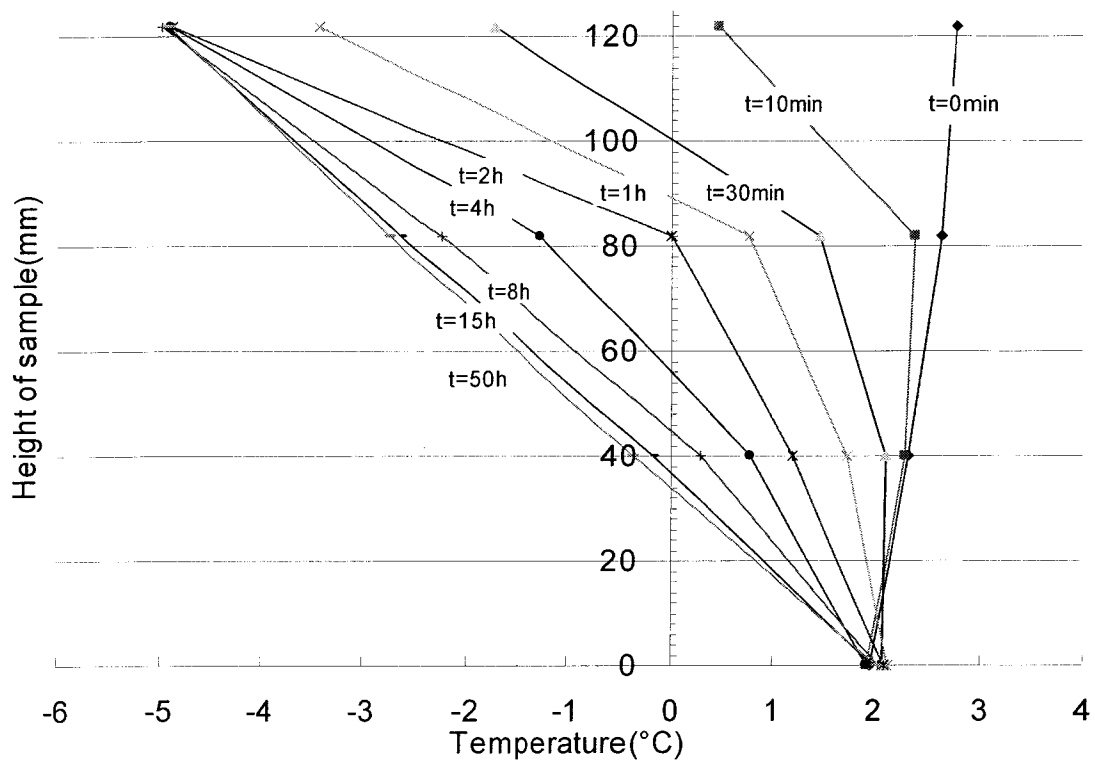


Figure 4.1.3 Temperature profiles at different time in test #1.

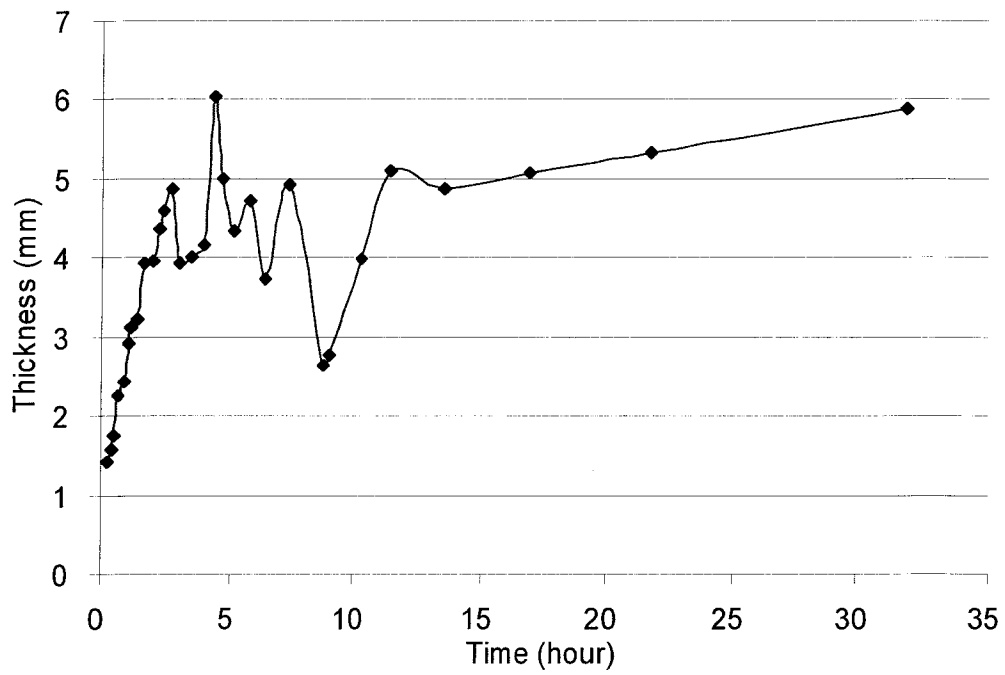


Figure 4.1.4 Frozen fringe thickness with time in test #1.

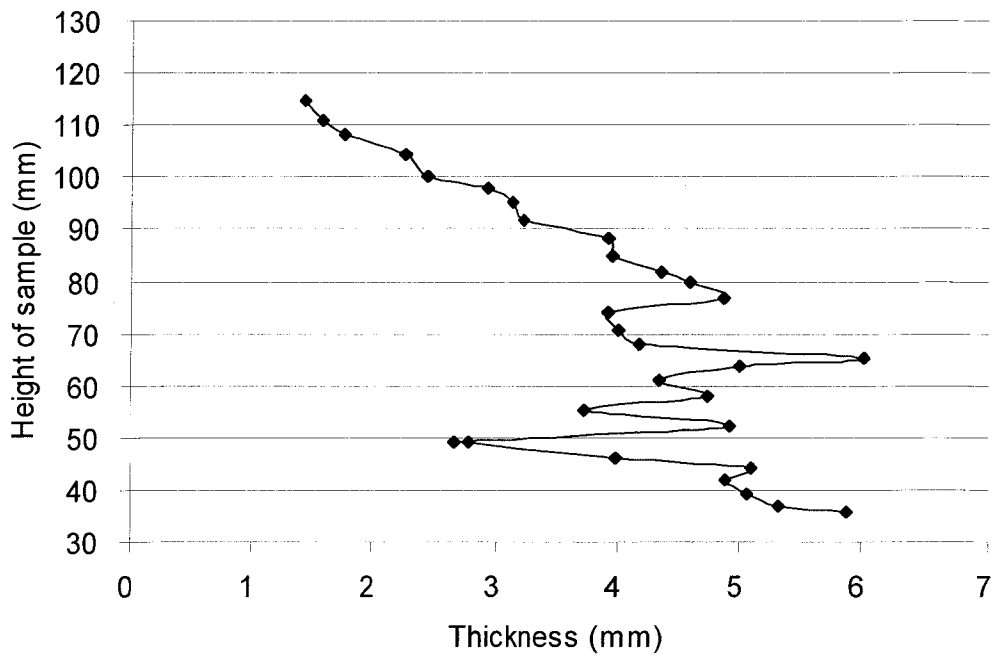


Figure 4.1.5 Frozen fringe thickness at different height of sample in test #1.

#### 4.1.2 Horizontal ice lens formation and development

During the initial and rapid freezing front advance, very fine and closely spaced ice lenses form as shown in Figure 4.1.1. With deeper frost penetration, the generated ice lenses became thicker and the distance between subsequent ice lenses increased until the final ice lens initiated at approximately 80 mm from the top after 21 hours of freezing (Figure 4.1.6). Then as the final ice lens continues to grow, the thermal steady state is reached. Figure 4.1.7 shows the growth of the final ice lens following its initiation after 21 hours in test #1. It can be seen that the ice lens grew faster at the beginning between 21 and 32 hours and then again after 63 hours. The thickness was measured using a caliper from the images taken by the digital camera during the test.

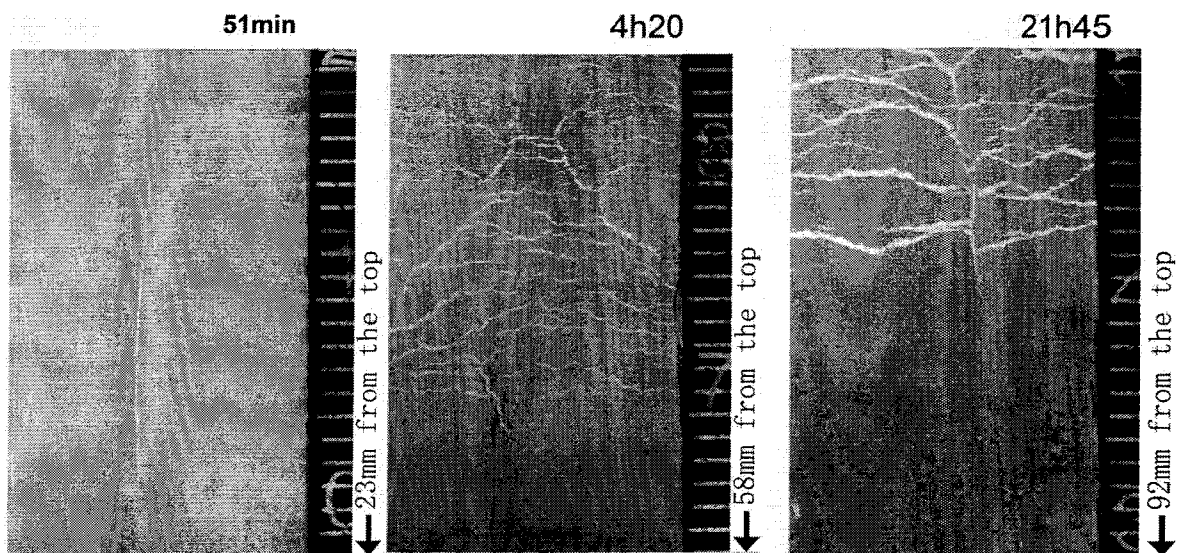
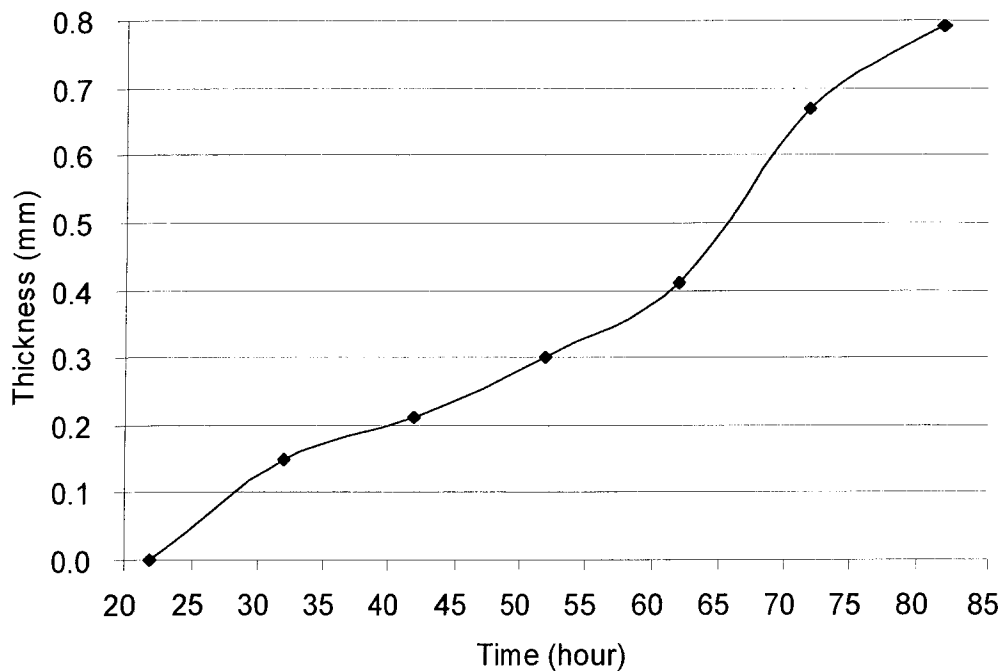


Figure 4.1.6 Horizontal ice lens at different depth of the sample in test #1



*Figure 4.1.7 Final ice lens growth in test #1.*

#### **4.1.3 Vertical ice lens formation**

The vertical ice lenses formed and developed as the horizontal ice lenses developed (Figure 4.1.1). The vertical ice lenses started to initiate and grow before the horizontal lenses at the given height. The vertical and horizontal ice lenses form a reticulate ice lens network with a polygonal shape. Figure 4.1.8 is an image of the sample cross section after the freezing. This shows the reticulate ice structure near the final ice lens within the frozen fringe. The image on the left is the frozen portion and on the right is the unfrozen portion.

#### **4.1.4 Heave and water intake**

During the freezing process, water migration into the sample occurs to feed the formation and growth of the ice lenses. Figure 4.1.9 shows the water migration, where the negative values indicate that water was expelled from the sample. Frost heave occurs when water is drawn into the sample after about 48 hours

(Figure 4.1.10). During the first 36 hours of freezing, water was continually expelled from the sample and no heave occurred. The water then started to be drawn into the sample at 36 hours of freezing and continuous heave was measured after 48 hours until the end of the test.

#### **4.1.5 Water migration within frozen zone**

Water migration within the frozen zone was observed in these investigations. For instance, in test #1, after the final ice lens was formed, the ice lens above it, emphasized by the (red) arrows in Figure 4.1.11, continued to grow with a measurable rate. This implies that additional water migration occurs even between ice lenses that have no access to the water from the unfrozen zone.

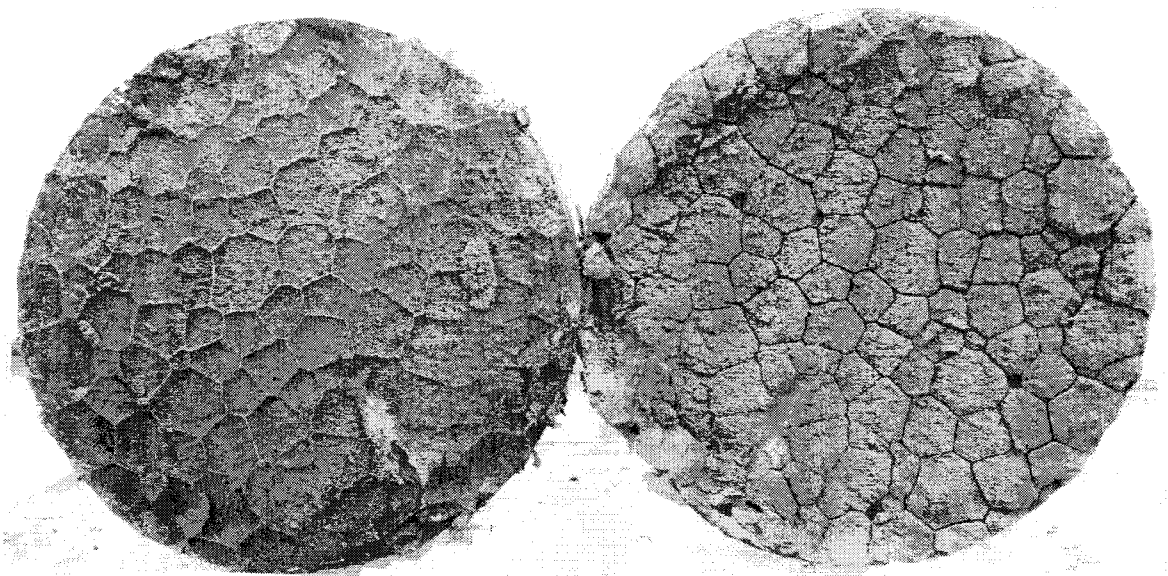


*Figure 4.1.8 Reticulate ice structure (the diameter of the sample is about 100 mm).*

Waterintake of test #1

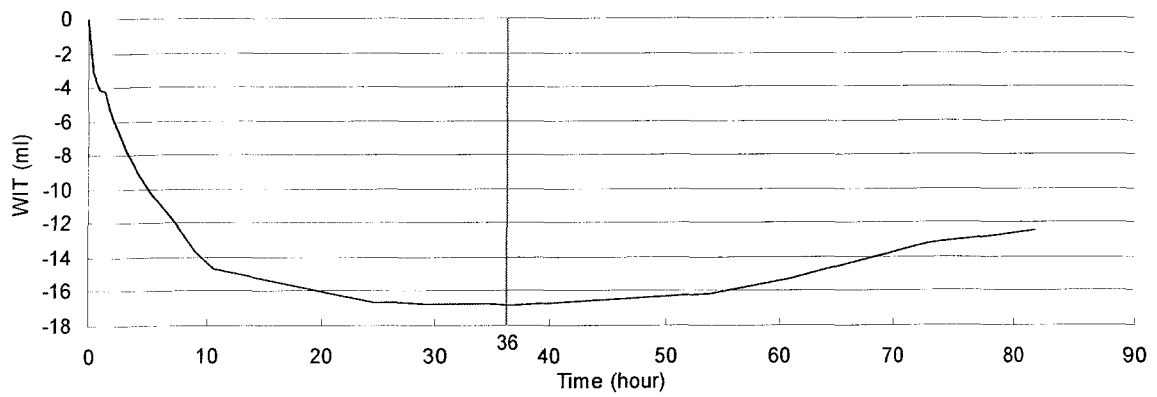


Figure 4.1.9 Water-intake (WIT) during freezing in test #1.

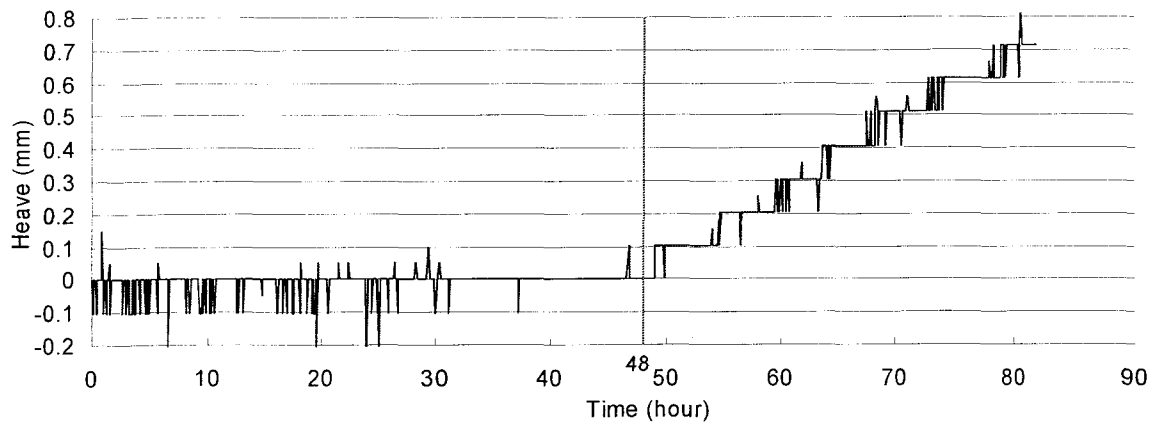


Figure 4.1.10 Heave of the top of the sample during freezing in test #1.

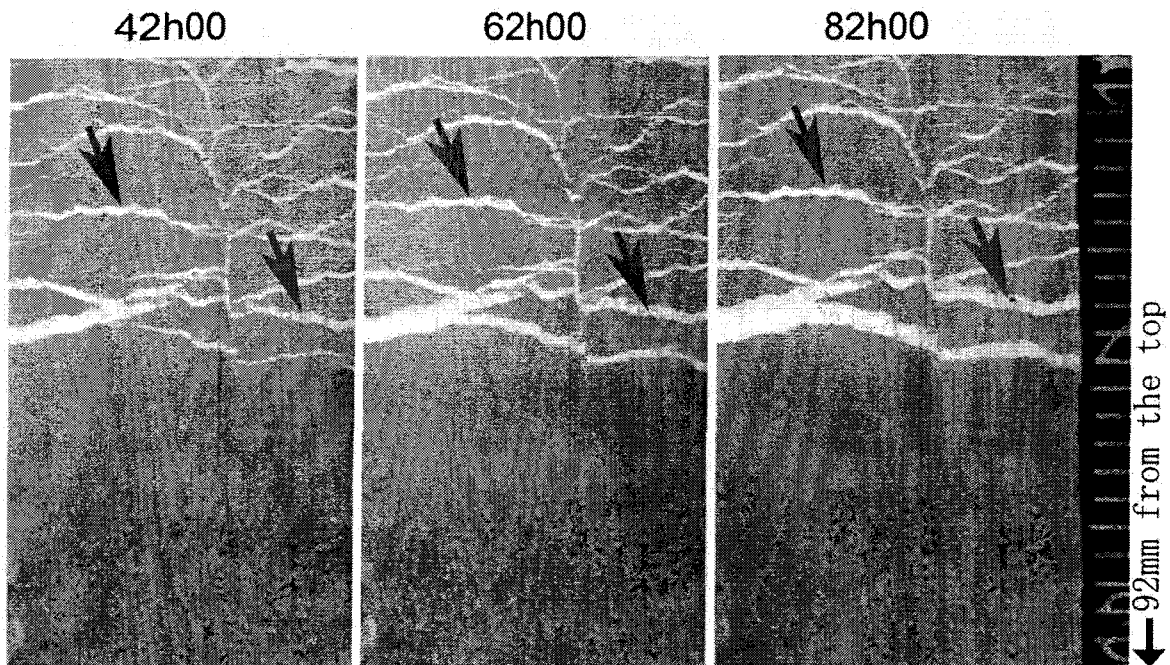


Figure 4.1.11 Thickness increasing of the ice lens above the final one in test #1.

#### 4.1.6 Moisture content (MC) redistribution

The water migration during freezing changes the initial moisture content distribution. Figure 4.1.12 shows the moisture content profile both before and after the test. The vertical straight line is the moisture content following consolidation but before freezing, and the jagged line illustrates the moisture content of the sample after the freezing test. The final ice lens was at 41 mm to 43 mm from the bottom of the sample. Because both soil and ice lenses in the frozen part were sampled for the actual moisture content measurement, the value of moisture content in the frozen zone included the water from the ice lenses. This indicates the soil between the ice lenses has actually lower moisture content than the value presented in Figure 4.1.12.

In general, the frozen zone has higher moisture content while the unfrozen zone has lower moisture content than at the start of freezing. The maximum moisture content value was recorded at the elevation of the final ice lens, and the minimum value was below this final ice lens. In the frozen zone, the moisture content decreases with distance above the final ice lens and tends towards the initial value. In the unfrozen zone, the moisture content is less than the initial value and gradually increases with distance from the final ice lens.

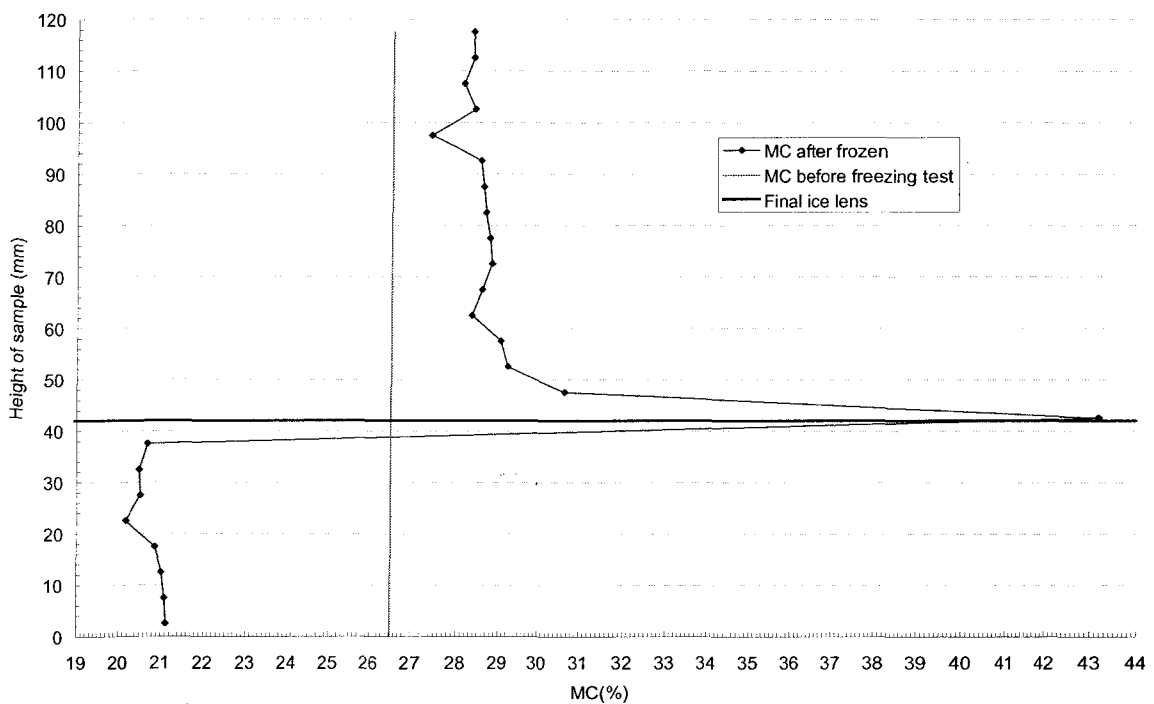


Figure 4.1.12 Moisture content (MC) profile in test #1.

#### 4.1.7 Water balance calculation

Two methods were used to analyze the water migration within the sample in these investigations. One was calculating the difference of the total mass of water in the sample before and after freezing based on the moisture content profile. The total mass of water in the sample was calculated using Equation [4.1.1]. The other

method was based on a direct measurement of the water intake during freezing (section 4.1.4). The comparison of the water mass from these two methods indicates the accuracy of determinations. The closer the two values, the more accurate the moisture content determination.

$$M_w = \sum_i \frac{MC_i G_s \rho_w A H_i}{(1 + MC_i G_s)} \quad [4.1.1]$$

Where  $M_w$ : the total mass of water in the sample (kg);

$MC_i$ : Moisture content of the section  $i$ ;

$G_s$ : Specific gravity of the soil;

$\rho_w$ : The density of water (1000kg/m<sup>3</sup>);

$A$ : The area of the cross section of the sample  
i.e. the freezing cell (m<sup>2</sup>);

$H_i$ : The thickness of the section  $i$  (m).

After each test, the water balance was calculated. The results from all 12 tests performed are listed in Table 4.1.2. It should be noted that only for test #9 was the whole cross section used for the moisture content (MC) determination. Approximately one quarter of each section of the sample was used for the MC determination for the other tests.

The results will be discussed in following section.

*Table 4.1.2 Water balance calculation.*

Test #	Water migration (g)		Test #	Water migration(g)	
	Calculated from MC of sample	Measured directly		Calculated from MC of sample	Measured directly
1	-10.9	-12.5	7	-1.2	-1.6
2	29.1	29.1	8	5.2	-1.4
3	18.6	18.2	9	32.7	28.2
4	-13.0	-14.4	10	-12.2	-16.3
5	-14.9	-13.4	11	-6.7	-11.5
6	-8.2	-7.9	12	9.9	18.1

Note:

1. MC: Moisture content
2. Negative value means water expelled from the soil sample during freezing.

#### **4.1.8 Discussion**

Freezing saturated fine-grained Devon silt results in not all the in-situ water changing phase at a unique temperature. In Figure 4.1.1, the digital images show that some unfrozen water exists in the frozen fringe which is colder than the low contamination water phase change temperature (0°C). In this study, the color within the images has an important role to indicate the existence of unfrozen water as described in Chapter 3. The frozen fringe was lighter in color than the unfrozen zone but darker than the frozen zone. This shows that unfrozen water and ice co-exist in this fringe. The temperature within the frozen fringe decreases upward in the sample. At a higher level the temperature is lower since the frost penetrated into the soil from the top. This is supported by the changing temperature profiles throughout the freezing test (Figure 4.1.3). Therefore, the unfrozen water at different elevations in the frozen fringe varies with the temperature. This interconnected unfrozen water provides paths for the water migration from the unfrozen zone to the active ice lens, nearest to the frozen fringe. It can also be seen in Figure 4.1.1 and Figure 4.1.2 that the warmest ice

lens is always located at the position colder than the freezing front ( $0^{\circ}\text{C}$ ). This implies that the warmest ice lens initiates at the segregation-freezing temperature, which is colder than  $0^{\circ}\text{C}$ .

The frost penetration into the soil sample is controlled by the boundary temperature conditions. The freezing front penetrates into the sample rapidly at the beginning of the test because the heat extraction from the unfrozen soil is high under the high gradient (Figure 4.1.1, Figure 4.1.2). Comparing the images (Figure 4.1.1) to the temperature profile (Figure 4.1.3), allows determination of the freezing front ( $0^{\circ}\text{C}$  isotherm). Note that it is not strictly correct to connect temperature points via a straight line when comparing Figure 4.1.3 to the images in Figure 4.1.1. The temperature profile below the top plate whose temperature is maintained constant, appears to be bilinear with the higher gradient in the frozen zone compared to the unfrozen zone.

The thickness of the frozen fringe changes with frost penetration into the sample. This phenomenon implies that the temperature of the warmest ice lens is not constant. The results shows this temperature varies between  $-0.04^{\circ}\text{C}$  and  $-0.54^{\circ}\text{C}$  (Figure 4.1.13) in this freezing test. The temperature of the top plate was reduced from  $2^{\circ}\text{C}$  to  $-5^{\circ}\text{C}$  during the first 2 hours of the freezing test and then remained at  $-5^{\circ}\text{C}$  afterwards as the frost penetrated from a height of 122 mm, to 82 mm (Figure 4.1.3). This temperature decrease of the top plate caused an increase in the cooling rate at the freezing front during the first 40 minutes. Then the cooling rate decreased. Figure 4.1.13 shows the relationship between the temperature of the warmest ice lens and cooling rate at the freezing front. For most conditions, the temperature of the warmest ice lens increases with a decrease in the cooling rate at the freezing front.

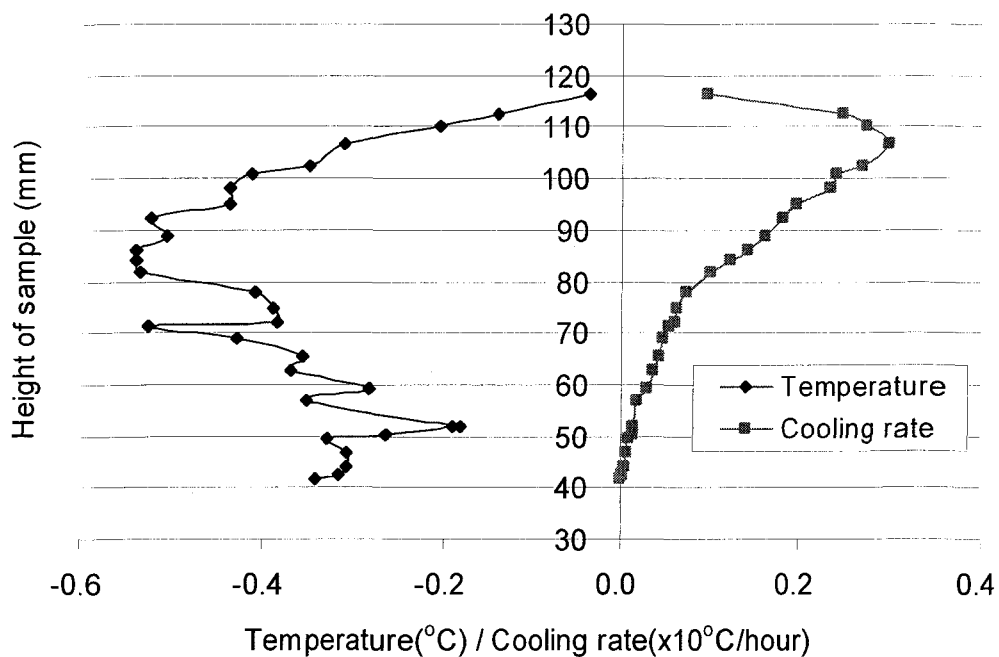


Figure 4.1.13 The temperature of the warmest ice lens (left) compared to the cooling rate of the freezing front (right) at different height of sample in test #1.

In this test, ice lenses oriented normal to the temperature gradient formed while the frost penetrated into the sample. Due to the initial rapid change in the temperature across the sample, some fine and closely spaced ice lenses formed. The subsequent lenses were thicker and further apart. The thickness of each ice lens, except for the final one, was only a few tenths of millimeter or even less whereas the final one grew to approximately 1 mm until the test was stopped. This implies that the frost heave is primarily induced by growth of the final ice lens. The final ice lens grew at a high rate initially, then decreased (Figure 4.1.7), and this observation was confirmed in the other freezing tests. This may result from the consolidation induced in the unfrozen soil by the suction generated as ice lenses form.

Three theories, have been advanced to explain the origin of the reticulate ice

veins observed in permafrost as discussed in Chapter 2. Vertical ice formation and development observed in these tests support Popov's theory (1967) for initiation of the vertical ice lens. In these tests, the vertical ice lenses formed before the warmest horizontal lens at a given elevation, in other words, the vertical ice lens initiated within the frozen fringe not above it. This is evidence that the soil in the unfrozen zone close to the frozen fringe shrinks to form cracks and these small vertical cracks filled with water drawn to the active horizontal ice lens. There was no evidence to support the growth of thick ice veins of tens of centimeters during these short-term tests.

In this open freezing system, the water can be expelled to and drawn from a reservoir connected to the base of the freezing cell. Heave occurred at approximately 48 hours after the start of the freezing and the final ice lens initiated after 34 hours (Figure 4.1.10 and Figure 4.1.1). The delay of frost heave was assumed to be caused by friction between the frozen soil and the inside of the cell wall. The heave started when the uplift pressure overcame this friction. This friction will be discussed later in this section and more discussion about heave and water intake will be pursued in sections 4.2.5, to 4.4.5.

Currently, it is thought that once an ice lens is formed over the whole area of a specimen, it cuts off water migration to the frozen soil above (Hoekstra 1969, Mageau and Morgenstern 1979). Therefore, at the base of the warmest ice lens, water flow is stopped and the conditions above are essentially static. It was observed in this test program, that after the final ice lens formed, the ice lenses above it within the frozen zone continued to grow throughout the test (Figure 4.1.6). The formation of the final ice lens in the sample did cut off water migration from the unfrozen zone. Therefore the growth of the ice lenses above the final one must have a different water sources. In other words, there must have been water

migration even within the frozen zone.

There are two possible water sources for this extra water migration. One, the water might be from the final ice lens melting at its top. It was noticed that temperature fluctuation exists during the thermal steady state, which was caused by the changes of room temperature with the defrost cycle (Figure A.1 in Appendix A). The images of test #1 (Figure 4.1.1) shows that even though the freezing front has some fluctuation, it was always lower than the final ice lens. This indicates that the temperature of the final ice lens was therefore always colder than the freezing point of pore water ( $0^{\circ}\text{C}$ ) during the freezing. It is unlikely the segregated ice thawed since its temperature remained below the freezing point. However, the ice on the upper side of the final ice lens may change phase due to suction, but no evidence was found to support such a large suction existing on the upper side of the final ice lens.

The second possible source for this extra water migration might be from the soil between two ice lenses. As commonly accepted, unfrozen water exists in frozen soils (e.g. Anderson and Tice 1972). The unfrozen water is presumed to coexist with ice in the pore space as thin films of adsorbed water and as capillary water that lies outside the adsorption forces but fails to freeze because it occupies spaces too narrow to be penetrated by a curved ice water interface (Konrad 1994, Rempel et. al. 2001). This unfrozen water content decreases with decreasing temperature of the soil (Figure 4.1.14). This decrease of unfrozen water content causes a slower ice lens growth rate in the frozen zone (Figure 4.1.15) since the hydraulic conductivity of the soil is much reduced as soil freezes. Furthermore, the water supply changes to a closed from an open-system due to the cut-off of the final ice lens. This change can further reduce the rate of the ice lens growth in the frozen zone. In this test, the temperature fluctuation also influenced this

phenomenon by melting the film water and capillary water in the soil located between two ice lenses, especially the final one and the above it, because this water freezes at the temperature colder than the freezing point ( $0^{\circ}\text{C}$ ) (Jumikis, 1966). Therefore, when the temperature of this zone increases, the ice in the soil between two ice lenses may melt even though its temperature is still colder than  $0^{\circ}\text{C}$ .

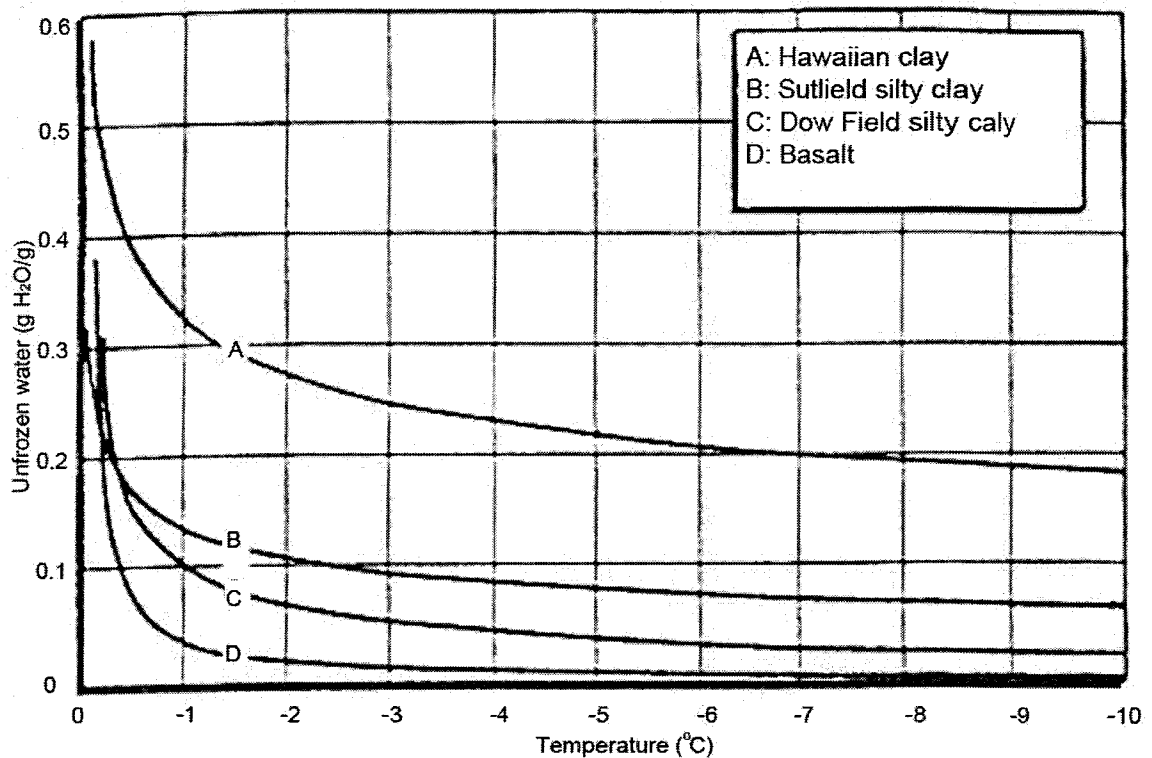


Figure 4.1.14 Typical unfrozen water contents (after Anderson and Tice 1972).

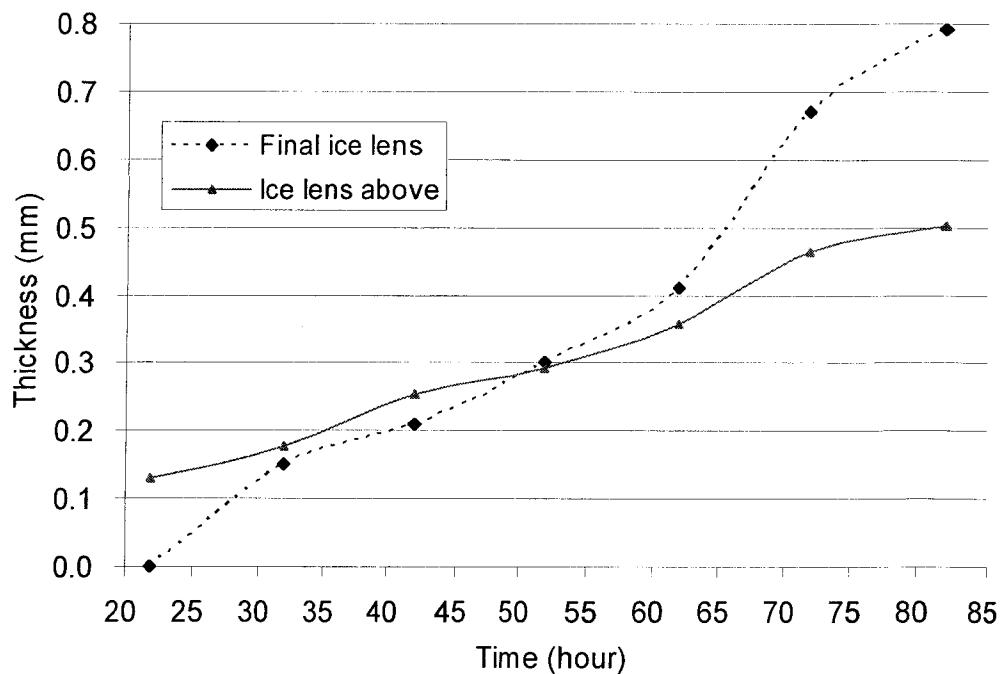


Figure 4.1.15 The growth of the ice lens right above the final one in test #1.

Water content redistribution occurs throughout the freezing test due to the moisture migration while the soil freezes under a temperature gradient. The water was attracted from the unfrozen zone to ice lenses during freezing in this open system. This induced an increase of moisture content throughout the frozen zone that contains many thin ice lenses. At the beginning of the freezing test, the frost penetration was rapid producing a few fine ice lenses. This behavior is confirmed by the moisture content profile. In Figure 4.1.12, the moisture content tends to be closed to the initial value in the frozen zone near the top of the sample. The exception shown by the top two data is assumed to be affected by non-uniform boundary conditions associated with consolidation before freezing was started. The maximum moisture content was at the location of the thick final ice lens. In the unfrozen zone, the moisture contents are always lower than the initial. It tends towards the initial value with distance from the final ice lens. Two processes are thought to cause the decrease in the moisture content in the unfrozen zone. The

first is the suction generated by the temperature gradient in the soil. This suction draws the water up towards the ice lenses and it also consolidates the unfrozen soil. The second is the friction between the inside of the cell wall and the sample, especially in the frozen zone. Water expands by about 9% in volume when it changes phase from a liquid to a solid. This expansion generally induces heave of the soil sample in fine grained soils. Furthermore, the segregated ice lenses should have contributed to the frost heave. However, in this test there was no heave and the water was expelled from the sample until the final ice lens formed. Considering the test equipment, the friction between the inside of the cell wall and the sample may limit the heave. The increase in volume due to freezing of the water and segregated ice lenses push the unfrozen soil down causing further consolidation. The increased positive pore stress induced by the volume expulsion is rapidly dispersed due to the high permeability and small size of the sample in this open system. This is verified by the expelling of the water from the sample observe during the first period of the freezing.

Water balance calculations were performed using two methods, described in 4.1.7, to determine the water migration between the sample and the water supply. There are some differences in the amounts of water migration determined by the two methods in each test (Table 4.1.3). Tests #1 to #6 had non-saline pore water. It can be seen in the images of each test, which will be discussed later in this chapter (Figure 4.1.1, 4.2.1, 4.2.2, 4.3.1, 4.3.2 and 4.3.3), that the ice lenses are more continuous compared to freezing tests, #7 to #12 (Figure 4.4.1 to 4.4.4). The difference in water balance calculation was small in the non-saline freezing tests even though only a part of each section was used for the moisture content test. The ice lenses were relatively well distributed in the section, whereas in the saline freezing tests, the ice lenses were heterogeneous in their distribution. This

caused the large differences in water balance calculation due to moisture content tests which only sampled a part of the section of the sample except for test #9 where the whole section was sampled to determine the moisture content at a particular location.

The water balance calculations show that the measurement of both moisture content and water intake in these laboratory tests can be used to explain the water redistribution within a sample as it freezes.

*Table 4.1.3 The difference of water amount in water balance calculation.*

Test#	Difference (%) (calculated – measured) /measured	Test#	Difference (%) (calculated – measured) /measured
1	12.7	7	26.1
2	0.0	8	460.3
3	2.2	9	15.8
4	9.7	10	25.4
5	10.9	11	41.7
6	3.3	12	45.3

## 4.2 Effects of temperature gradient (Cooling rate)

In this section, the results of tests #1, #2 and #3 are discussed to demonstrate the effect of the temperature gradient on the freezing process of Devon silt. Figure 4.2.1 and Figure 4.2.2 provide a series of selected images to show the freezing processes of tests #2 and #3, respectively. Table 4.2.1 and Table 4.2.2 summarize the locations of each row of pictures in the two separate freezing tests. The images of test #1 were previously presented in Figure 4.1.1.

Figure 4.2.1 A through C show the development of ice lenses during the transient state of freezing, and from image 19h30 to image 66h02 the development of the final ice lens in test #2 is presented. Figure 4.2.2 A through F show the development of ice lenses during the transient state of freezing for test #3, and the image beginning at 10h11 to image 191h5 show the development of final ice lens.

*Table 4.2.1 Image locations for Figure 4.2.1.*

Row #	Distance for the top of the sample*	
	Top edge (mm)	Bottom edge (mm)
A	2	24
B	20	42
C	27	49
D	27	49
* the top of the sample is the top of the sample after consolidation		

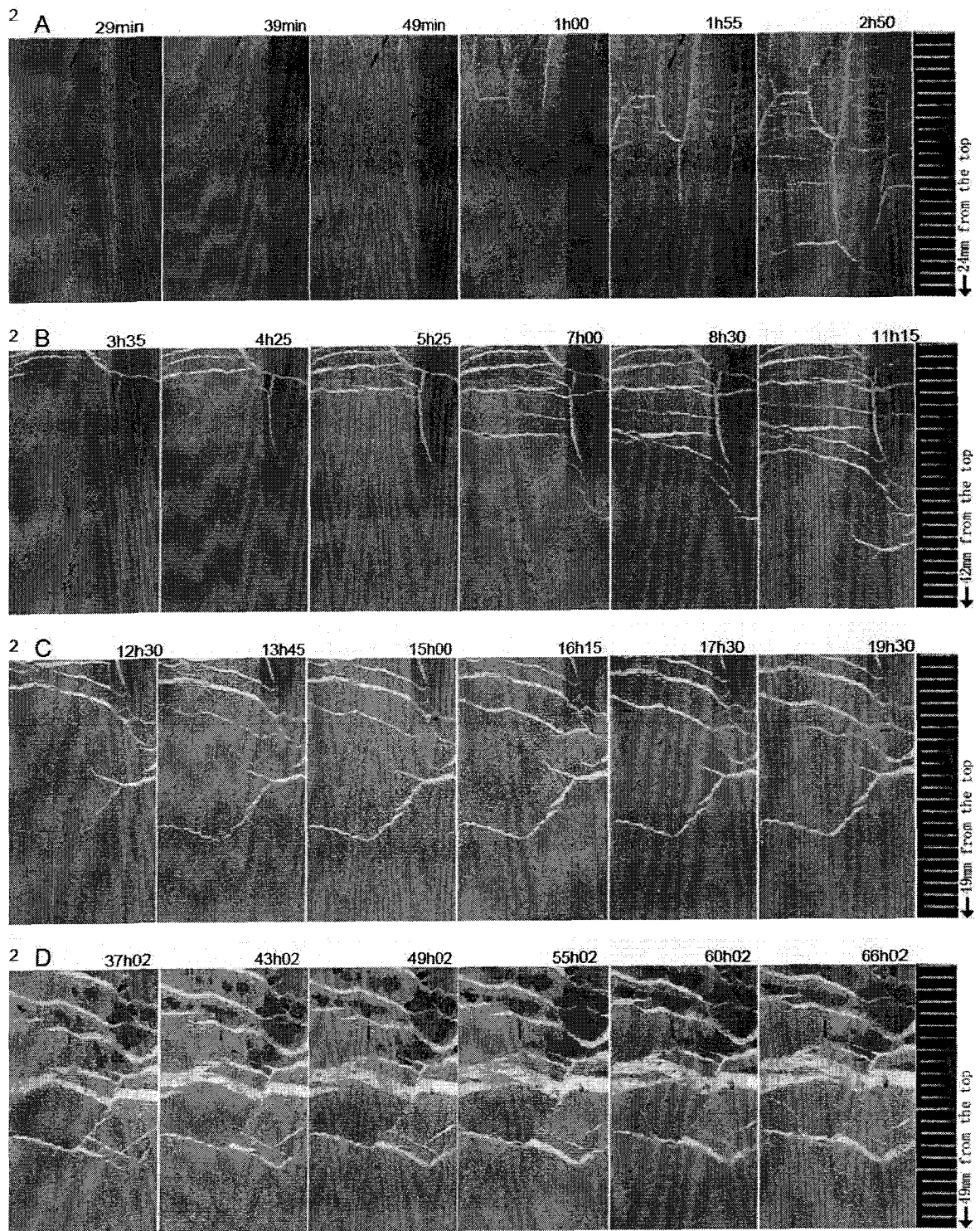
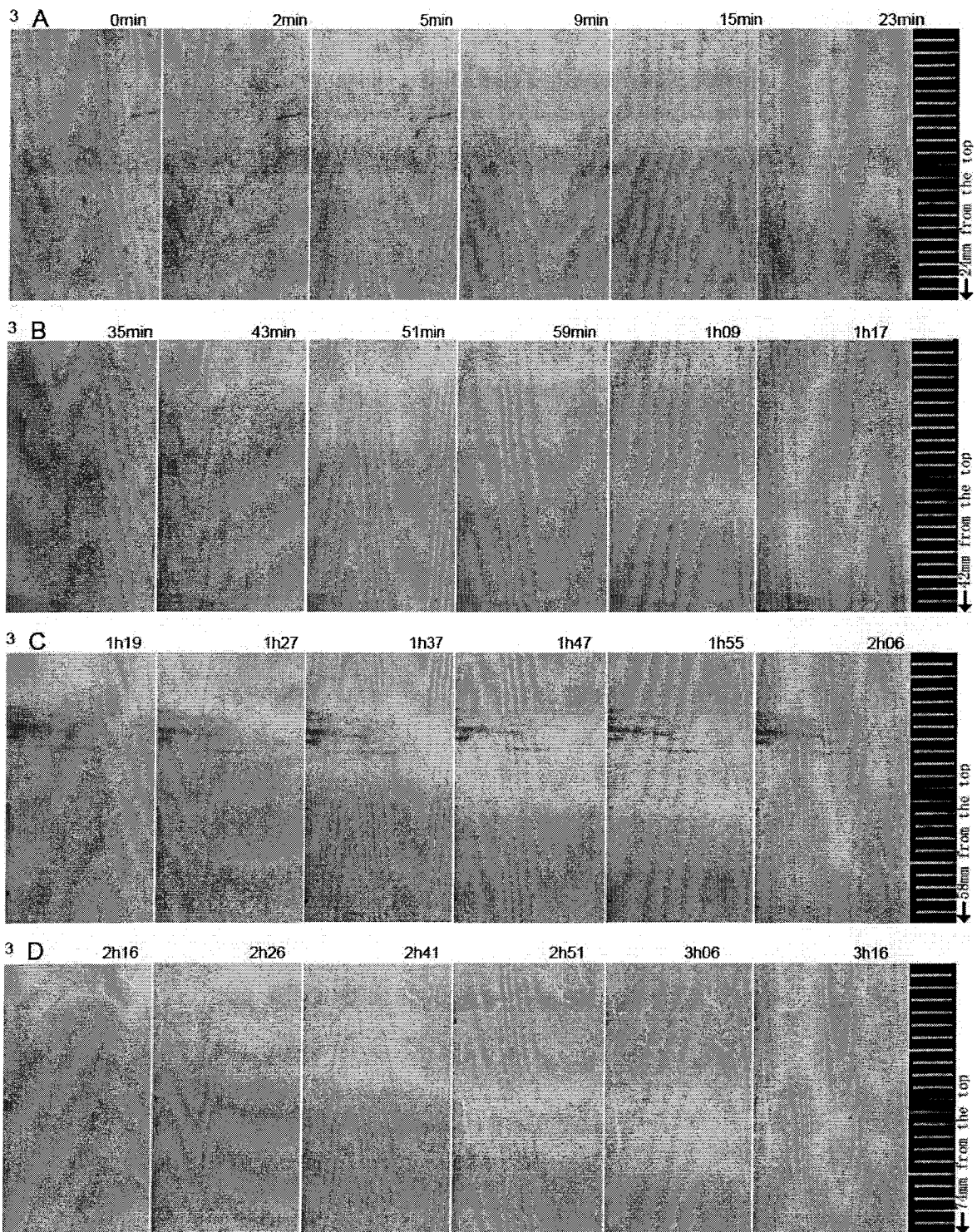


Figure 4.2.1 Serial images of the freezing process of test #2 (scale in millimeter).



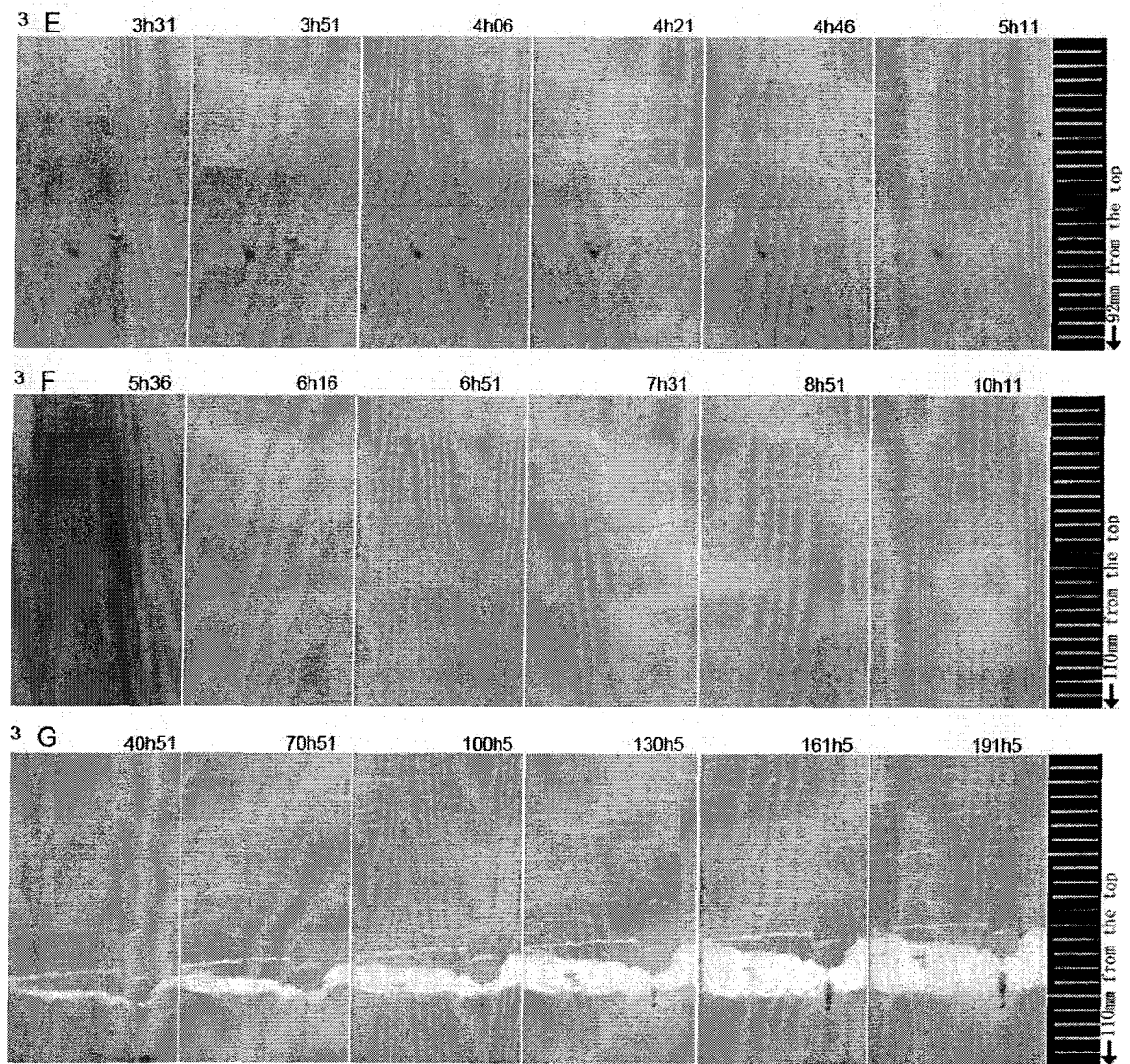


Figure 4.2.2 Serial images of the freezing process of test #3 (scale in millimeter).

Table 4.2.2 Image locations for Figure 4.2.2.

Row #	Distance for the top of the sample*	
	Top edge(mm)	Bottom edge(mm)
A	2	24
B	20	42
C	36	58
D	52	74
E	70	92
F	88	110
G	88	110

\* the top of the sample is the top of the sample after consolidation

#### 4.2.1 Frost penetration and frozen fringe

The frost penetration rate is related to the temperature gradient, which controls the cooling rate of the frozen fringe. The three tests discussed in this section have the same temperature at the bottom plate, 2°C and the other test conditions are summarized in Table 3.1. The top plate temperatures are -2°C, -5°C, and -15°C for test #2, test #1 and test #3, respectively. With the similar total height of the soil sample, test #3 had the largest temperature gradient while test #2 the smallest in the thermal steady state. Consequently, the temperature gradient in the frozen zone of test # 3 was the greatest, and in test #2 the smallest during transient freezing, when the freezing front was located at similar depths within the sample. Figure 4.2.3 shows that test #3 had the fastest frost penetration rate compared to test #2 with the slowest.

The frozen fringe changes its thickness with temperature gradient. Figure 4.2.4 illustrates the thickness changes of the frozen fringe with time and Figure 4.2.5 illustrates the changes at different locations within each sample of tests #1, #2 and #3. For similar time after start of freezing, test #3 had the smallest frozen fringe whereas test #2 had the largest (Figure 4.2.4). At the same location within

each sample, test #3 has the smallest frozen fringe with the greatest temperature gradient whereas test #2 has the largest frozen fringe associated with the lowest temperature gradient (Figure 4.2.5).

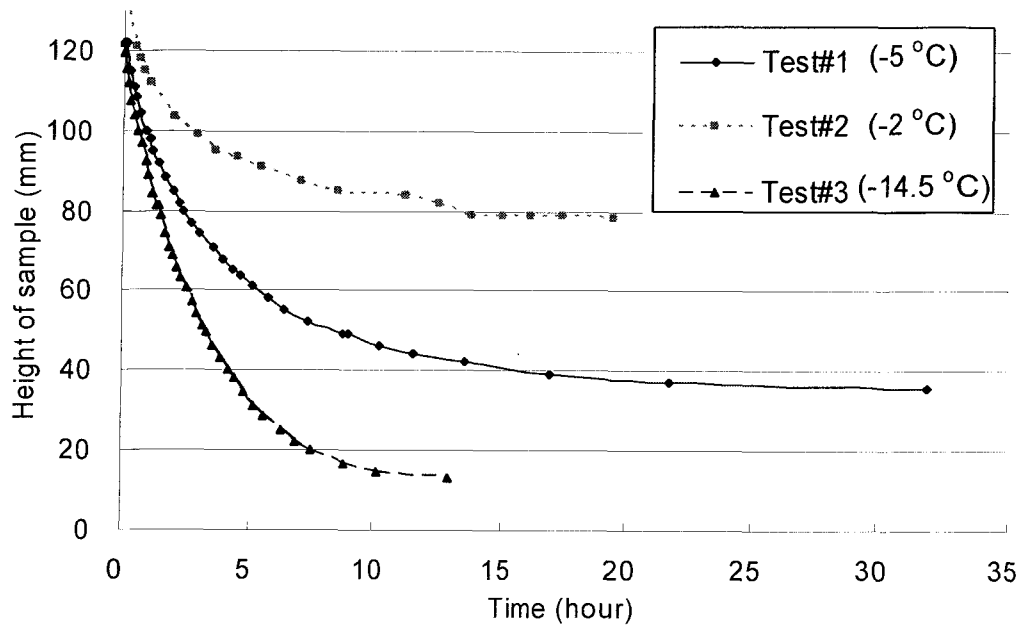


Figure 4.2.3 Frost penetration (freezing front) under different temperature gradients.

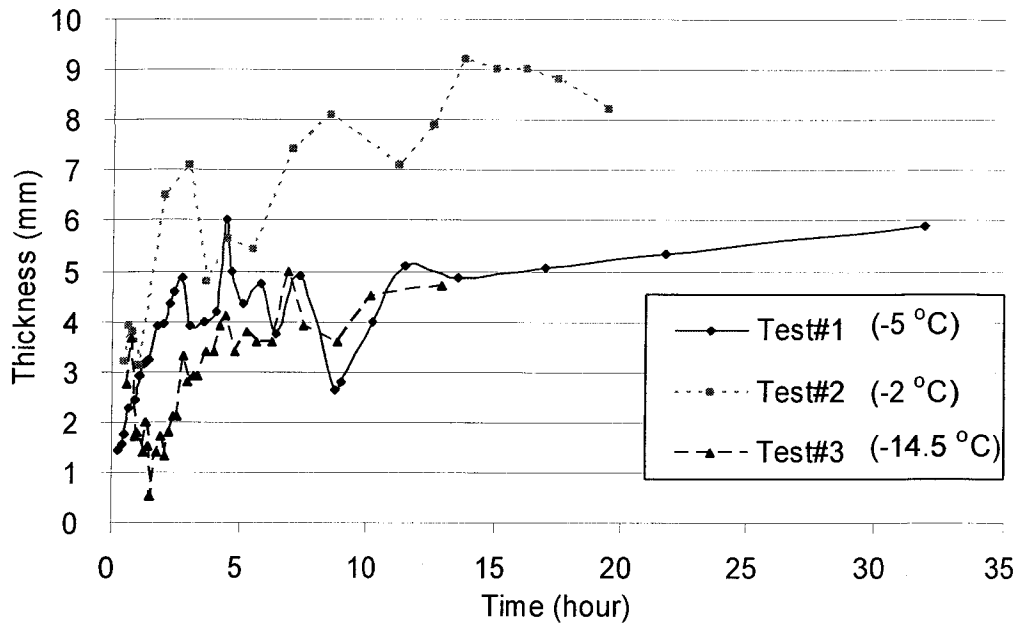


Figure 4.2.4 Frozen fringe thickness changes with time under different temperature gradients.

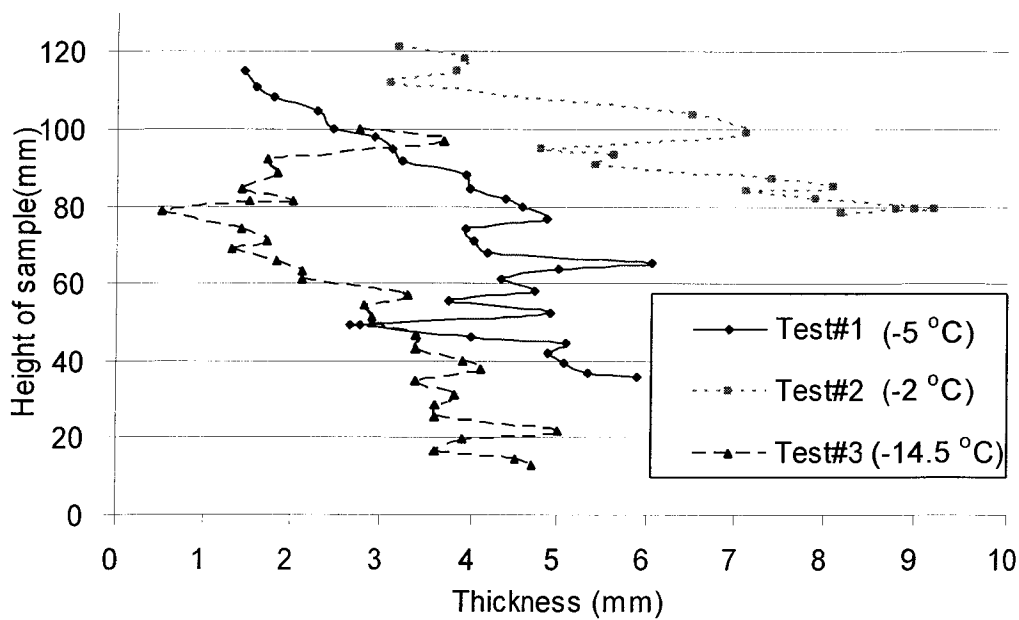


Figure 4.2.5 Frozen fringe thickness along the height of the sample in tests #1, #2 and #3.

#### 4.2.2 Horizontal ice lens formation and growth

Figure 4.1.1, Figure 4.2.1 and Figure 4.2.2 illustrate via digital images the formation and development of the horizontal ice lenses during both transient and steady state freezing under different boundary temperature conditions as summarized in Table 3.1. Figure 4.2.1 shows that visible ice lenses formed at the beginning of the freezing in test #2 with the lowest boundary temperature gradient of  $0.033^{\circ}\text{C}/\text{mm}$ . In test #3, with the highest boundary temperature gradient of  $0.139^{\circ}\text{C}/\text{mm}$  (4 times of test #2), it was difficult to observe ice lenses above a frost penetration depth of about 20 mm (Figure 4.2.2). The observed ice lenses were fine and closely spaced even as the final ice lens was approached. Test #1 had a temperature gradient condition of  $0.057^{\circ}\text{C}/\text{mm}$ , between that of test #2 and test #3. It shows features of ice lenses initiation and development just between tests #2 and #3 at the beginning. Some visible ice lenses formed, but they were finer than the ice lenses at the same height in test #2. As frost penetrated deeper into the sample, thicker ice lenses developed and the distance between two ice lenses increased until the initiation of the final ice lens within the sample.

Figures 4.1.1, 4.2.1 and 4.2.2 show the location of the final ice lens was at 80 mm from the top of the sample in test #1, 36 mm in test #2, and 104 mm in test #3. Figure 4.2.6 presents the growth of the final ice lens thickness with time. Test #3 was frozen for a longer time than test #1, and test #2. The data shown in Figure 4.2.6 were directly measured from the images in certain time interval after the final ice lens initiated in each test. The average rate of final ice lens growth in test #1 was  $0.013\text{ mm}/\text{hour}$ . The average rates of the final ice lens growth in tests #2 and #3 were  $0.032\text{ mm}/\text{hour}$  and  $0.022\text{ mm}/\text{hour}$ , respectively.

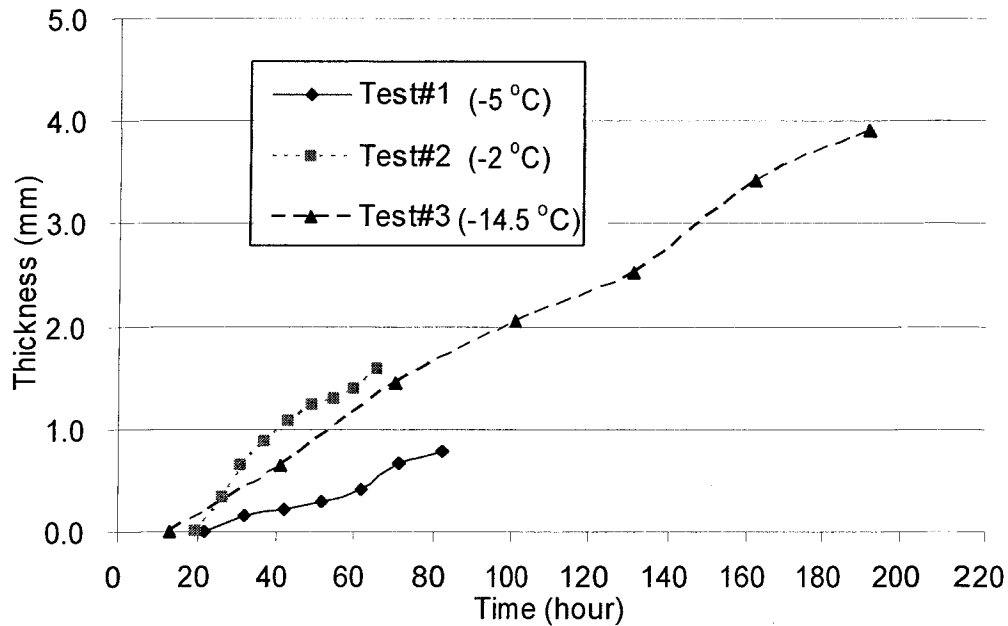


Figure 4.2.6 Final ice lens growth under different temperature gradient.

#### 4.2.3 Heave and water intake

In test #2, heave started almost immediately after the start of the freezing. Water was expelled from the sample during the first 2 hours and then was drawn into the sample. Both sample heave and water intake continued until the end of the test (Figure 4.2.7 and Figure 4.2.8). In test #3, no heave was monitored during the first 10 hours after the start of freezing. Water was expelled from the soil sample for the first 7 hours and then the water was drawn into the sample. Both heave and water intake took place until the end of the test. The heave and water intake results of test #1 were presented in section 4.1

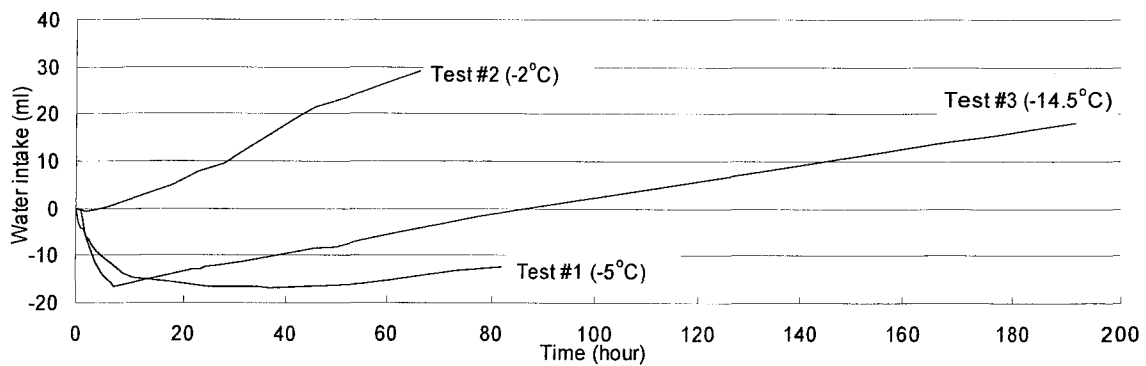


Figure 4.2.7 Water intake in tests #1, #2 and #3.

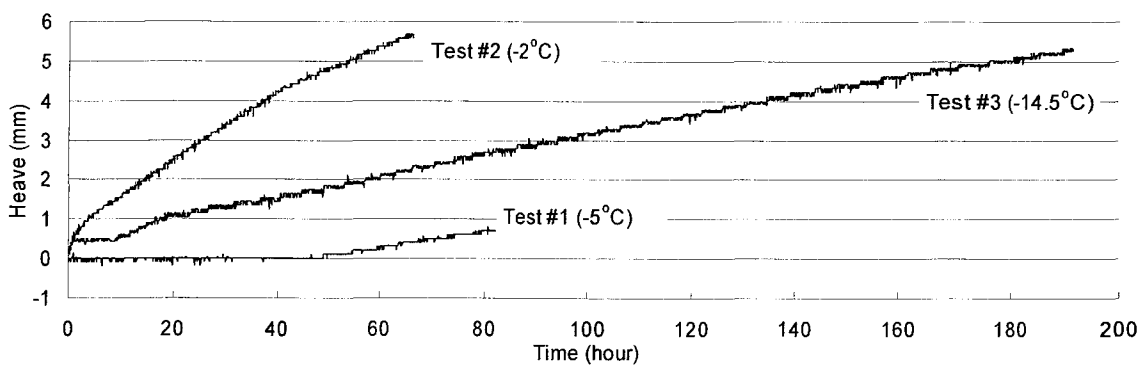


Figure 4.2.8 Frost heave in tests #1, #2 and #3.

#### 4.2.4 Moisture content redistribution

The moisture was redistributed within the sample during the freezing in all tests. The moisture content profile in each test can be compared in Figure 4.2.9. The moisture contents following freezing were normalized to the initial moisture content ( $MC_0$ ). The maximum moisture content occurs at the location of final ice lens within each sample. After freezing, test #2 had the greatest moisture content ratio whereas test #3 had the lowest within the frozen zone. In the unfrozen zone the moisture content ratio of test #2 was closest to the initial moisture content while in the other tests the moisture content in the unfrozen zone was lower than the initial.

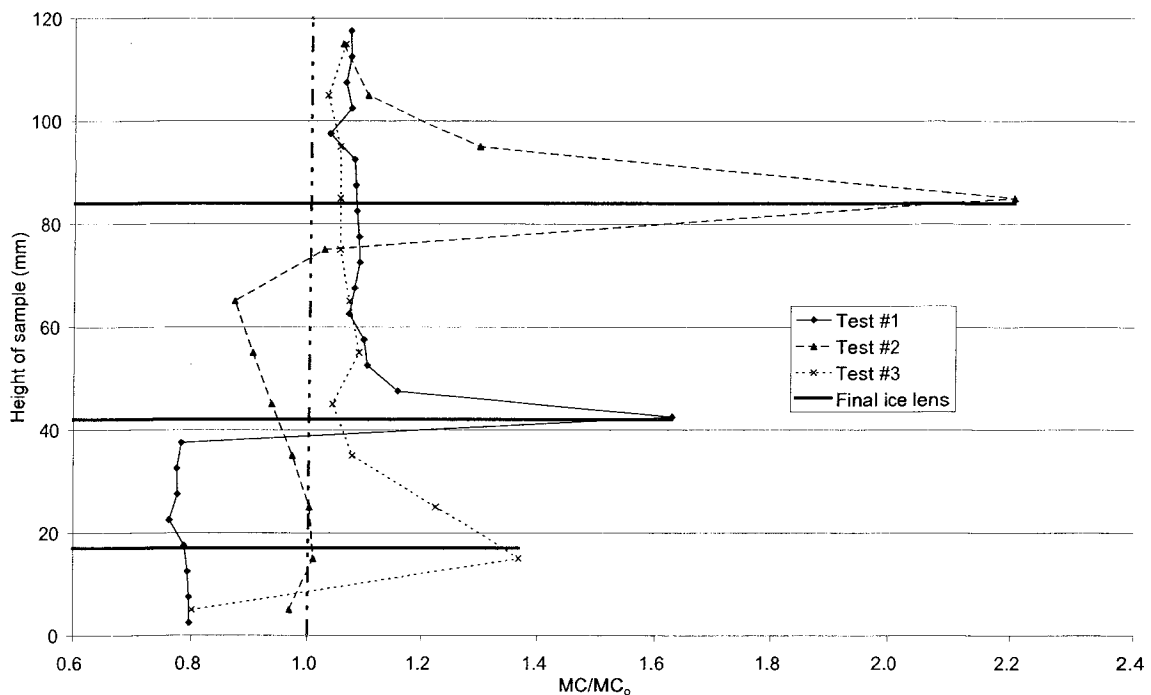


Figure 4.2.9 Moisture content ratio profile in tests #1, #2 and #3

#### 4.2.5 Discussion of the effects of temperature gradient

The frost penetration rate depends on the rate of heat flow, which is related to the temperature gradient and thermal conductivity of the soil. When heat is extracted from the unfrozen zone at a rapid rate, the frost rapidly penetrates into the sample. In this series of tests, the greatest temperature gradient caused the highest heat flow rate, which induced the most rapid frost penetration rate. The results of these tests confirmed the relationship between the temperature gradient and the frost penetration rate outlined in section 4.1.

The temperature gradient not only affects the frost penetration, but also affects the thickness of the frozen fringe throughout the test. At similar positions in the samples, the thinnest frozen fringe was found with the highest temperature gradient (Figure 4.2.5). In a step-freezing test, the temperature is usually linear

through both the frozen and unfrozen zone. As shown in Figure 2.3(a), it is assumed that the change of segregation temperature  $T_s$  with cooling rate can be neglected in a freezing test. The lower temperature  $T_c$  at the top boundary causes a thinner frozen fringe to develop as the freezing front penetrates.

The temperature gradient also controls the formation of the horizontal ice lenses in these step-freezing tests. In tests #1 and #2, the visible ice lenses appeared at the beginning of the freezing because the temperature at the top plate was decreased from about 2°C to -2°C and -5°C, respectively. This did not result in a rapid temperature change across the sample. The maximum cooling rates for test #1 and test #2 are 3.0°C/hour and 1.6°C/hour, respectively. In test #3, the high cooling rate did not allow for the initiation of visible ice lens at the start of freezing. Only when the cooling rate decreased to about 4.1°C/hour, did visible ice lenses start to form.

Konrad and Morgenstern (1980, 1981) introduced the segregation potential (SP), which is defined as the ratio of the water intake velocity to the temperature gradient in the frozen fringe. The effects of factors such as vertical stress and soil type on it during the formation of the final ice lens can be accounted for using:

$$SP = SP_0 e^{-aP_e}$$

Where  $SP_0$  is the segregation potential obtained with no applied load for a given soil,

$P_e$  is the vertical stress

$a$  is a soil specific parameter.

The average rate of the final ice lens growth was 0.013 mm/hour in test #1, 0.032 mm/hour in test #2 and 0.022 mm/hour in test #3. According to the segregation

potential concept, the SP during the final ice lens formation does not change if only the temperature gradient changes. Therefore, the rate of final ice lens growth, which represents the rate of water intake during steady state, in test #1 should be greater than the rate in test #2 but smaller than the rate in test #3 due to differences in temperature gradients. These tests however show that the largest rate of final ice lens growth was recorded for test #2, then test #3 and the smallest for test #1. The discrepancy of these results implies that another factor, at least, affects these freezing tests. The results of water intake and frost heave shown in Figure 4.2.7 and Figure 4.2.8 also confirm the existence of this factor because the rate of heave and water intake in test #1 is smaller than the rate for tests #2 and #3.

A suction gradient is generated at the warm side of the active ice lens and into the unfrozen zone of the sample (Figure 4.2.10). This gradient not only induces the migration of water from the unfrozen zone to the warmest ice lens, but also results in consolidation of the unfrozen soil. The maximum suction is generated at the warm side of the active ice lens and decreases to 0kPa at the sample base. Therefore no consolidation should be generated at the bottom of the sample. However, the moisture content profiles after freezing (Figure 4.2.9) suggest that tests #1 and #3 were consolidated even in the lower unfrozen zone of each sample. This implies that not only the suction caused this consolidation at the unfrozen zone. The friction between the inside of the cell wall and the frozen part of the soil is thought also to have an influence according to the limitation of this test setup. Further discussion and this influence on the segregation potential measured in this research can be found in section 4.3.

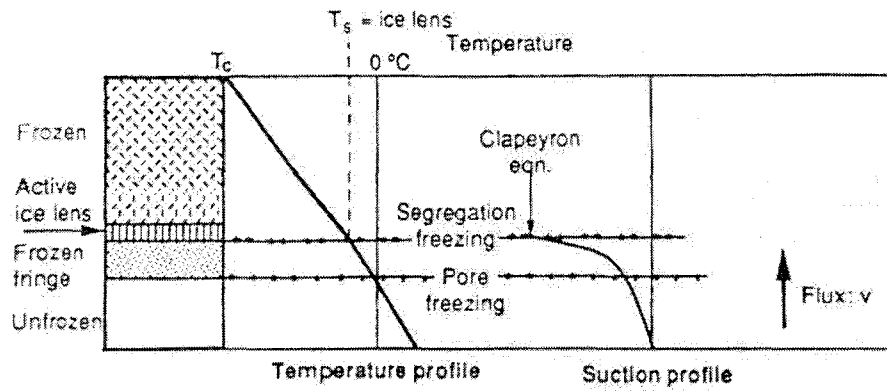


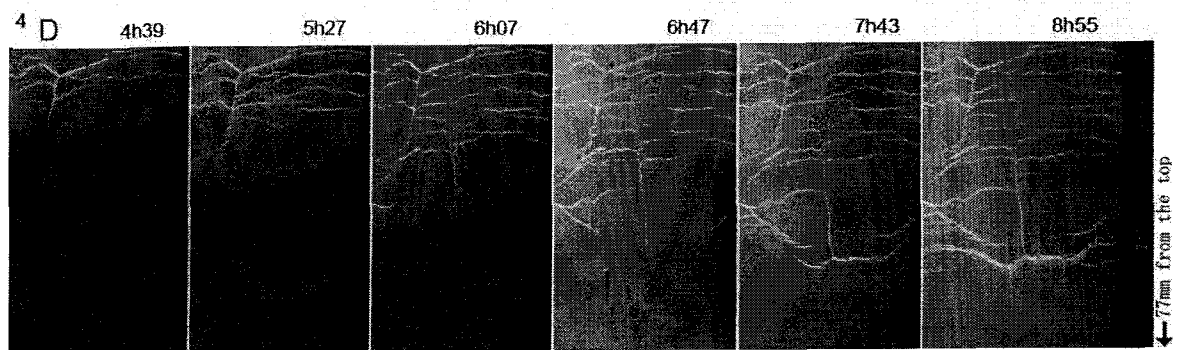
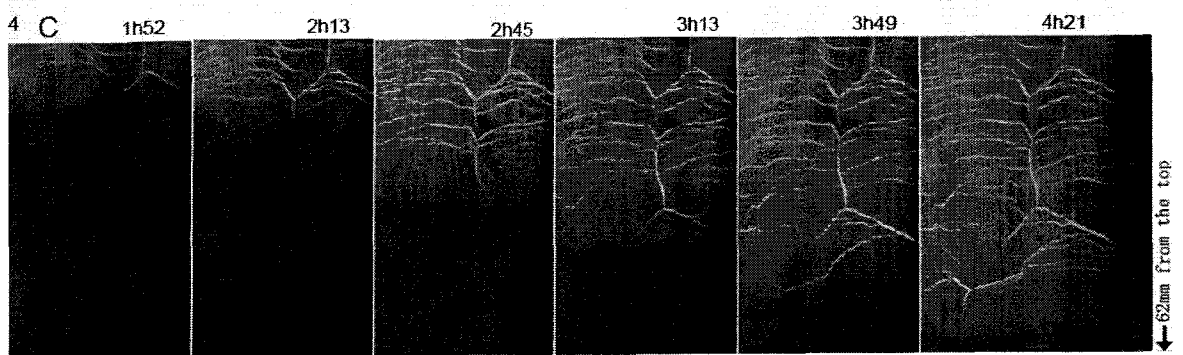
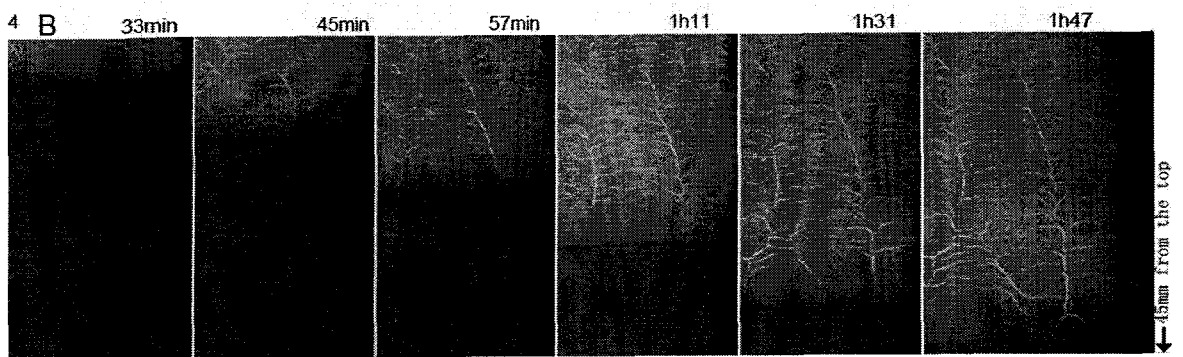
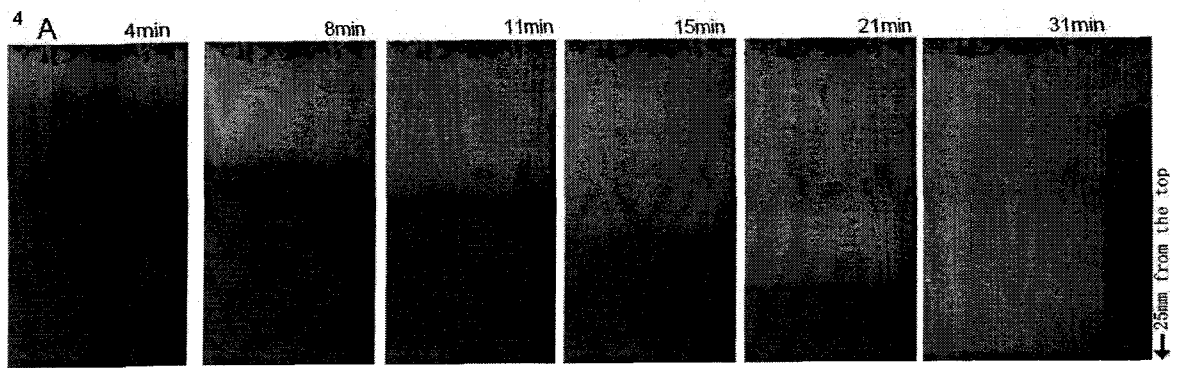
Figure 4.2.10 Temperature profile and suction profile of freezing soil (after Konrad 1994).

### 4.3 Effects of applied stress

The results of tests #1, #4, #5 and #6 are reviewed to demonstrate the influence of vertical stress on the soil sample as it freezes. A series of images (Figure 4.3.1, Figure 4.3.2 and Figure 4.3.3) are selected to demonstrate the freezing process in tests #4 (100kPa), #5 (200kPa), and #6 (400kPa). Table 4.3.1 through Table 4.3.3 explain the locations of each row of images and time after the start of freezing is shown on each image. Similar images for test #1(0kPa) are presented in section 4.1.

Figure 4.3.1 A through E show the development of ice lenses during the transient freezing state, as well as the development of the final ice lens from 18h45 to 77h01 in test #4. Figure 4.3.2 A through D show similar development of ice lenses during the transient state of freezing for test #5, and E shows the development of the final ice lens. Figure 4.3.3 A through E show the development of ice lenses during the transient state of freezing, and the development of the final ice lens from 34h00 to 175h00 in test #6.

Obvious changes of ice lens formation can be found from the images shown in Figures 4.1.1, and 4.3.1 through 4.3.3. The following sections will present this change with other effects of vertical stress on freezing process.



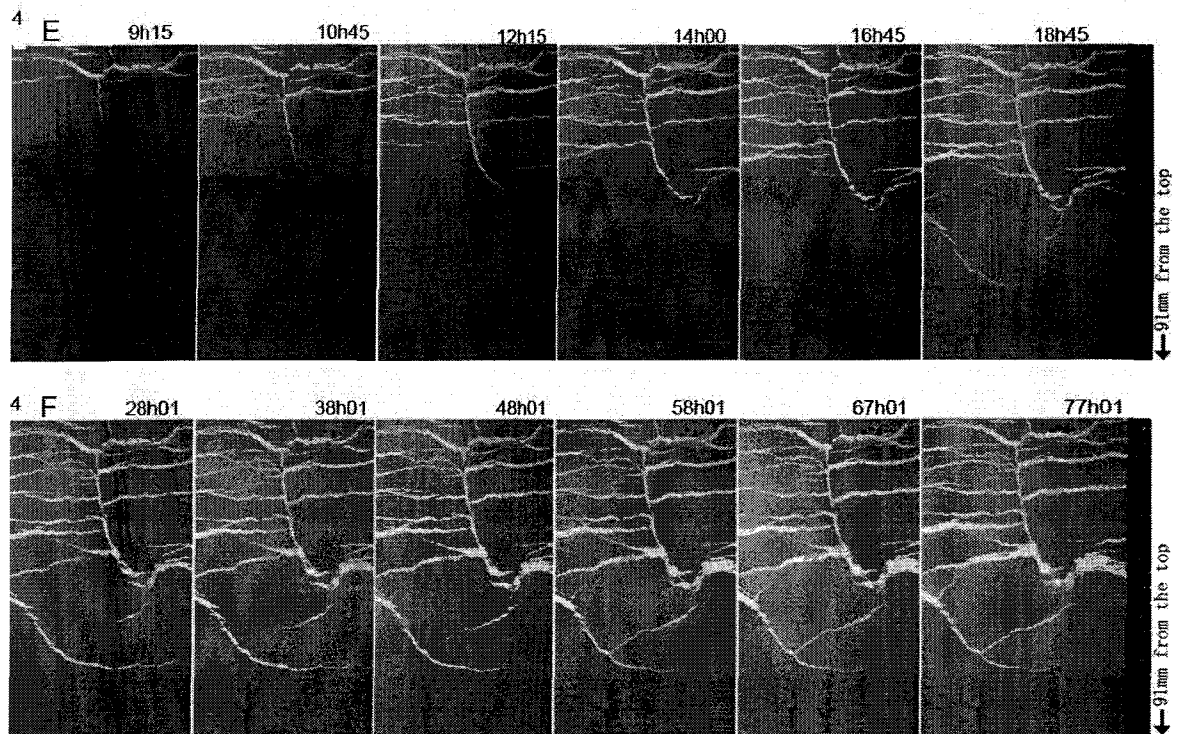
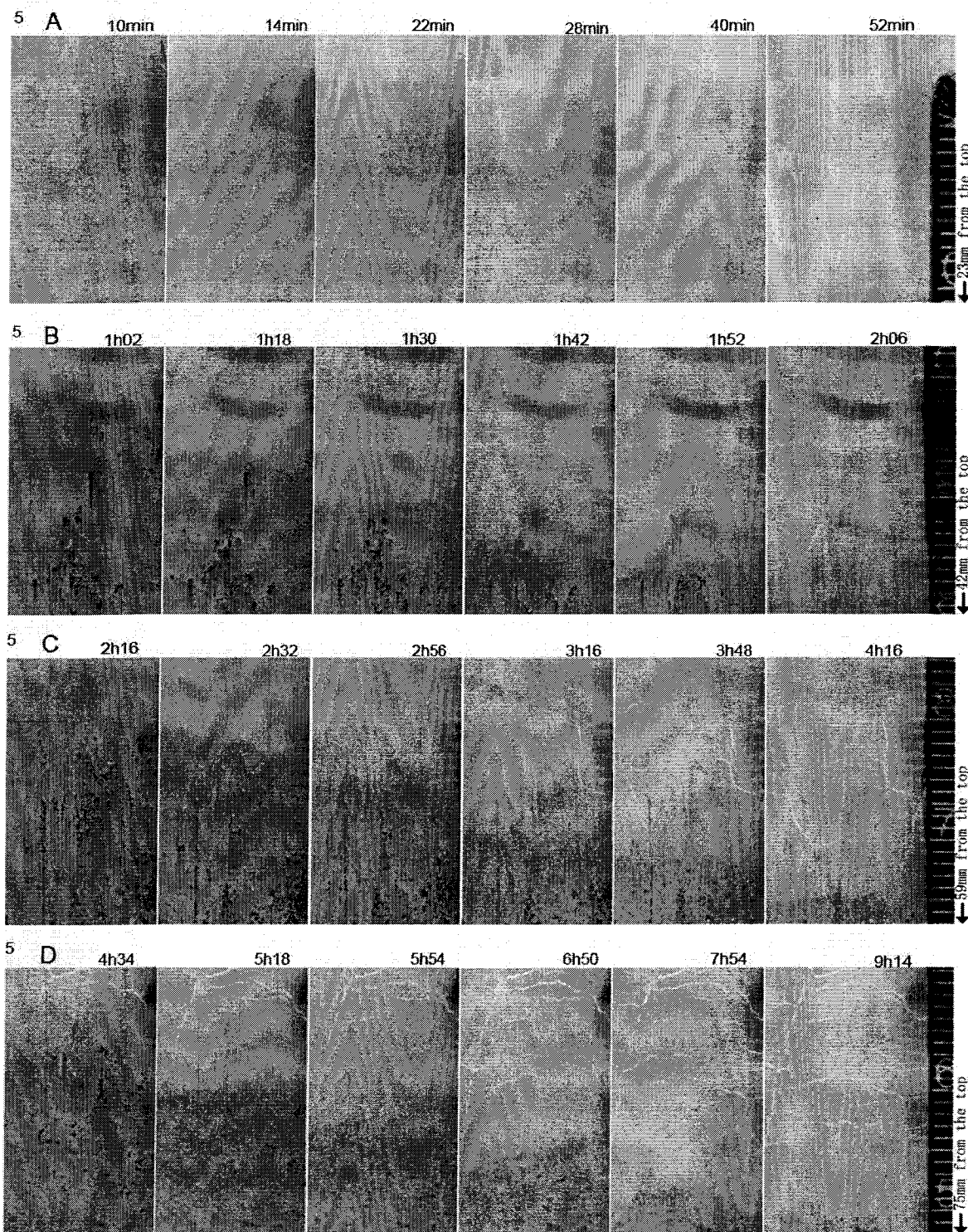


Figure 4.3.1 Serial images of the freezing process of test #4 (scale in millimeter).

Table 4.3.1 Image locations for Figure 4.3.1

Row #	Distance for the top of the sample*	
	Top edge (mm)	Bottom edge (mm)
A	3	25
B	23	45
C	40	62
D	55	77
E	69	91
F	69	91

\* the top of the sample is the top of the sample after consolidation



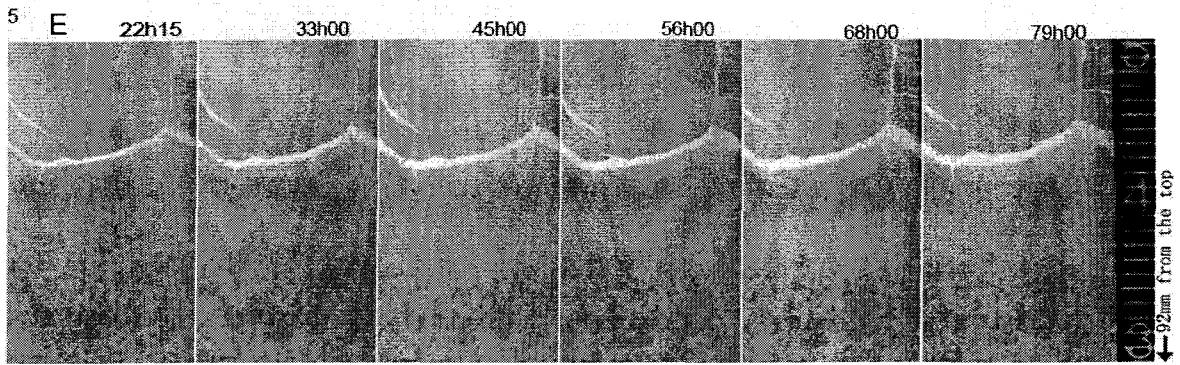
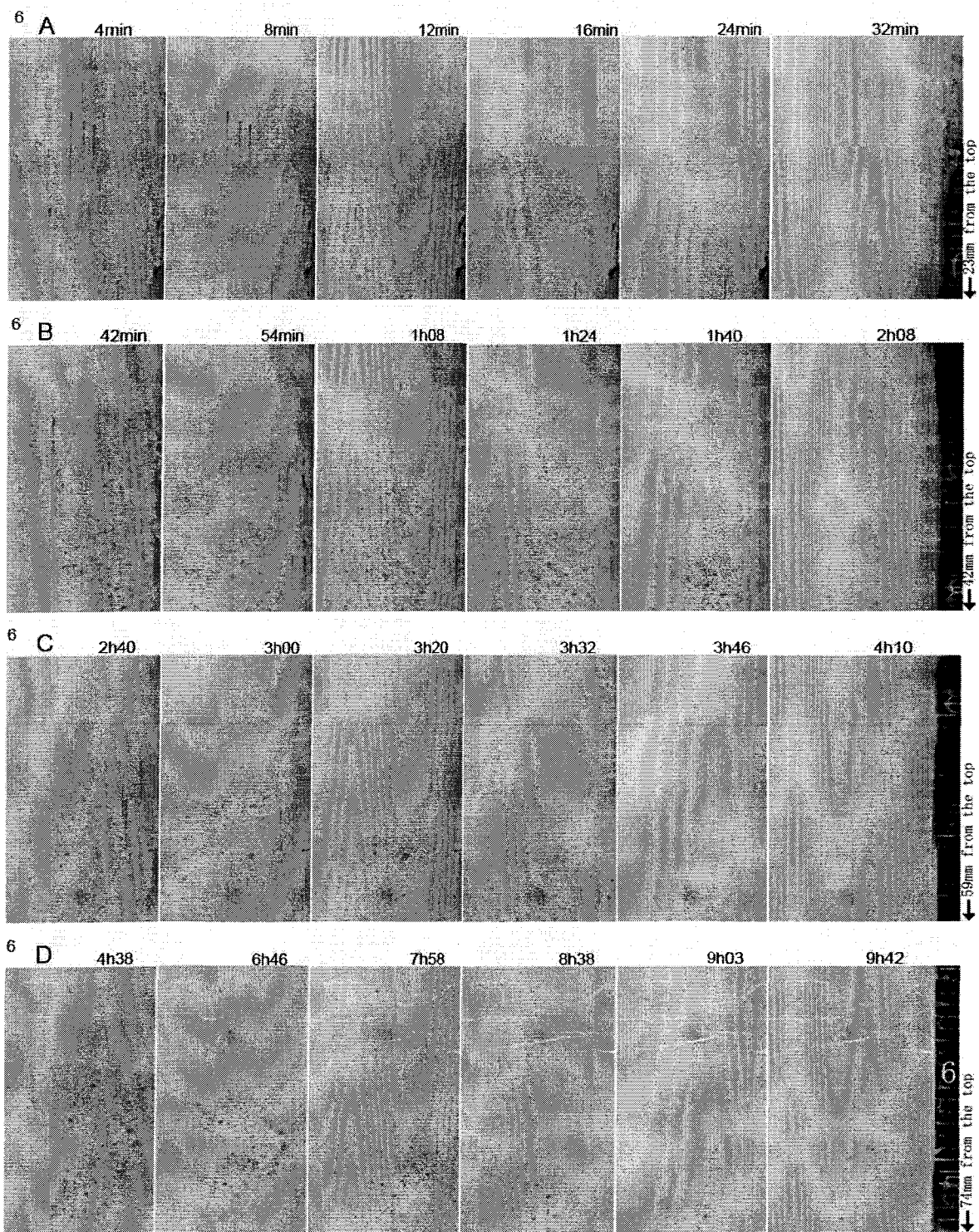


Figure 4.3.2 Serial images of the freezing process of test #5 (scale in millimeter).

Table 4.3.2 Image locations for Figure 4.3.2

Row #	Distance for the top of the sample*	
	Top edge (mm)	Bottom edge (mm)
A	1	23
B	20	42
C	37	59
D	53	75
E	70	92

\* the top of the sample is the top of the sample after consolidation



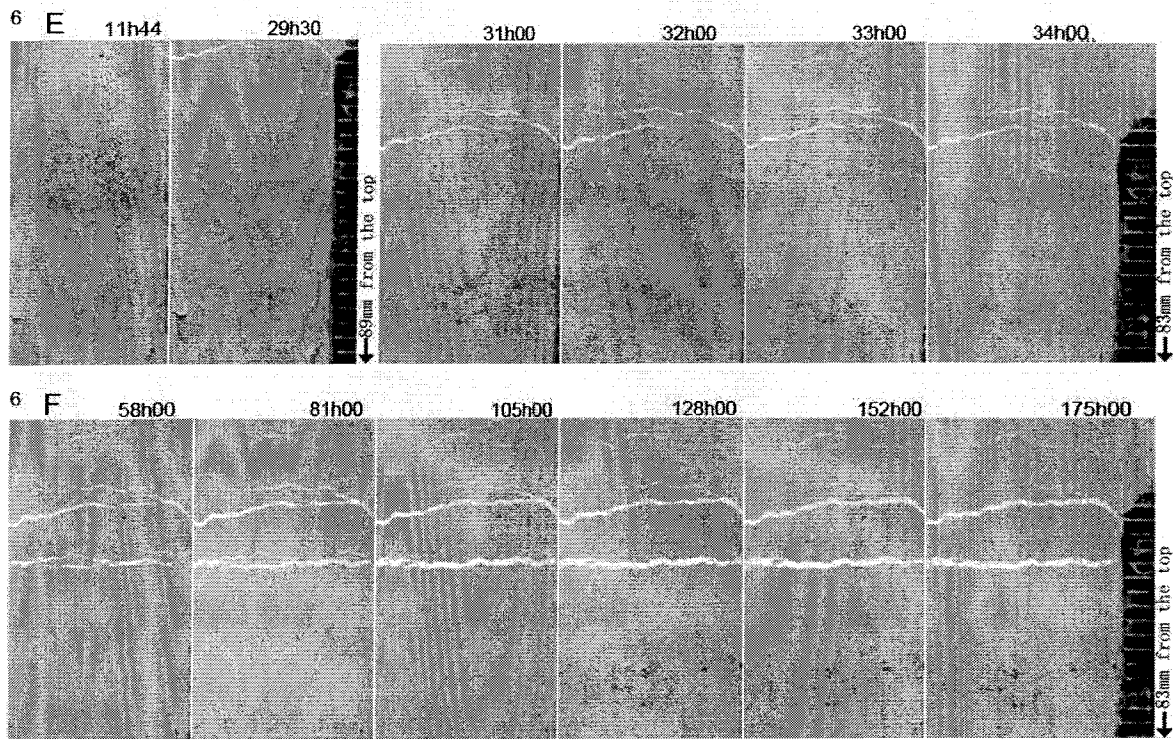


Figure 4.3.3 Serial images of the freezing process of test #6(scale in millimeter)

Table 4.3.3 Image locations for Figure 4.3.3

Row #	Distance for the top of the freezing sample*	
	Top edge (mm)	Bottom edge (mm)
A	1	23
B	20	42
C	37	59
D	52	74
E	(67)**61	(89)**83
F	61	83

\* the top of the sample is the top of the sample after consolidation.  
 \*\* the data in ( ) represents the data for first two images of 4.4.3 E.

### 4.3.1 Frost penetration

As shown in Figure 4.3.4, in all four tests the freezing fronts penetrated into the samples at almost the same rate during the first 10 hours of freezing. Then the rate in test #6 decreases compared to the others. As a result, the freezing front during thermal steady state is located at a higher position within this sample. Tests #1, #4, and #5 showed similar behaviour to each other.

The frozen fringe thickness generally increases with increased vertical stress. Figure 4.3.5 illustrates the changes of the frozen fringe with time and Figure 4.3.6 illustrates the changes with the location for tests #1, #4, #5 and #6. At similar times following the start of freezing, test #6 had the thickest frozen fringe whereas tests #4 and #1 had the thinnest (Figure 4.3.5). At the same location in the sample, test #6 had the largest frozen fringe thickness, followed by test #5 (Figure 4.3.6). The frozen fringes in both test #4 and test #1 were thinner. Test #1 has the thicker frozen fringe in the upper 60 mm of sample compared to test #4, which has the thicker frozen fringe between 40 mm and the freezing front under steady state.

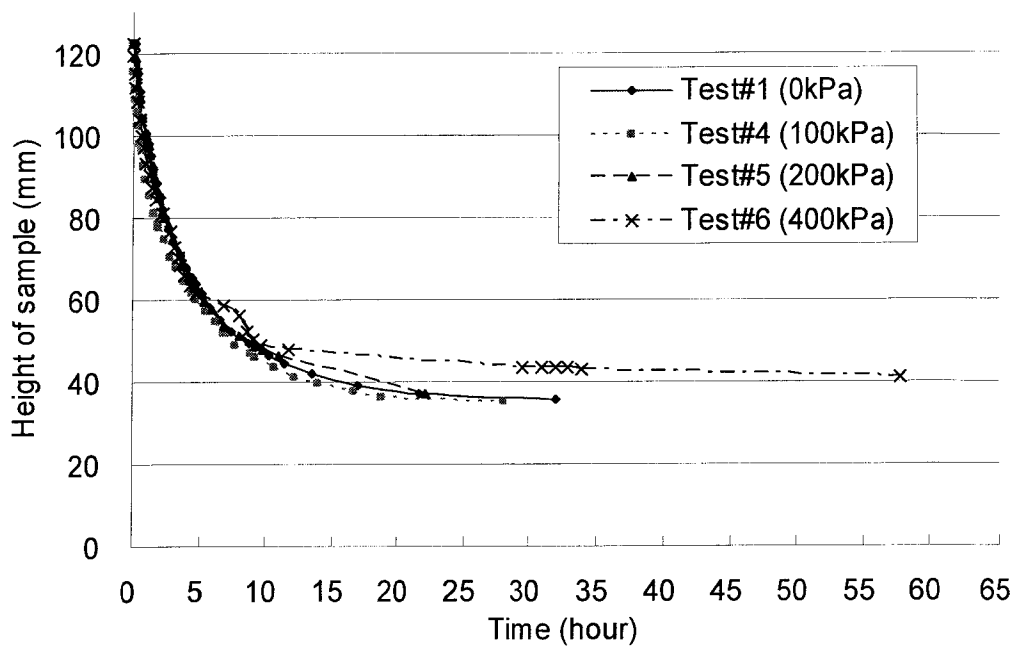


Figure 4.3.4 Frost penetration under different vertical stress.

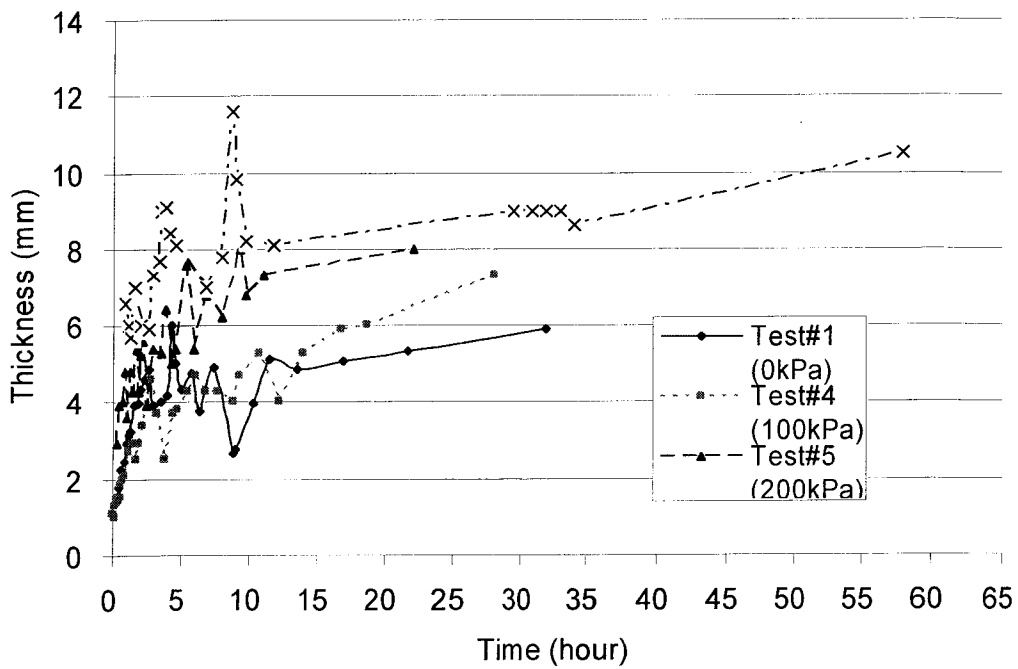


Figure 4.3.5 Frozen fringe thickness changes with time under different vertical stresses.

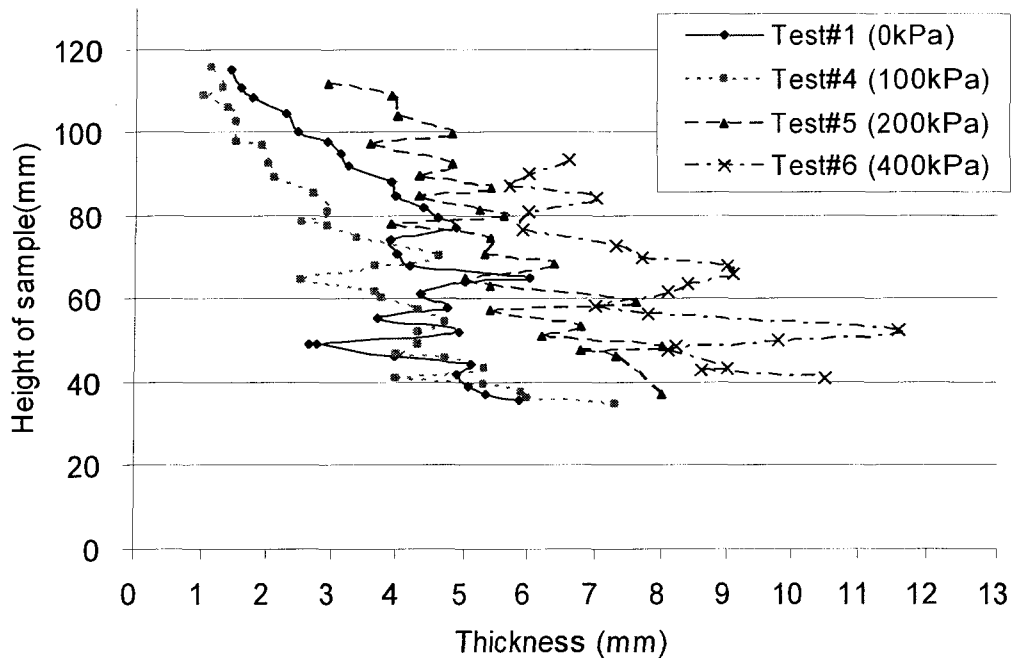


Figure 4.3.6 Frozen fringe thickness along the height of the sample under different vertical stresses.

#### 4.3.2 Horizontal ice lens formation and its development

Figures 4.1.1, 4.3.1, 4.3.2, and 4.3.3 show the formation and growth of the horizontal ice lenses during both transient freezing and steady state freezing under different vertical stresses. In test #4, the applied vertical stress during freezing is 100 kPa, which is the same as the consolidation stress applied to test #1. The ice lens feature of test #4 shown in Figure 4.3.1 is similar to the one in test #1 shown in Figure 4.1.1. In test #5, no visible ice lens formed during the first 28 minutes of freezing before the frost penetrated 10 mm. Very fine and discontinuous ice lenses formed between 28 minutes and 240 minutes following the start of freezing. The frost penetrated from 10 mm to 52 mm in the sample in this period. The ice lenses formed during this stage are heterogeneous. Starting at

about 4 hours after freezing, layers of ice lenses formed prior to the onset of the final ice lens at a depth of 78 mm. Under a vertical stress of 400 kPa (test #6 ), no ice lens was observed during the first 54 minutes of freezing, at which the frost had penetrated 29mm into the sample(Figure 4.3.3). Very fine and discontinuous ice lenses formed between 54 minutes and 240 minutes, as the frost penetrated from 29mm to 57mm depth. The ice lenses formed in this period were heterogeneous and non-continuous. After about 4 hours of freezing, layers of ice lenses formed until the final ice lens initiated at a depth of 71mm.

The growth of the final ice lenses in tests #1, #4, #5 and #6 are shown in Figure 4.3.7. The data were directly measured on the digital images taken during each freezing test. In test #1, the final ice lens initiated at 21.75 hours after the start of freezing and grew at an average rate of 0.013 mm/hour until the end of the test. In test #4 under a 100 kPa applied vertical stress, the final ice lens initiated after 18.75 hours and grew at an average rate of 0.007 mm/hour until the end of the test. In test #5 (200 kPa vertical stress), the final ice lens initiated after 11 hours and grew at an average rate of 0.006 mm/hour until the end of the test. In test #6 (400 kPa vertical stress), the final ice lens initiated after 34 hours and grew at an average rate of 0.004 mm/hour until the end of the test.

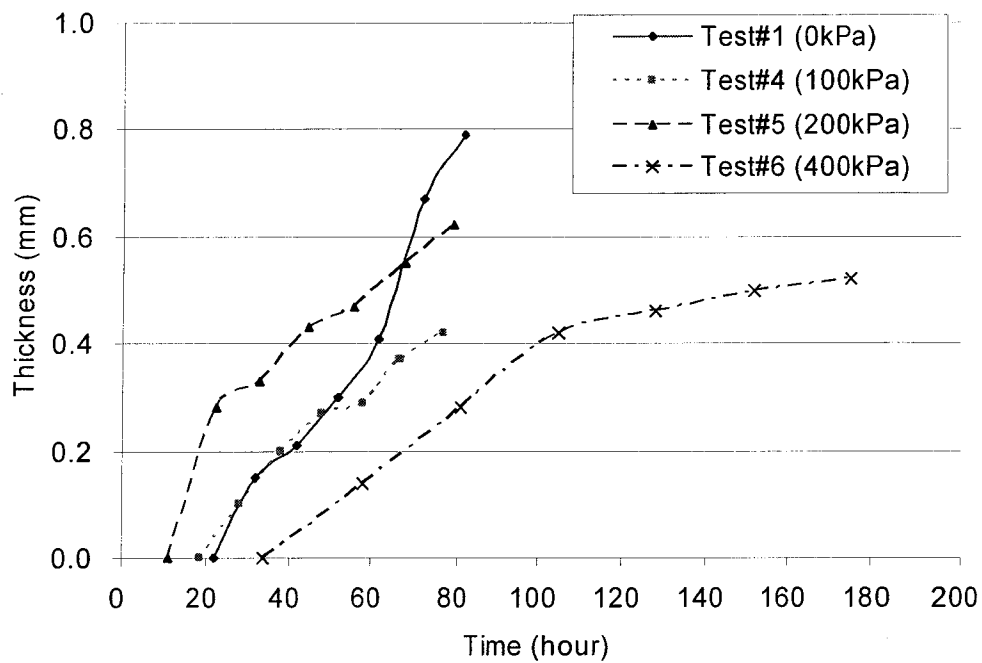


Figure 4.3.7 Final ice lens growth under different vertical stresses.

### 4.3.3 Heave and water intake

Figure 4.3.8 and Figure 4.3.9 show the results of heave and water intake for these same four tests. The times for onset of heave and water expulsion are summarized in Table 4.3.4.

Table 4.3.4 Summary of the time for onset of heave and water ejection.

Test #	Time (hour)	
	Onset of heave	Water expulsion
1	32	36
4	21	47
5	47	32
6	73	54

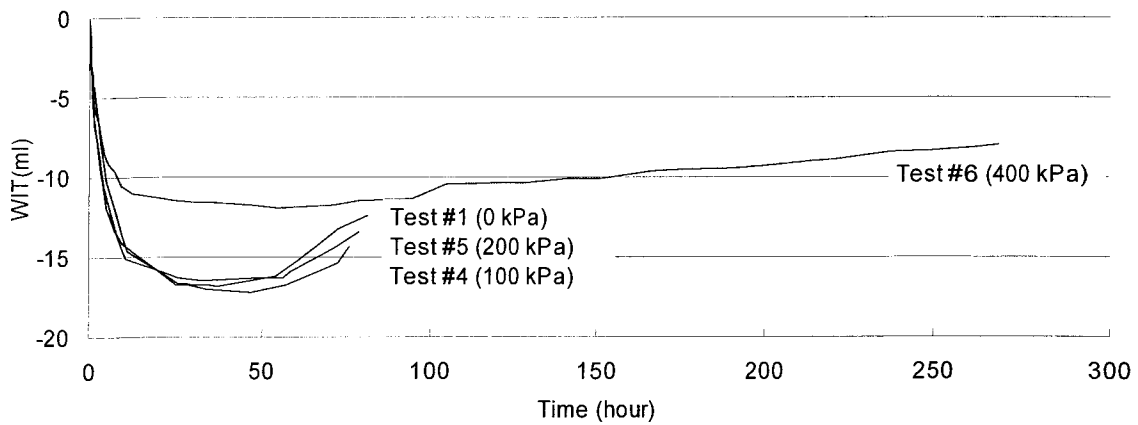


Figure 4.3.8 Water intake under different vertical stresses.

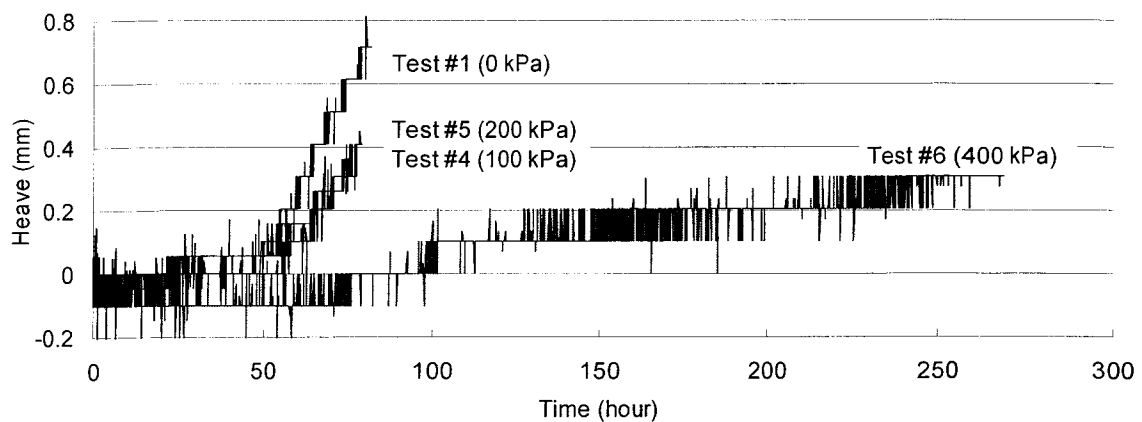


Figure 4.3.9 Frost heave under different vertical stresses.

#### 4.3.4 Moisture content redistribution

The moisture content redistribution in the sample during freezing occurred in all tests. Figure 4.3.10 shows the maximum moisture content is at the location of final ice lenses. In the frozen zone, tests #1 and #4 have higher relative moisture contents than tests #5 and #6, but in the unfrozen zone, tests #1 and #4 have lower values. However, test #5 shows similar values in the unfrozen zone as tests #1 and #4 and is significantly lower than test #6.

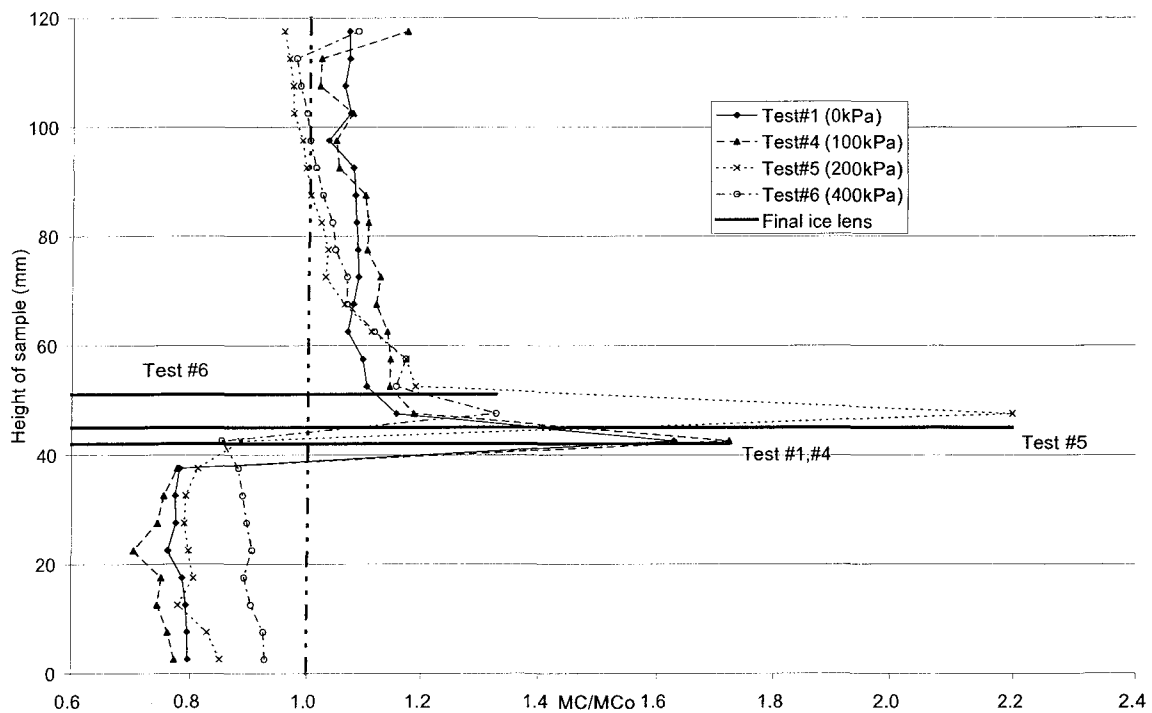


Figure 4.3.10 Moisture content (ratio) profile after frozen in tests #1, #4, #5 and #6.

#### 4.3.5 Discussion of the effects of applied vertical stress

It has been previously discussed that frost penetration rate is related to the temperature gradient. The results presented in this section show that the applied vertical stress within this study has little effect on the frost penetration. The penetration was similar for all the tests discussed in this section. Figures 4.3.5 and 4.3.6 show the thickness of the frozen fringe increases with increase in vertical stress.

As the applied vertical stress increases, the growth of the ice lens was inhibited (Figures 4.1.1, and 4.3.1 to 4.3.3) since the suction at the warm side of the active ice lens decreases with increasing stress in the soil (Konrad and Morgenstern 1982). Furthermore, the increase in frozen fringe thickness with increasing vertical stress (Figure 4.3.5 and 4.3.6) requires a longer flow path for the water to

migrate from the unfrozen zone to the growing ice lens. The hydraulic conductivity in the soil is further reduced as a result of the increased state of consolidation. According to Darcy's law, the longer the drainage path, the lower the gradient along with the lower the hydraulic conductivity results in reduced water migration to the ice lens. These observations are confirmed by the decrease in average rate of the final ice lens growth (Table 4.3.5, Figure 4.3.11) with increasing applied vertical stress. The effects of friction between the soil sample and the inside wall of the freezing cell, which induced additional vertical stress, are discussed below.

The applied vertical stress affects the frost heave by reducing the water intake rate (Figure 4.3.8 and Figure 4.3.9). This influence of stress can be explained in terms of changes in suction at the ice-water interface, which results in changes in segregation freezing temperatures, and reduced hydraulic conductivity within the frozen fringe as confirmed by the results of the changes of the frozen fringe outlined above. The SP calculated from tests #1 to #6 are shown in Figure 4.3.12 with the results from Konrad (1982) for Devon silt. For this data analysis, the final ice lens growth rate was used to calculate the segregation potential instead of the water intake rate since the ice lens growth rate was less influenced by the friction between the sidewall of the cell and the frozen soil sample. Curve *a* represents the data from the current test using the vertical stress applied on the top of the sample, so-called nominal stress, whereas curve *b* is the corrected result after considering the influence of friction as discussed below.

In these investigations, the friction between the frozen soil and the sidewall of the cell was an issue that affects the final ice lens growth, the measured heave, and thus the calculated segregation potential. The existence of the friction is confirmed by the moisture content redistribution profile. The soil at the bottom boundary should not be consolidated during freezing since the suction generated

at the warm side of the ice lenses decreases to zero at the base of the sample in the open system (Figure 4.2.11). However, the result of moisture content distribution in each test shows that the soil on the bottom boundary was consolidated during the freezing due to the lower moisture content compared to the initial one. This inconsistency implies that additional consolidation stresses existed during freezing. According to the setup used in these freezing tests, it is considered that the extra stress results from friction between the frozen part of the sample and the cell wall due to the expansion of the frozen soil against the sidewall.

A consolidation index of  $C_c=0.257$  was determined from a consolidation test on Devon silt prior to the freezing tests (Figure 3.4). The moisture content at the bottom of the sample after freezing were used to back-analyze the total stresses, including friction, applied on the final ice lens. The specific gravity of the Devon silt is 2.65. The void ratio at the base of the sample can be calculated using the measured moisture content at the same location after freezing. The total vertical stress inducing this consolidation can then be calculated using the relationship between the void ratio and consolidation stress show in Figure 3.4 or the consolidation index ( $C_c$ ). All the data of moisture content after freezing are presented in Appendix B. Curve b in Figure 4.3.12 uses these total stresses. This curve is closer to the one presented by Konrad (1982) on Devon silt.

Table 4.3.5 Summary of final ice lens growth rate and SP at the onset of the final ice lens formation.

Test #	Vertical stress (kPa)		Final ice lens growth rate ( $10^{-6}$ mm/s)	SP ( $10^{-5}$ mm <sup>2</sup> /s.°C)
	Nominal	Plus friction		
1	0	471	2.64	4.62
2	0	118	14.4	44.2
3	0	422	6.37	4.83
4	100	580	2.64	4.44
5	200	506	1.53	2.65
6	400	622	1.51	2.38

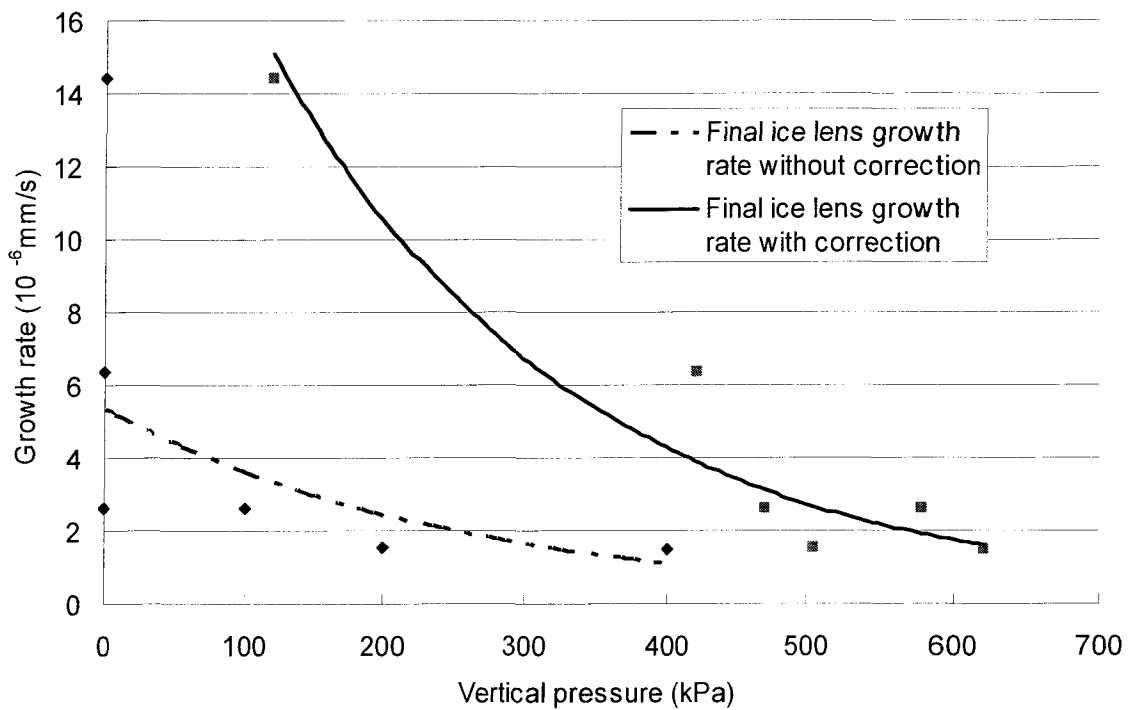


Figure 4.3.11 The final ice lens growth rate at the onset of the final ice lens formation under different vertical stress.

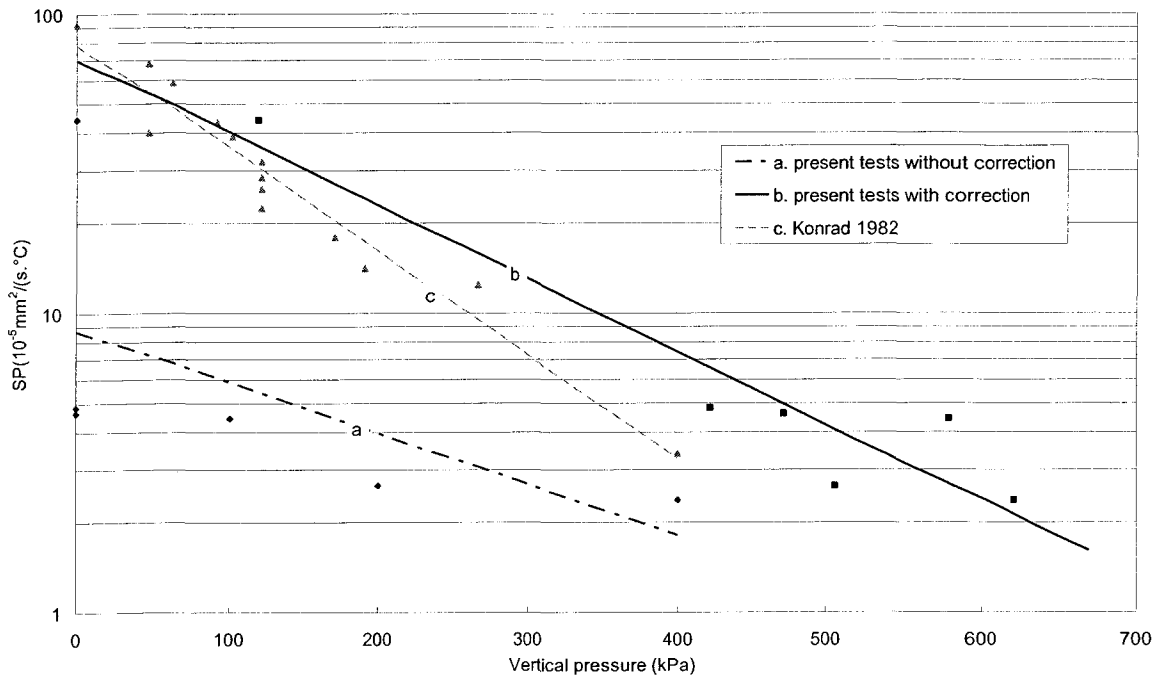
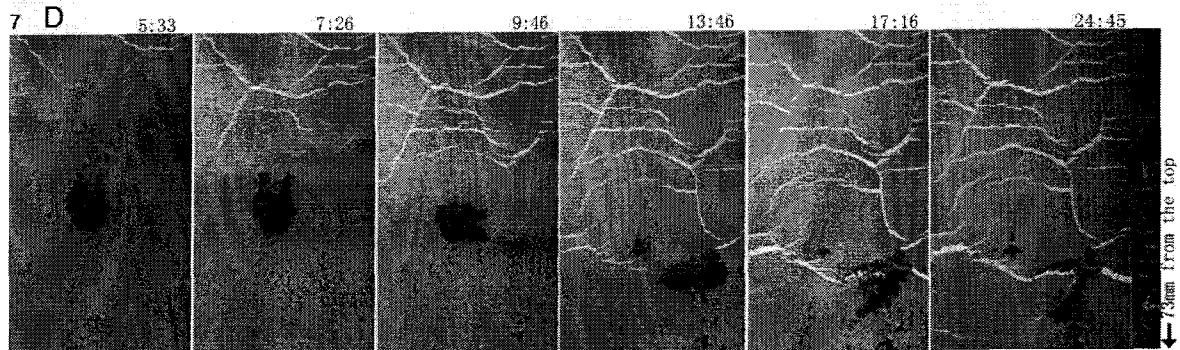
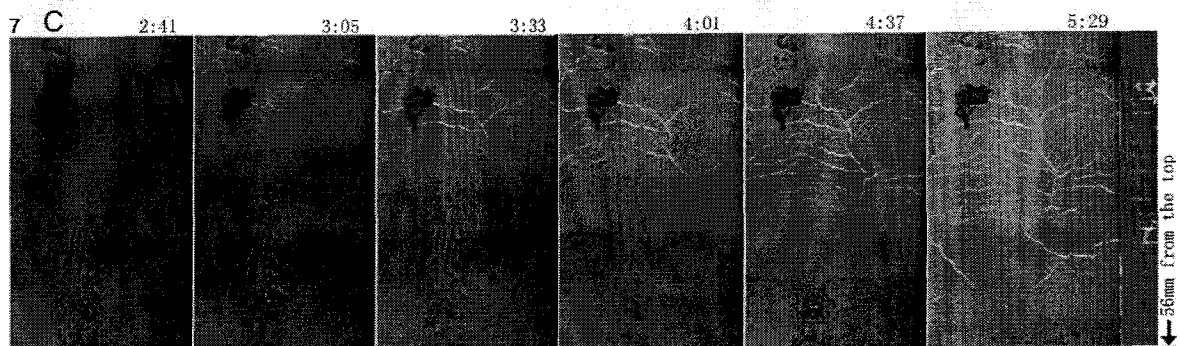
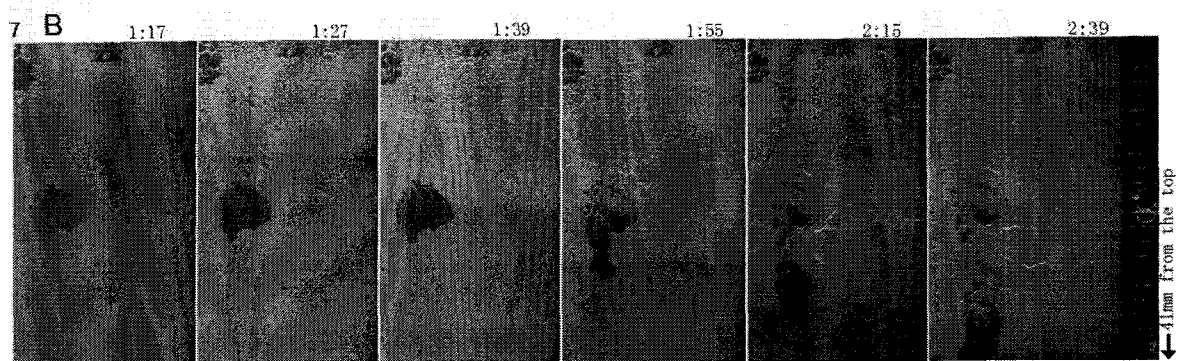
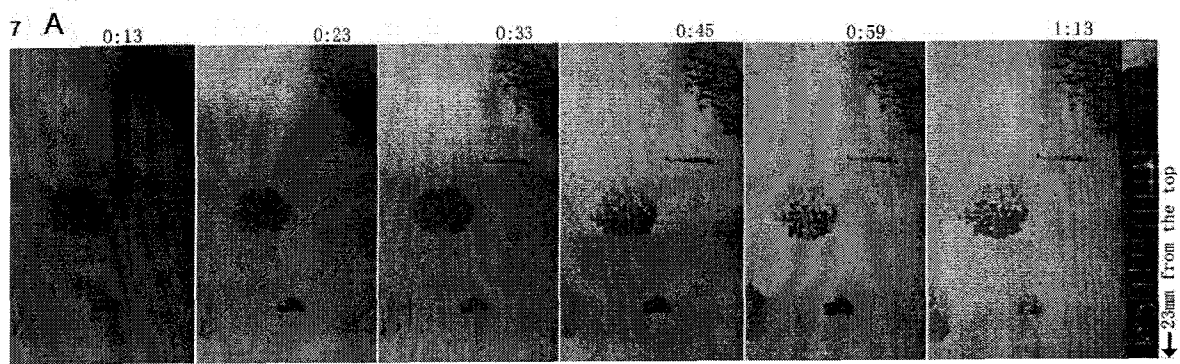


Figure 4.3.12 The segregation potential (SP) at the onset of the final ice lens formation under different vertical stress.

## 4.4 Effects of water salinity

In this section, the results from tests #1 (0 g/L), #7 (5.9 g/L), #8 (10.2 g/L) and #9 (25.7 g/L) are presented to show the influence of pore water salinity on soil freezing. Tests #9, #10, #11 and #12 will show the influence of changing boundary conditions for samples prepared using the highest salinity of 25 g/L (nominal). The actual salinity varied from 23.6 to 25.7 g/L in each test (Table 3.1). Figure 4.4.1, to Figure 4.4.6 are six separate series of digital images to show the freezing process of tests #7 to #12, and each figure is followed by a table, which explains the location of each row of images. The images and their locations of test #1 have been presented in section 4.1. The elapsed time at which each image was taken is provide above each image.

Figure 4.4.1 A through D show the development of ice lenses during the transient state of freezing, and images taken between 13:46h and 77:00h show the development of the final ice lens in test #7. Figure 4.4.2 A through D show the development of ice lenses during the transient state of freezing, and the final ice lens begins to form after 15:02h and its development continues to 72:00h in test #8. No distinct final ice lens formed in test #9 through test #12 with 25g/L (nominal) pore water salinity (Figure 4.4.3 to Figure 4.4.6). In each figure, the last row of images shows the growth of the ice lenses at thermal steady state, and the others show the processes during transient freezing.



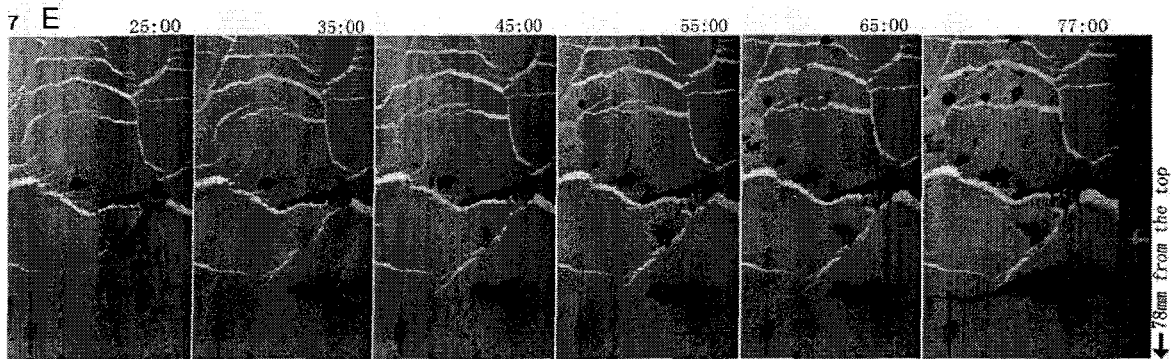
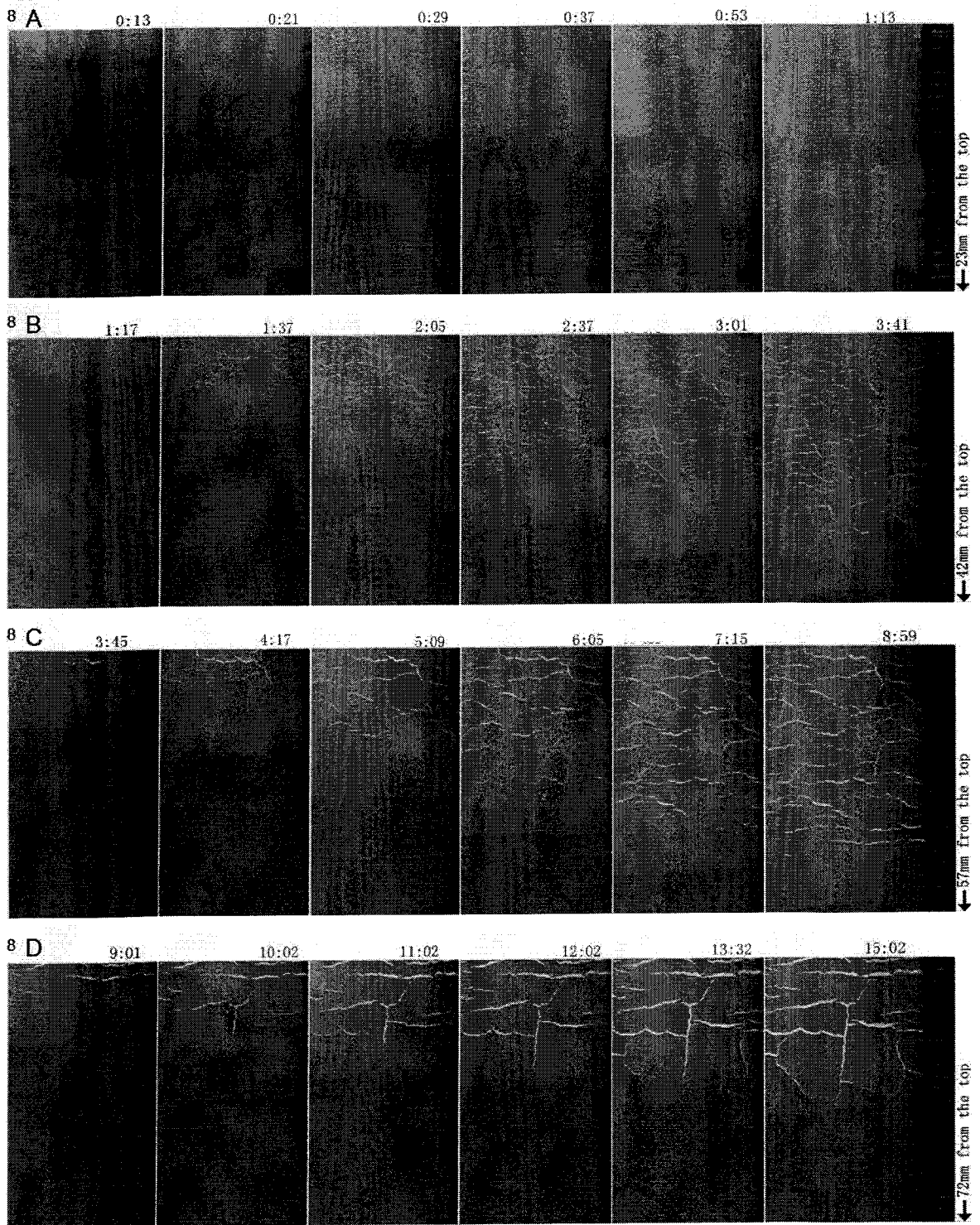


Figure 4.4.1 Serial images of the freezing process of test #7  
 (5.9 g/L, -5°C on the top, 0 kPa, scale in millimeter).  
 scale in millimeter).

Table 4.4.1 Image locations for Figure 4.4.1.

Row #	Distance for the top of the sample*	
	Top edge (mm)	Bottom edge (mm)
A	1	23
B	19	41
C	34	56
D	51	73
E	56	78

\* the top of the sample is the top of the sample after consolidation



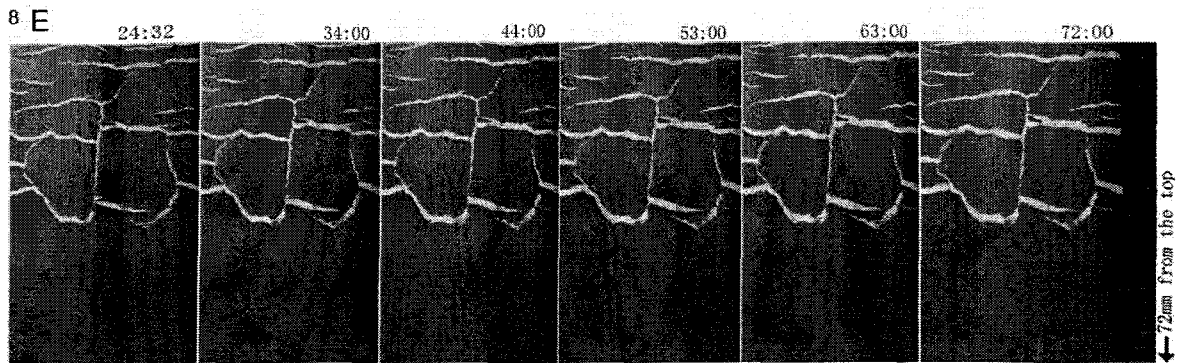


Figure 4.4.2 Serial images of the freezing process of test #8  
(10.2 g/L,  $-5^{\circ}\text{C}$  on the top, 0 kPa, scale in millimeter).

Table 4.4.2 Image locations for Figure 4.4.2.

Row #	Distance for the top of the sample*	
	Top edge (mm)	Bottom edge (mm)
A	1	23
B	20	42
C	35	57
D	50	72
E	50	72

\* the top of the sample is the top of the sample after consolidation

Table 4.4.3 Image locations for Figure 4.4.3.

Row #	Distance for the top of the sample*	
	Top edge (mm)	Bottom edge (mm)
A	1	23
B	20	42
C	31	53
D	31	53

\* the top of the sample is the top of the sample after consolidation

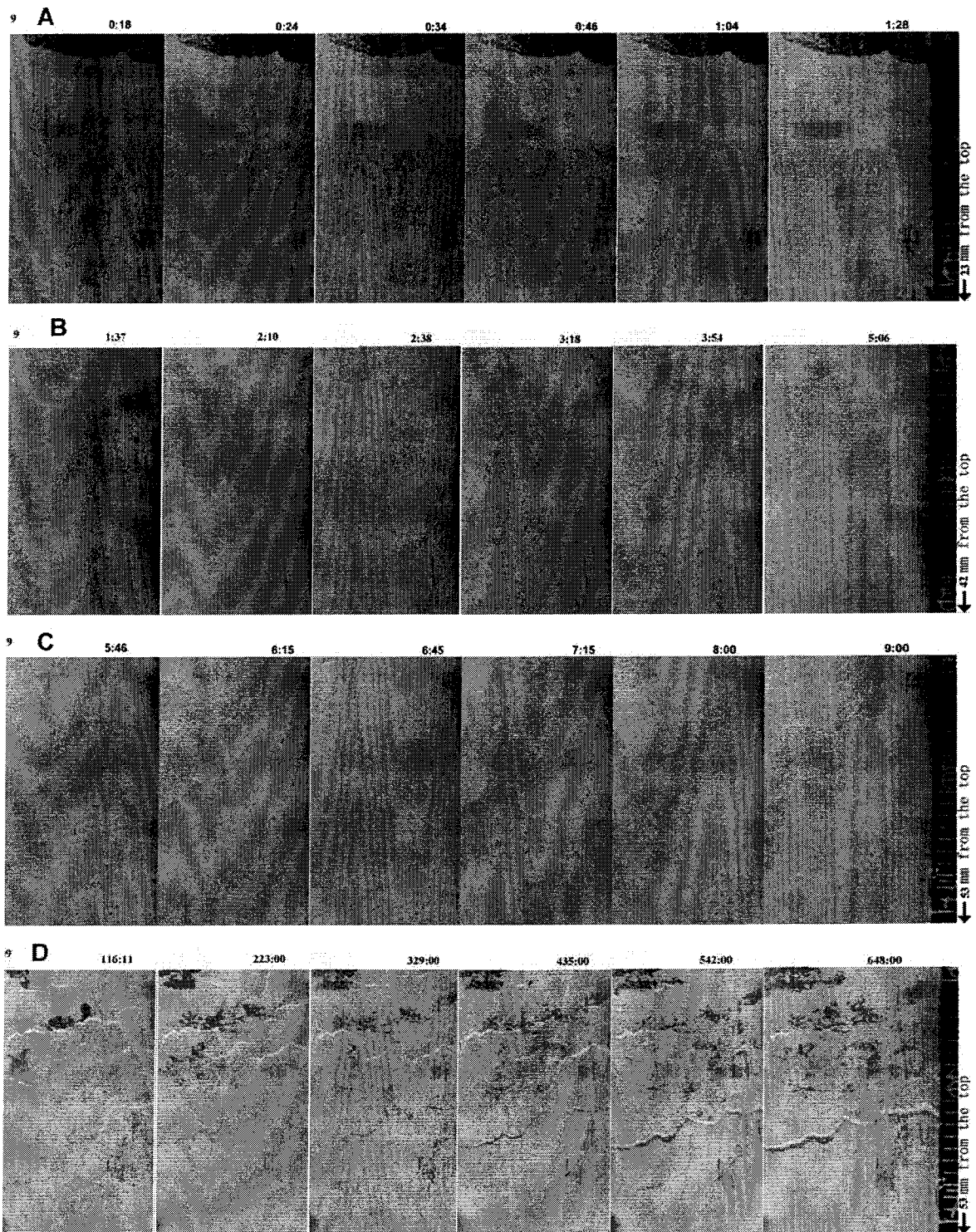
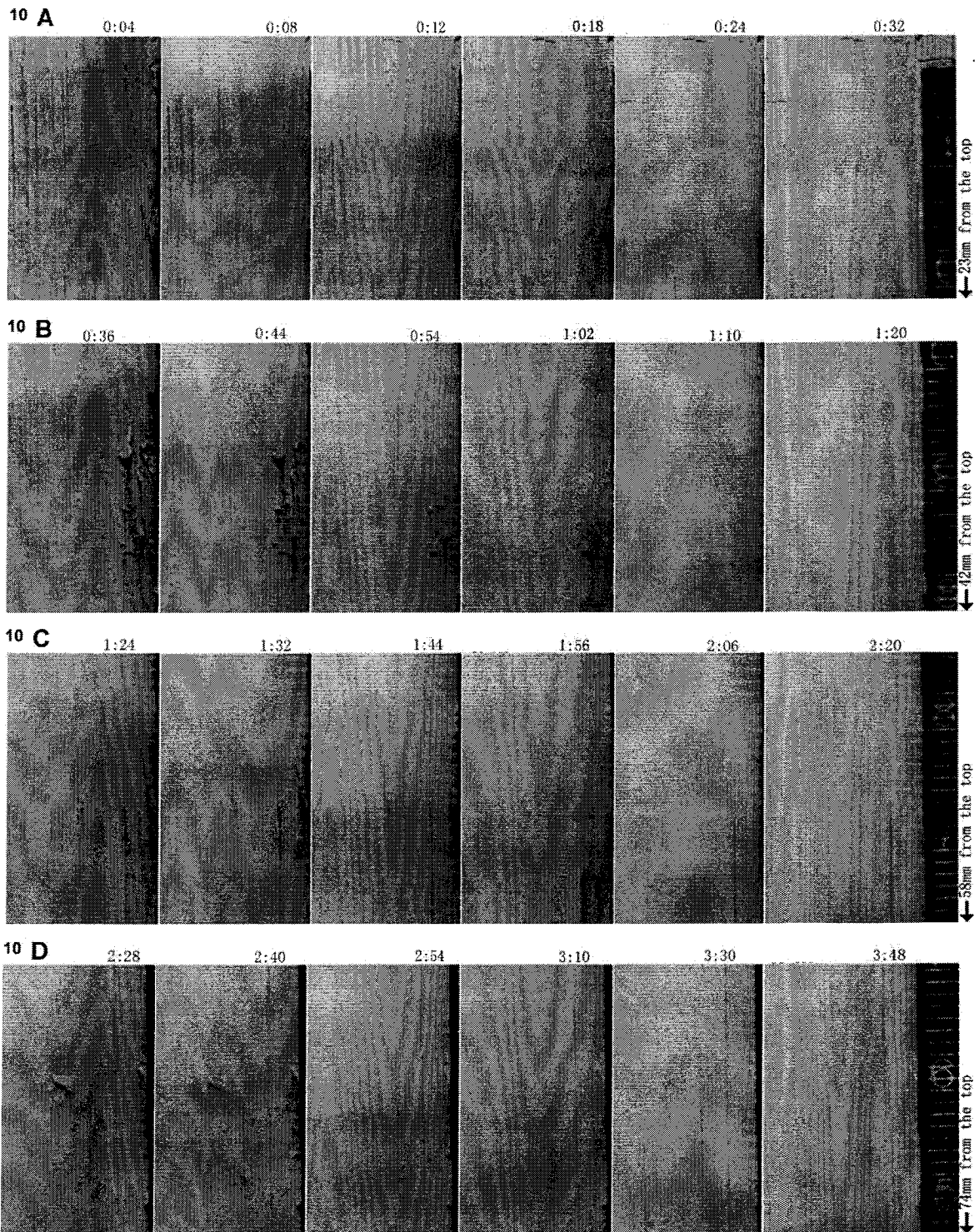


Figure 4.4.3 Serial images of the freezing process of test #9 (25.7g/L, -5°C on the top, 0 kPa, scale in millimeter).



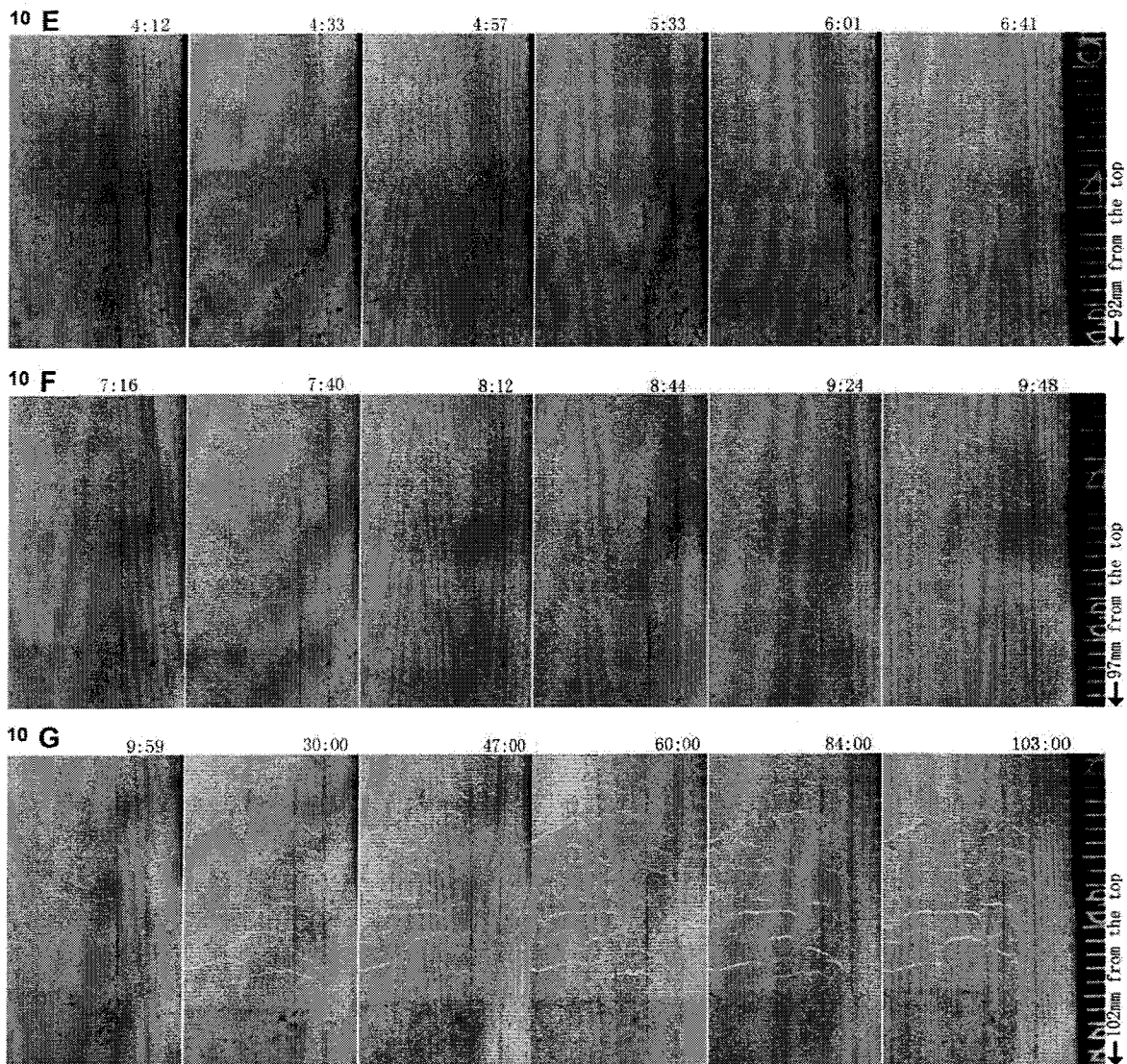


Figure 4.4.4 Serial images of the freezing process of test #10 (23.6g/L, -14.5°C on the top, 0 kPa, scale in millimeter).

Table 4.4.4 Image locations for Figure 4.4.4.

Row #	Distance for the top of the sample *	
	Top edge (mm)	Bottom edge (mm)
A	1	23
B	20	42
C	36	58
D	52	74
E	70	92
F	75	97
G	80	102

\* the top of the sample is the top of the sample after consolidation

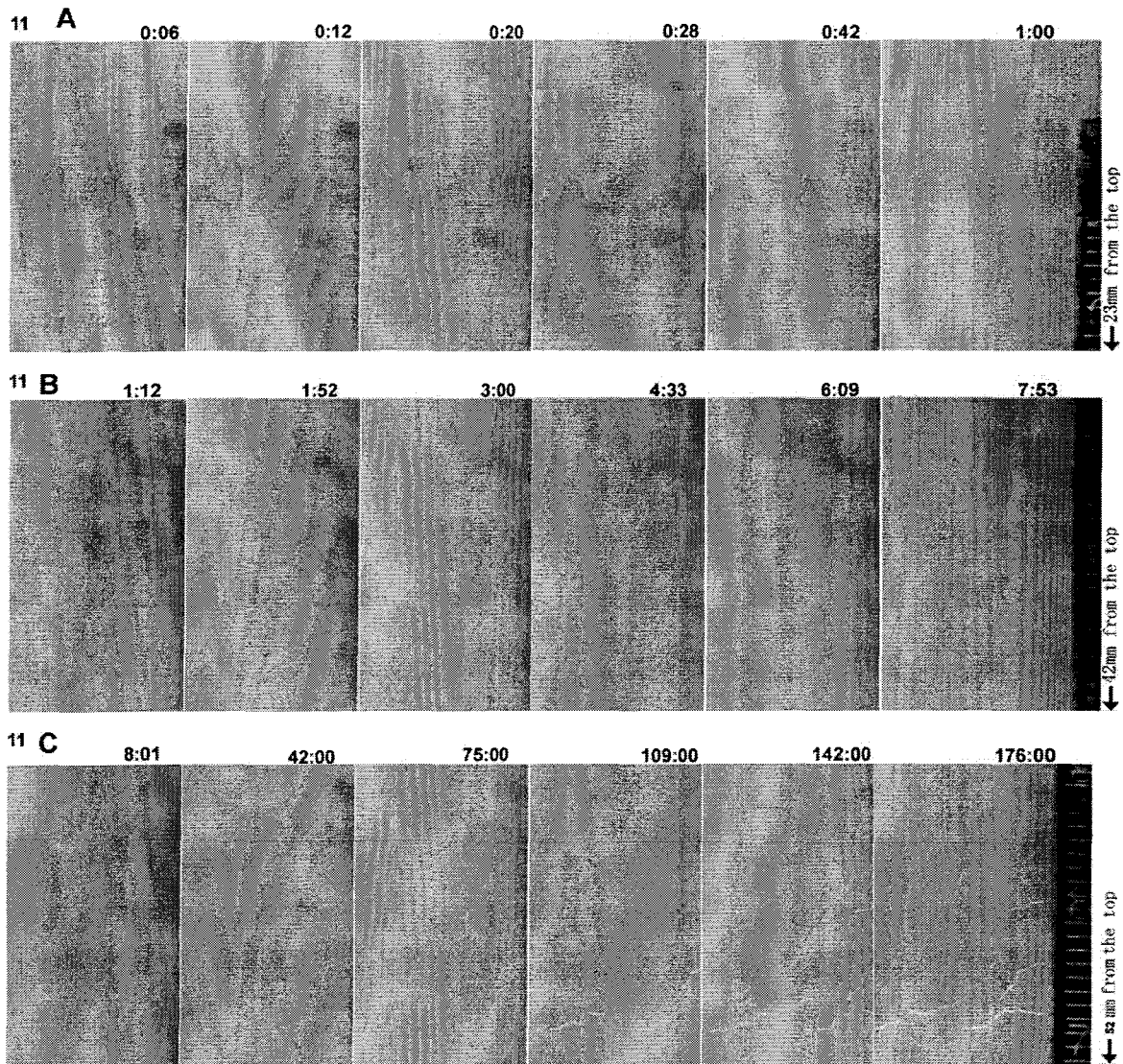


Figure 4.4.5 Serial images of the freezing process of test #11 (24.4g/L,  $-5^{\circ}\text{C}$  on the top, 200 kPa, scale in millimeter).

Table 4.4.5 Image locations for Figure 4.4.5.

Row #	Distance for the top of the sample*	
	Top edge (mm)	Bottom edge (mm)
A	1	23
B	20	42
C	30	52

\* the top of the sample is the top of the sample after consolidation

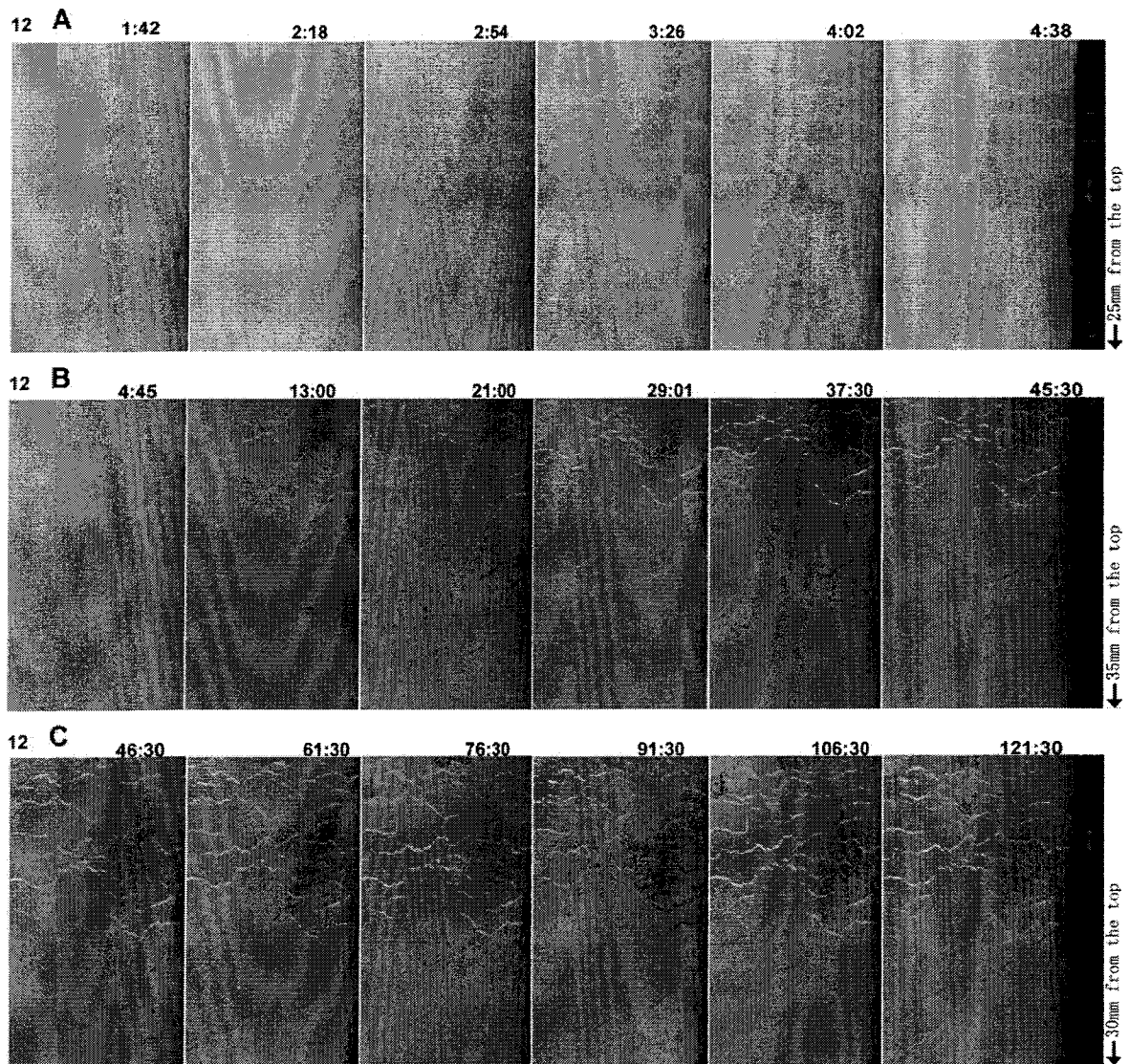


Figure 4.4.6 Serial images of the freezing process of test #12 (24.7g/L,  $-2.5^{\circ}\text{C}$  on the top, 0 kPa, scale in millimeter).

Table 4.4.6 Image locations for Figure 4.4.6.

Row #	Distance for the top of the sample *	
	Top edge (mm)	Bottom edge (mm)
A	3	25
B	13	35
C	18	30

\* the top of the sample is the top of the sample after consolidation

#### **4.4.1 Frost penetration during tests with saline pore fluid**

The results already show that the frost penetration rate is influenced by the pore water salinity, which affects the freezing point. Table 3.1 summarized conditions for tests #1, #7, #8 and #9 that freeze under similar boundary temperature gradient and vertical stress, but each had different pore water salinities (0, 5.9, 10.2, 25.7g/L). Figure 4.4.7 illustrates the frost penetration during these tests. The fastest penetration rate occurred in test #1, followed by tests #7, #8, and test #9. At steady state, the frozen front remained at the height of 36 mm in test #1, 48 mm in test #7, 56 mm in test #8, and 75 mm in test #9.

In test #9, the salinity (25.7g/L) was so high that it was difficult to locate the active ice lens (discussed in 4.4.2). Therefore, both Figures 4.4.8 and 4.4.9 showing frozen fringe thickness do not include data from test #9. These figures show that the thickness of the frozen fringe does not differ significantly for these different salinities from 0 to 10.2 g/L.

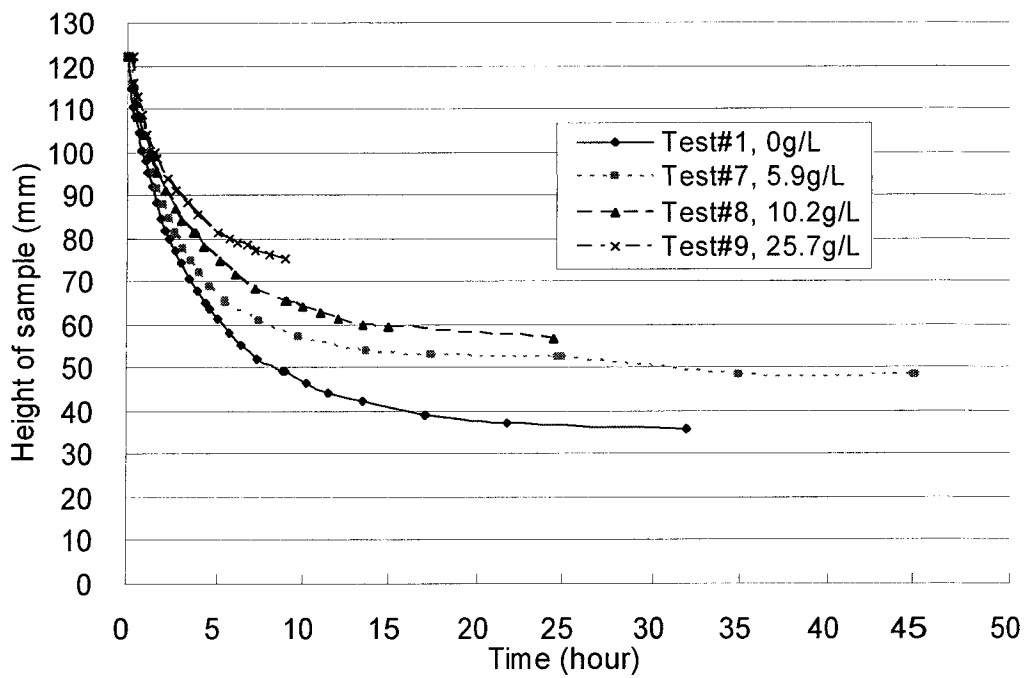


Figure 4.4.7 Frost penetration under different pore water salinities.

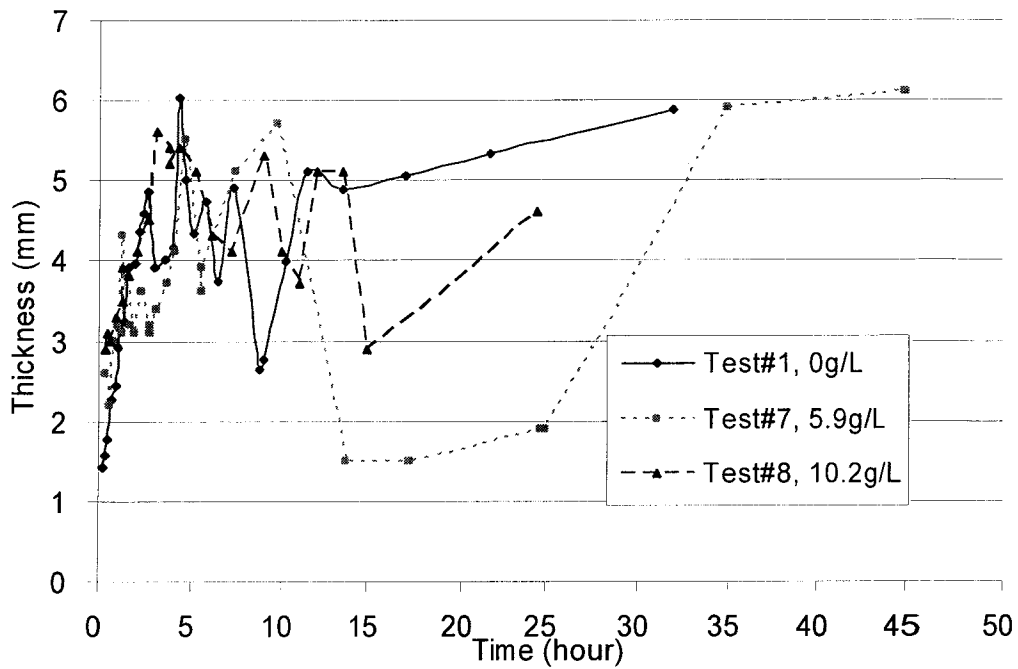


Figure 4.4.8 Frozen fringe thicknesses with time with different pore water salinities.

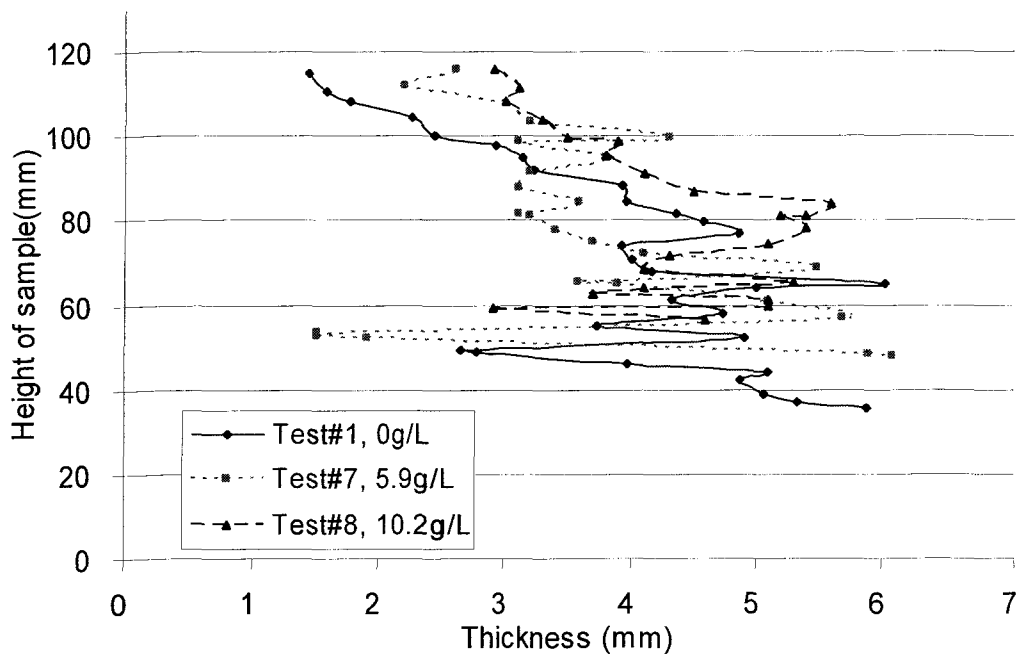


Figure 4.4.9 Frozen fringe thicknesses along the height of the samples with different pore water salinities.

#### 4.4.2 Ice lens formation and development

Figure 4.1.1 and Figures 4.4.1 through 4.4.3 show the formation and development of the horizontal ice lenses during both transient and steady state freezing under similar temperature conditions and vertical applied stresses but with different pore water salinities (Table 3.1). At the beginning of test #1, there was no visible ice lens (Figure 4.1.1). After the frost penetrated 7 mm into the sample (15 minutes), the ice lenses were visible but were very fine and tightly spaced. With further frost penetration, the ice lenses grew thicker and the distance separating ice lenses increased until the final ice lens initiated at a depth of 80 mm, after 21 hours (Figure 4.1.6). In test #7, with a pore water salinity of 5.9 g/L, visible ice lenses started to appear after 23 minutes as the freezing front penetrated 6mm into the sample. The ice lens arrangement in test #7 is shown in Figure 4.4.1, which is similar to the ice lens distribution in test #1 but it appears more three dimensional,

especially in the first two rows of the images in Figure 4.4.1. In test #8, with a pore water salinity of 10.2 g/L, visible ice lenses started to form after 21 minutes as the freezing front penetrated 6 mm into the sample. Compared to test #7, the ice lenses in test #8 appear more three dimensional throughout the frozen zone. The depths of the final ice lens are at 68 mm in test #7, and 63 mm in test #8. The ice lens formation in test #9 (25.7 g/L) dramatically changed from that observed in tests #7 and #8. The ice lenses were hardly visible during the first 34 minutes after freezing as the freezing front penetrated to 9 mm depth. Only a few, fine and reticular ice lenses became visible during the freezing. The active ice lenses were well distributed at different elevations of the sample. Furthermore, no continuous final ice lens formed in test #9. The location of the final ice lens for each of the four tests discussed above is presented in Figure 4.4.10. The same characteristics of ice lens formation as in test #9 were also found in tests #10, #11 and #12, which had similar salinities.

The final ice lens thicknesses in tests #1, #7 and #8 are plotted versus time in Figure 4.4.11. The data used for this figure were directly measured from the images taken during each freezing test. In test #1, the final ice lens initiated 21.75 hours after the start of freezing and grew at an average rate of 0.013mm/hour until the end of the test. In test #7, with 5.9 g/L pore water salinity, the final ice lens initiated 13.77 hours after the start of freezing and grew at an average rate of 0.0127mm/hour until the end of the test. In test #8, with the pore water salinity of 10g/L, the final ice lens initiated at 15.03 hours after the start of freezing and grew at an average rate of 0.0095mm/hour until the end of the test. In tests #9, #10, #11 and #12, there were no layered final ice lenses during each test.

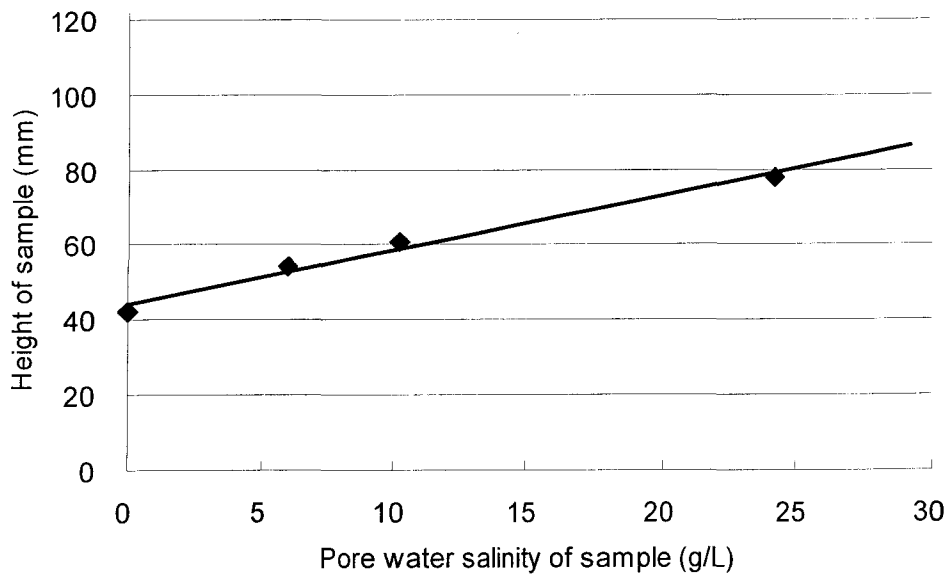


Figure 4.4.10 Location of the final ice lens with different pore water salinities .

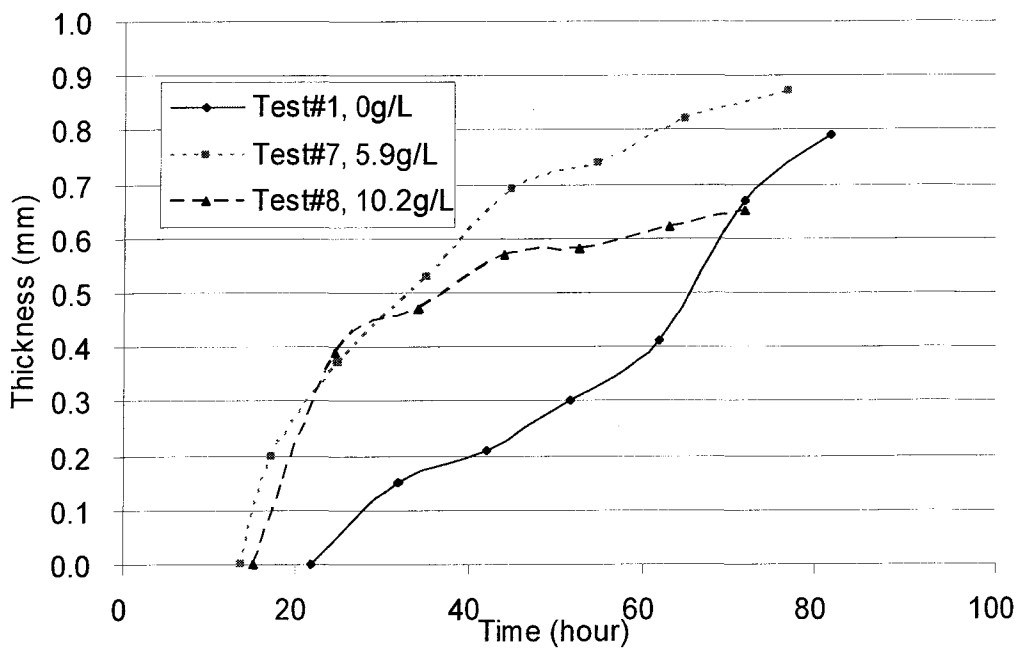


Figure 4.4.11 Final ice lens growth with different pore water salinities.

### 4.4.3 Heave and water intake

The frost heave and water intake were monitored and recorded during each test. Figures 4.4.12 and 4.4.13 show the water intake and frost heave for tests #1, #7, #8 and #9 while Figures 4.4.14 and 4.4.15 illustrate the water intake and frost heave in tests #9, #10, #11 and #12. The boundary condition for each test is summarized in Table 3.1. The time for water to start flowing into the sample and the onset of heave, and water intake and heave are presented in Table 4.4.7. Except for tests #9 and #12, all other tests exhibited pore water expulsion. Tests #10 had the greatest and that of tests #7 and #8 were close to 0 mL.

*Table 4.4.7 Starting time and total amount for water in take and frost heave for all the saline tests.*

Test #	T <sub>top</sub> (oC)	σ <sub>f</sub> (kPa)	S (g/L)	Water intake		Frost heave	
				Starting time (hours)	Total amount (mL)	Starting time (hours)	Total amount (mm)
1	-5	0	0	36	-12.4	32	0.71
7	-5	0	5.9	24	-1.6	21	1.53
8	-5	0	10.2	25	-1.4	0	1.94
9	-5	0	25.7	3.5	28.2	0	5.51
10	-14.5	0	23.6	23	-16.3	0	0.61
11	-5	200	24.4	154	-11.5	0	0.92
12	-2.5	0	24.7	6.5	19.1	0	2.96

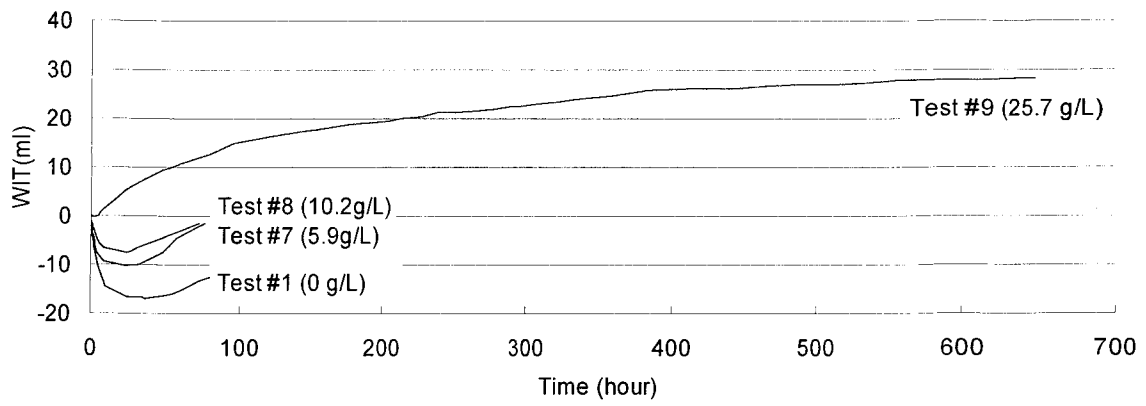


Figure 4.4.12 Water intake with different pore water salinities.

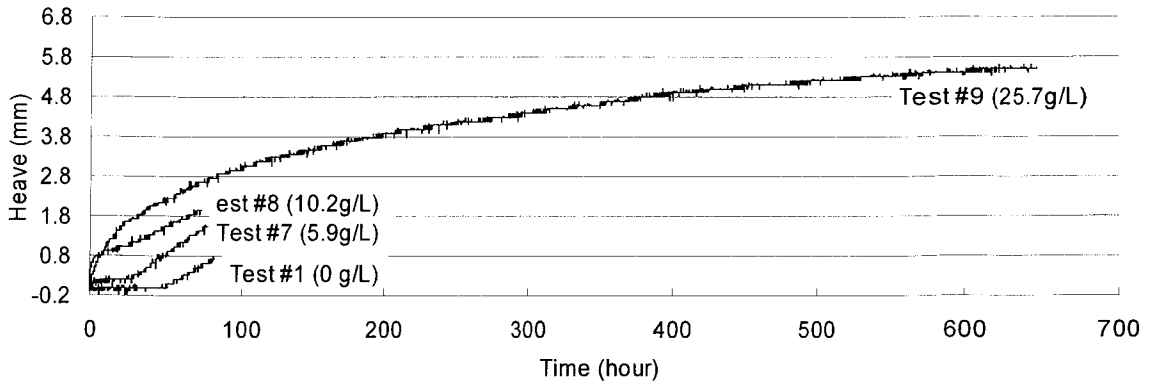


Figure 4.4.13 Frost heave with different pore water salinities.

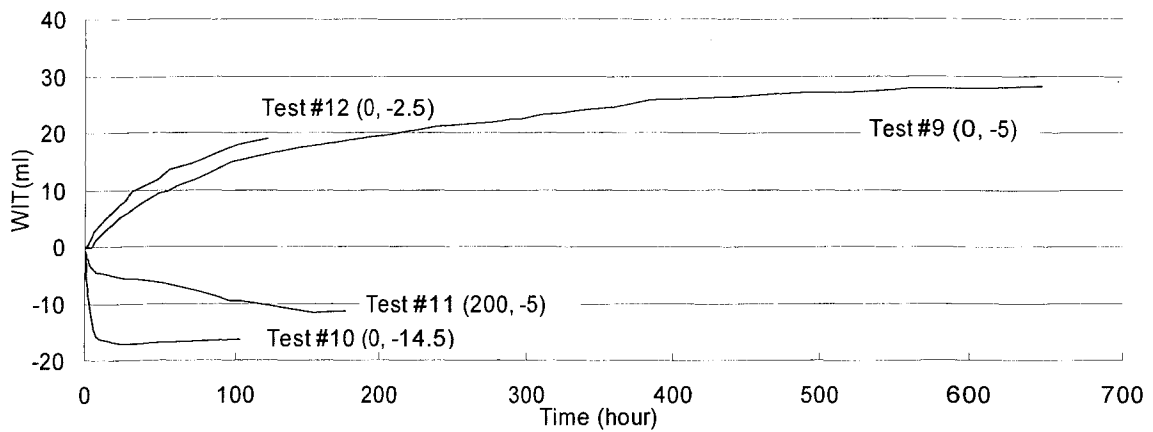


Figure 4.4.14 Water intake in tests #9, #10, #11 and #12 (vertical pressure (kPa), top plate temperature( $^{\circ}$ C)).

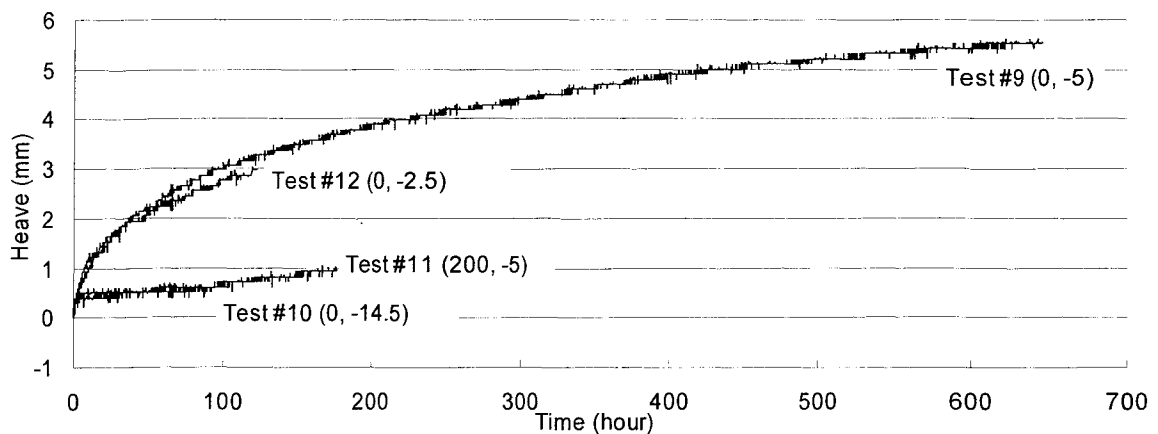


Figure 4.4.15 Frost heave in tests #9, #10, #11 and #12 (vertical pressure (kPa), top plate temperature( $^{\circ}$ C))

#### 4.4.4 Moisture content and redistribution, and salinity rejection

Normalized moisture content profiles after testing are shown in Figure 4.4.16 and 4.4.17. Figure 4.4.16, shows the lowest relative moisture content recorded in the unfrozen zone in test #1, followed by tests #7, #8 and #9. The moisture content was close to the initial value in the lower 20 mm in tests #8 and #9. In the frozen

zone (above the final ice lens in each test), the values of relative moisture contents in tests #1, #7 and #8 are similar above of 70 mm, but the value in test #9 is substantially larger. The thickness of the zone in which the moisture content increased dramatically with increasing salinity: 7.5mm in test #1, 10mm in test #7, 12.5mm in test #8 and 20mm in test #9. Compared to test #9 (Figure 4.4.17) the moisture contents in both the frozen and unfrozen zones are lower for tests #10 and #11, and the value for test #12 is lower in frozen zone but higher in the unfrozen zone.

The salinity distribution changed during freezing in each test. The results of tests #7, #8 and #9 are shown in Figure 4.4.18 and the results of tests #9, #10, #11 and #12 are shown in Figure 4.4.19. To compare the salinity profiles in each test, the values in Figure 4.4.18 and 4.4.19 were normalized to the initial value. In each test, the salinity of the pore water (including ice lenses) along the height of the sample changes near the final ice lens. The salinity just beneath the final ice lens in each test suddenly increases while the salinity immediately above the final ice lens dramatically decreases, which indicates that solute rejection occurs when the final ice lens forms.

It is noticed that the elevation of the final ice lens and the maximum value of moisture content does not coincide in the high salinity tests (salinity of about 25 g/L) as it does in non-saline tests. The final ice lens is lower than the location of maximum moisture content at 5 to 25 g/L. The reason for this phenomenon is that several ice lenses grow simultaneously above the final one. No continuous and thick final ice lenses were observed during the high salinity freezing tests.

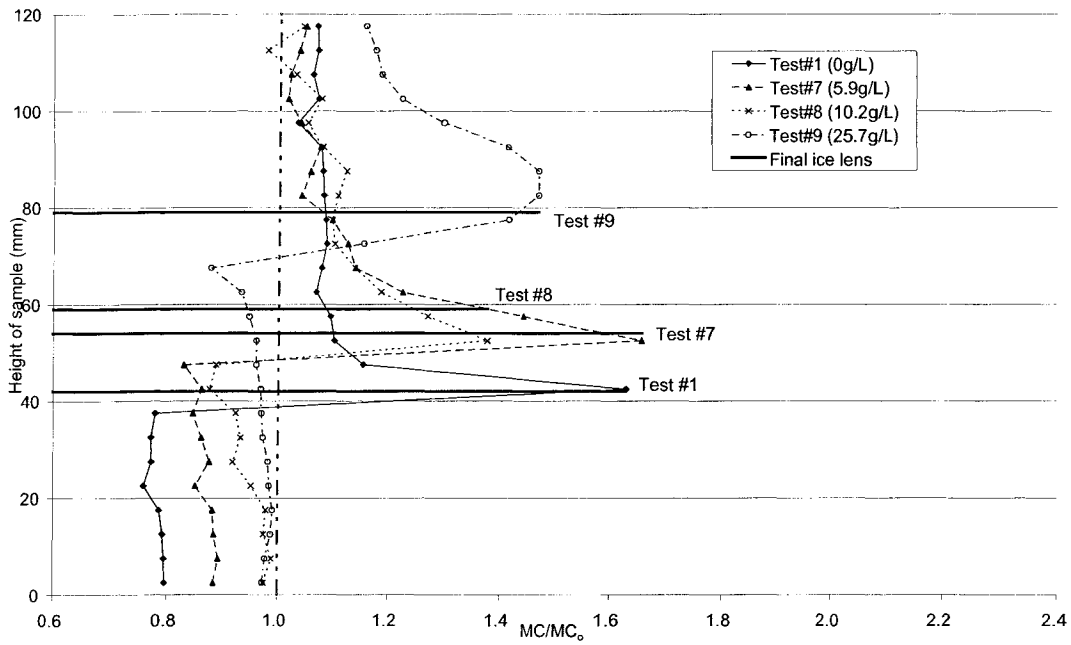


Figure 4.4.16 Moisture content (ratio) profiles after frozen in tests #1, #7, #8 and #9

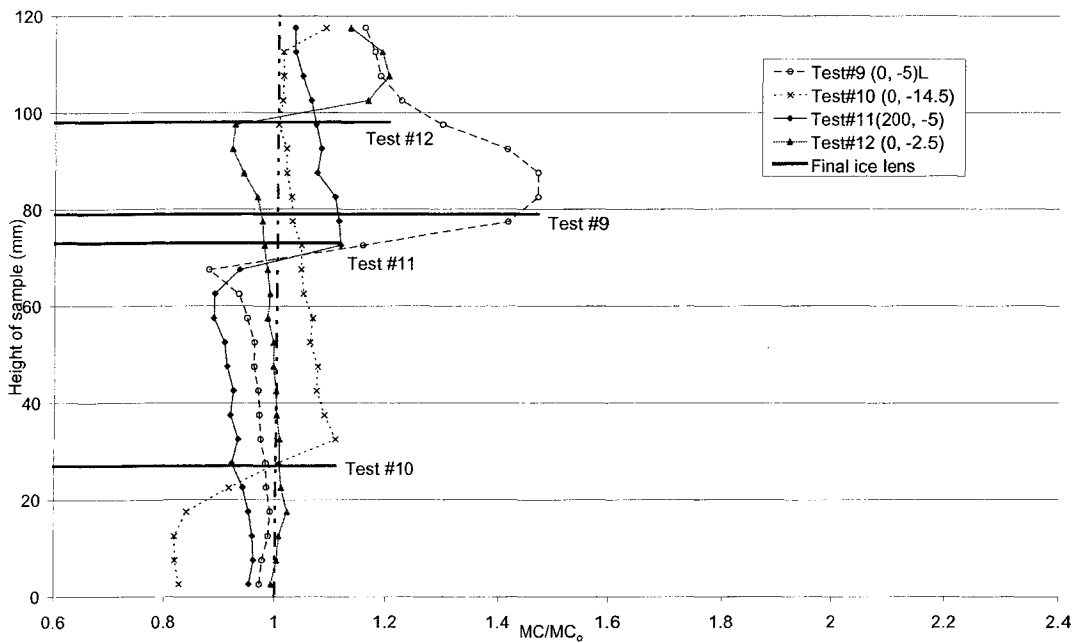


Figure 4.4.17 Moisture content (ratio) profiles after frozen in tests #9, #10, #11 and #12 (vertical pressure (kPa), top plate temperature( $^{\circ}$ C))

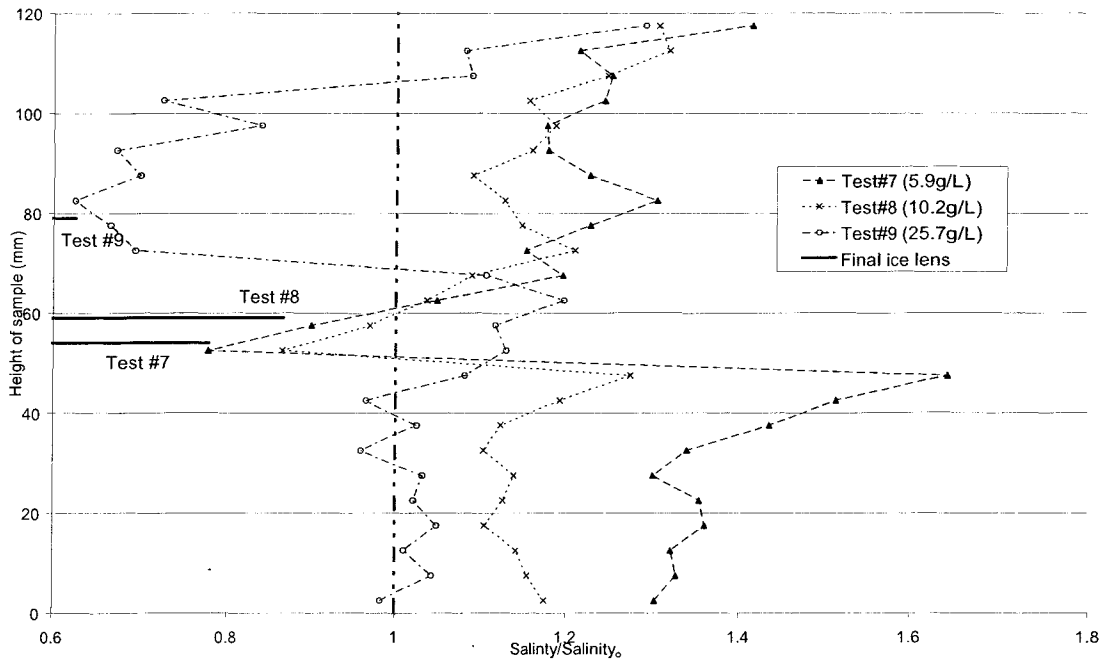


Figure 4.4.18 Salinity (ratio) profile after frozen in tests #7, #8 and #9

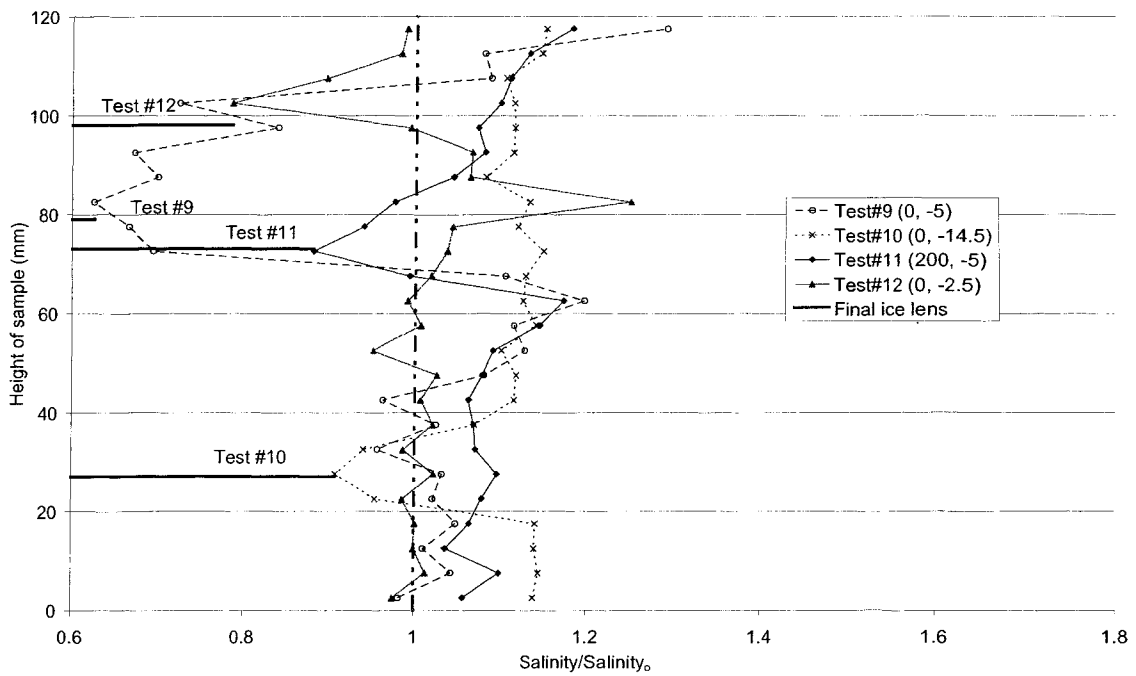
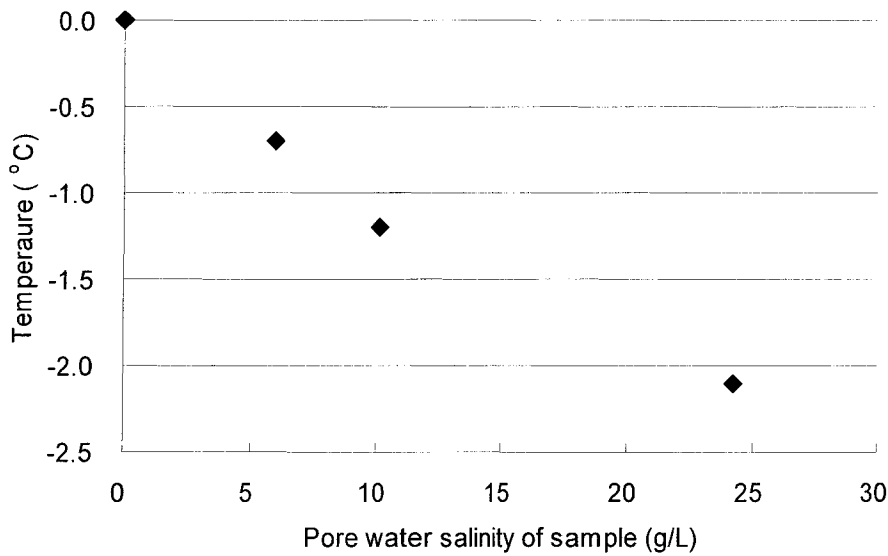


Figure 4.4.19 Salinity (ratio) profile after frozen in tests #9, #10, #11 and #12 (vertical pressure (kPa), top plate temperature( $^{\circ}$ C)).

#### **4.4.5 Discussion of the effects of pore water salinity**

Six freezing tests were designed to study the effect of salinity on the freezing process. As shown in Figure 4.4.7, the frost penetration was influenced significantly by the salinity of the pore water. Higher salinity causes a lower frost penetration rate and decreases the depth of the frost penetration. The frost penetration herein refers to the freezing front as observed by the fluorescein in the water, not the 0°C isotherm. It is well known that the freezing point of the saline water decreases with increasing salinity of the solution. In Figures 4.4.8 and 4.4.9, the thicknesses of the frozen fringe in tests #1, #7 and #8 is similar even though the salinities of the tests differ. The temperature profile in both the frozen and unfrozen zones is linear in these freezing tests of saline soil similar to that in Section 4.1. The similar frozen fringe thickness for different salinities implies that the temperature of the active ice lens decreases with increasing pore water salinity and this temperature corresponds to the decreased freezing point. Figure 4.4.20 shows the freezing point with different pore water salinities, The values presented in this figure are determined by comparing the images and the temperature profile within each test.



*Figure 4.4.20 Observed pore freezing temperature with different salinities.*

In tests #9, #11 and #12 (Figures 4.4.3, 4.4.5 and 4.4.6), the freezing front was not as distinct as the freezing front at low salinity, such as tests #7 and #8. Greater unfrozen water was observed in the frozen zone. However, in test #10 with similar pore water salinity, the freezing front appeared clearly in Figure 4.4.4 and unfrozen water was hardly observed in the frozen zone. This might be due to the effect of the high temperature gradient,  $1.38^{\circ}\text{C}/\text{cm}$  at steady state. The temperature gradient in tests #9 was  $0.57^{\circ}\text{C}/\text{cm}$ ,  $0.55^{\circ}\text{C}/\text{cm}$  for test #11 and  $0.40^{\circ}\text{C}/\text{cm}$  for #12 at thermal steady state. The salinities in tests #9, #10, #11 and #12 were all 25 g/L, which is close to the salinity of sea water. Since the temperature gradients in nature are much smaller, e.g.  $0.28^{\circ}\text{C}/\text{cm}$  in the high Arctic (Nakawo and Sinha, 1981), unfrozen water is expected to be present in frozen zones in the natural frozen saline soils. This unfrozen water in the frozen zone may result in significant engineering problems in saline soils because the strength of the frozen soil is strongly influenced by the amount of the unfrozen water (Hivon and Segó 1995).

More evidence for the existence of unfrozen water in the frozen zone is that ice lenses in part of the frozen zone grew simultaneously while the sample was at thermal steady state. In tests #9, #11, and #12, several ice lenses at different elevations developed above the last ice lens at the same time. This was also confirmed by the relatively wide range of enhanced moisture content in the frozen zone as observed in the moisture profile (Figures 4.4.16 and 4.4.17).

The ice lens formation is related to the pore water salinity. Higher pore water salinity reduces the ice lens formation due to the decreased suction at the ice water interface. Konrad (1990) showed the decreased suction during thermal steady state for saline Devon silt. This was confirmed by the decrease of the final ice lens growth, the heave and the water intake rate (Figures 4.4.11 through 4.4.13). It was further found that the formation of the ice lenses during the transient heat flow was also inhibited with increasing pore water salinity (Figures 4.1.1 and 4.4.1 through 4.4.3). The hydraulic conductivity does not decrease with increasing pore water salinity. This implies that the suction at the ice-water interface decreases with increasing pore water salinity resulting in a limited ice lens formation.

Not only ice lenses are inhibited by the pore water salinity, but also ice lenses generated during freezing grow in a more 3-dimensional structured pattern compared to during the freezing of non-saline soils (Figure 4.1.1, Figures 4.4.1 to 4.4.6). The salinity of the pore water may not be uniform in the sample. When a segregated ice lens initiates, it is likely to develop in the direction where the salinity is the lowest. This non-uniformity of pore water salinity allows the ice lens to grow in a different way compared to a non-saline sample. More 3-dimensional ice lenses are therefore formed in a saline soil sample as they freeze.

The salinity redistribution (Figures 4.4.18 and 4.4.19) shows that nearly no solute rejection occurred until the freezing reached thermal steady state. Konrad and McCammon (1990) established the relationship between solute rejection and freezing conditions. They proposed a threshold rate of cooling of  $3^{\circ}\text{C}/\text{day}$  above which no solutes are rejected from the ice matrix. The cooling rate is the product of the frost penetration rate and the temperature gradient near the freezing front. In this step-freezing test, both the temperature gradient and the frost penetration rate decreased with the increasing frost penetration. The significant changes of salinity in Figures 4.4.18 and 4.4.19 imply that the solute rejection only takes place close to the final ice lens when the freezing is at thermal steady state, i.e. the cooling rate is close to zero.

Other evidence for solute rejection is the melting at the bottom of the frozen fringe at thermal steady state during the freezing test with saline pore fluid. After the final ice lens formed, the freezing front should remain at the same level until the end of the test if the pore freezing point did not change. However, the freezing front in all saline tests moved up continuously during thermal steady state, i.e. part of the frozen fringe melted (Figures 4.4.1 to 4.4.6). This shows that the pore freezing point decreased with time because the higher position in the soil sample has a lower temperature in a step-freezing test during thermal steady state. According to the test procedure, the water supplied has the same salinity as the pore water. When the water is drawn in to the final ice lens and freezes, solutes are expelled and remain in the unfrozen water in the frozen fringe. This results in an increase in the salinity of the unfrozen water in the frozen fringe. The increased salinity decreases the freezing point of the pore fluid in the frozen fringe, and induces the freezing front to move to a higher position, where the temperature is lower .

## 5 SUMMARY AND CONCLUSIONS

To study the freezing behaviour of saturated fine grained soils under different boundary conditions, 12 one-dimensional freezing tests on Devon Silt were carried out. The formation of ice lenses and frost penetration were visually recorded using a special tracer and a digital camera during the experiments. The tracer appears green under ultra violet light when dissolved in water and does not change the freezing point of the water. When the solution is frozen it loses its green colour. All tests were carried out in a cold room under open-system freezing and step-freezing boundary temperature condition. To simulate natural freezing conditions, the tests were set up so that the frost penetrated into the sample from the top downward.

A total of 12 laboratory freezing tests (Table 3.1 in Chapter 3) were carried out to study the effects of different temperature gradients, applied vertical pressures and pore water salinities on the freezing process, ice lens formation, and frost heave. Test #1, with non-saline pore water and zero vertical pressure, was used as a reference with temperatures of  $-5^{\circ}\text{C}$  of the top plate and  $2^{\circ}\text{C}$  of the bottom plate. This test revealed information about the general freezing process. A series of tests (tests #1, #2 and #3) were used to study different temperature gradients. Four tests (tests #1, #4, #5 and #6) were carried out to investigate the freezing under different vertical pressures. A series of tests (tests #1, #7, #8 and #9) were carried out to study the freezing with different pore water salinities. Finally, Tests #9, #10, #11 and #12 were tested at similar water salinities (23.6 to 25.7 g/L), to study the effects of different vertical pressures and temperature gradients on the freezing process and solute rejection. The boundary conditions of each series of tests are summarized in Table 5.1

Table 5.1 Summary of test conditions of each series of tests

Tests No.	Boundary temperatures (°C )	Vertical pressure (kPa)	Pore water salinity (g/L)
1	-5 (top) 2(bottom)	0	0
1, 2, 3	-2, -5, -14.5 (top) 2 (bottom)	0	0)
1, 4, 5, 6	-5 (top) 2 (bottom)	0 to 400	0
1, 7, 8, 9	-5 (top) 2 (bottom)	0	0 to 25
9, 10, 11, 12	-2.5, -5, -14.5 (top) 2 (bottom)	0, 200	Similar (~25)

The rate of frost penetration decreases with increasing time and depth of frost penetration due to the decreasing cooling rate at the freezing front in a step-freezing test. The temperature profile and the existence of a frozen fringe indicate that the segregated ice lenses form in the frozen zone at the temperature slightly below the pore water freezing point. The changed frozen fringe thickness further implies that the temperature of ice lens formation is not constant but depends on the boundary conditions.

Both horizontal and vertical ice lenses are formed during the freezing. The horizontal ice lenses get thicker, and the space between two adjacent ice lenses increases as the frost front penetrates deeper into the sample. The vertical ice lenses initiate before the warmest horizontal ice lens forms in the frozen fringe. It

is thought that water is drawn up to the active horizontal ice lens causing the soil in unfrozen zone close to the frozen fringe to dehydrate and shrink so that small vertical cracks to be formed where the vertical ice lens initiates.

The final ice lens keeps growing until the end of the freezing. The ice lens growth rate decreases with time due to the consolidation of the unfrozen layers below, which reduces its hydraulic conductivity. This consolidation is caused by the suction generated on the warm side of the active ice lens.

Additional water migration in the frozen zone above the final ice lens was further observed in these investigations, which has not been previously reported. The ice lens above the final one still grew after the final ice lens had been formed, which has generally been thought as a cutoff with regard to water migration from the unfrozen soil.

Due to the water migration caused by the suction, the moisture content is redistributed in the soil sample during freezing. The frozen zone has a higher moisture content whereas the unfrozen zone is lower than the initial value. The moisture contents tend to be the initial value at the top and bottom of the sample. Figure 5.1 schematically shows the soil sample and moisture content redistribution after a freezing test.

The temperature gradient affects the frost penetration rate, thickness of the frozen fringe, the ice lens formation and structure, the final ice lens growth rate and the frost heave. Obviously, the frost penetration rate increases with increasing the temperature gradient due to the higher heat flow, which is related to the temperature gradient and thermal conductivity of the medium. The frozen fringe changes its thickness according to the temperature gradient. A higher

temperature gradient results in a thinner frozen fringe. The ice lens formation and structure are also related to the temperature gradient. Under very high temperature gradient, it is hard to form visible segregated ice lenses due to the fast frost penetration. With decreasing temperature gradient, fine closely spaced ice lenses are formed; decreasing the temperature gradient further, the ice lenses get thicker and the space between two adjacent ice lenses increases. The final ice lens growth rate increases with increasing temperature gradient due to the stronger suction generated by the larger temperature gradient. Most frost heave is induced by the final ice lens growth. The temperature gradient therefore affects the frost heave and water intake rate through affecting this final ice lens growth.

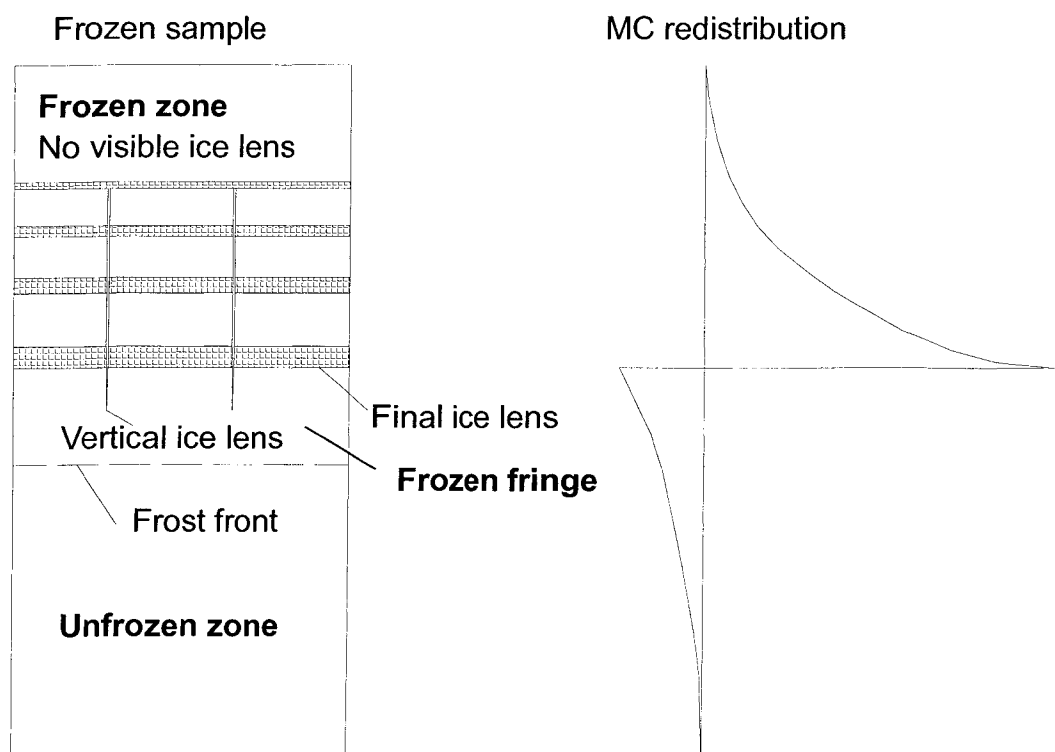


Figure 5.1 Schematic frozen sample and MC redistribution after freezing

The heat flow is governed by the temperature gradient and the thermal conductivity of the medium. Generally, a reduction in the void ratio of a soil increases the thermal conductivity of the soil mixture. However, in these investigations, the frost penetration rates did not change obviously (Figure 4.3.4 in Chapter 4) even though the vertical stresses varied but the boundary temperature gradients remain similar. This implies that the change of the conductivity of the soil with different vertical stress was small in these investigations. However, the thickness of the frozen fringe is affected by different vertical stresses applied. For an increased vertical stress, the freezing point of the pore water does not change significantly but the ice lenses initiated at a lower temperature due to the increase of the suction on the capillary water caused by the reduced void ratio. This resulted in an increase in the thickness of the frozen fringe with increasing vertical stress. In addition, an increased vertical stress reduces the suction at the warm side of the active ice lens as well as the hydraulic conductivity of the soil due to the decreased void ratio by reducing the unfrozen water amount within the frozen fringe. All of these inhibit the formation and development of the ice lenses including the final ice lens. The vertical stress therefore limits the frost heave.

Increasing the pore water salinity depresses the freezing point of the fluid. This results in an increased amount of unfrozen water in the frozen zone and also reduces the frost penetration rate. The frozen fringe thicknesses did not change obviously with the change in the pore fluid salinity (Figure 4.4.9 in chapter 4). Solutes in the pore water reduce the suction at the warm side of the active ice lens, which cause the ice lens to grow at a smaller rate than non-saline tests. The higher the salinity the smaller the growth rate of the ice lenses, including the final one. In addition, ice lenses in saline freezing appear to have a more 3D-structure compared to non-saline tests. The lower ice lens growth rate results in a lower

frost heave rate. Salinity redistribution was only noticed at the zone close to the final ice lens, where the cooling rate is low. This confirms earlier findings that show a threshold for the cooling rate, below which solute rejection can occur (Konrad and McCammon 1990).

For similar salinity tests, the effects of the temperature gradient and vertical stress are similar to the results obtained from the non-saline tests described above.

Freezing behaviour influenced by factors discussed is summarized in Table 5.2.

Table 5.2 Freezing behaviour influenced by temperature gradient, stress and salinity.

Freezing Behaviour	Temperature Gradients	Applied Stresses	Pore water Salinities
Frost penetration rate	Yes	-	Yes
Frozen fringe thickness	Yes	Yes	-
Ice lens formation and structure	Yes	Yes	Yes
Final ice lens growth rate	Yes	Yes	Yes
Frost heave and water migration	Yes	Yes	Yes

## 6 RECOMMENDATIONS

The detailed observations on the freezing process of fine-grained soils revealed phenomena that have never been observed and visually documented before. A unique observation is that after the final ice lens formed, the ice lenses within the frozen zone, especially the one immediately above the final one, continued to grow. This implies that additional water migration takes place even between ice lenses that have no access to water from the unfrozen layer below the final ice lens. Further tests need to be carried out to establish the mechanism responsible for and consequence of this phenomenon.

In further tests, the ambient temperature around the freezing cell needs to be improved to ensure no temperature fluctuation of the freezing cell. Improved insulation is recommended. In the present investigations, the room temperature fluctuated with time, which resulted in melting of the ice near the final ice lens in each test. The melted ice might be the water supply for the growth of the ice lenses above the final one. If the room temperature is controlled properly and the ice lenses above the final one are still observed to grow, current theory of ice lens growth and water migration may need to be adjusted.

Furthermore, to study the suction which causes the water migration and the consolidation of unfrozen zone, pore water pressure measurement during freezing is highly recommended. Using this measurement, the pore water pressure profile and the change of pore pressure with time can be obtained. This can provide useful information to establish the mechanism for water migration both to the warmest ice lens and to the ice lens above it.

Two other factors influencing the accuracy of the present freezing tests are the

friction between the cell wall and the frozen soil, and the measuring method of the height of the soil samples.

The friction resulted in an increase in the vertical pressure on the warmest ice lens and the frozen fringe in each test, which reduced the accuracy of studying the effects of vertical pressure on freezing process. To solve this problem, a special material with lower friction for the cell wall or other efficient method to reduce this friction is recommended.

Sample height measurement inaccuracy affected the accuracy of the initial moisture content calculation. In the present freezing tests, the moisture contents of soil samples before freezing were calculated using the moisture content determined before consolidation and the sample height before and after consolidation. The measurement of the sample height in the present tests used a tape scale outside the freezing cell. Due to the thickness of the cell wall, error (less than 0.5 mm) could not be avoided. A scale engraved on the inside of the cell wall can reduce this error on the sample height measurement.

## 7 REFERENCE

Anderson, D.M. and Tice, A.R. 1972. Predicting unfrozen water contents in frozen soils from surface area measurements. U.S. Highway Research Record, Report No. 393: 12-18.

Arenson, L.U. and Segó D.C., 2004. Freezing processes for a coarse sand with varying salinities. In Proceedings of the Cold Regions Engineering & Construction conference. Edmonton, Alberta, Canada, May 16-19, 2004: CD\_ROM.

Beskow, D.M. 1935. Soil freezing and frost heaving with special application to roads and railroads. (Translated by J. Osterberg, Northwestern University Technological Institute, Evanston, Ill., 1947) Sveriges Geologiska Undersökning, Serie C.

Bouyoucos, G.J. 1916. The freezing point method as a new means of measuring the concentration of the soil solution directly in the soil. Michigan Agricultural College Experiment Station, Technical Bulletin 24: 1-44.

Danilov, I.D. 1969. The permafrost-facies structure of the watershed relief forming deposits of the lower Enisei. (In Russian). In problems of cryolithology. Vol. 1. Edited by Popov, A. I. Moscow University Press, Moscow, U.S.S.R. 93-105.

Hivon, E.G. and Segó, D.C. 1995. Strength of frozen soils. Canadian Geotechnical Journal, 32(2): 336-354.

Hass, H. and Seegers, J., 2000. Design of ground freezing as temporary support during the construction of underground structures of the subway line "U5" in Berlin. Proceedings of the international symposium on ground freezing and frost action in

soils, Louvain, Belgium, Sept. 11-13, 2000, 9: 295-298.

Hoekstra, P., 1969. The physics and chemistry of frozen soils. Highway research Board, Special Report No. 103: 78-90.

Huang, S. L., Bray, M.T., Akagawa, S., and Fukuda, M., 2004. Field investigation of soil heave by a large diameter chilled gas pipeline experiment, Fairbanks, Alaska. *Journal of Cold Regions Engineering*, 18:1:2-34.

Jumikis, A.R. 1966 Thermal soil mechanics. Rutgers University Press, New Jersey.

Kaplar, C.W. 1970. Phenomenon and mechanism of frost heaving. U.S. Highway Research Record, Report No. 304: 1-13.

Katasonov, E. M. 1960. Cryogenic texture of alluvial deposits in permafrost, (In Russian). *Acad. Sci. U.S.S.R., Inst. Permafrost Stud., Yakutsk, U.S.S.R.* 2:15-21.

Katasonov, E. M. 1961. Composition and cryogenic structure of permafrost. In permafrost investigations in the field, Part1 Chapter II. *Acad. Sci. U.S.S.R., V. A. Obruchev Inst. Permafrost Stud., Moscow, U.S.S.R.* Translated by Poppe, V., NRCC TT 1358, 1969, 25-36.

Katasonov, E. M. 1967. Features of deposits formed under permafrost conditions. In *Arctic and alpine environments*. Edited by Wright Jr., H.E., and Osburn, W.H. Indiana University Press, Bloomington, Ind. 237-240.

Konrad, J.M. 1987. The influence of heat extraction rate in freezing soils, *Cold Regions Science and Technology*, 14: 129-137.

Konrad, J.M. 1988. Influence of freezing mode on frost heave characteristics, *Cold Regions Science and Technology*, 15: 161-175.

Konrad, J.M. 1990. Segregation potential – pressure – salinity relationships near thermal steady state for a clayey silt, *Canadian Geotechnical Journal*, 27: 203-215.

Konrad, J.M. 1994. Sixteenth Canadian geotechnical colloquium: frost heave in soils: concept and engineering, *Canadian Geotechnical Journal*, 31: 223-245.

Konrad, J.M. and McCammon, A.W. 1990. Solute partitioning in freezing soils. *Canadian Geotechnical Journal*, 67: 726-736.

Konrad, J.M. and Morgenstern, N.R. 1980. A mechanistic theory of ice lens formation in fine-grained soils. *Canadian Geotechnical Journal*, 17: 473-486.

Konrad, J.M. and Morgenstern, N.R. 1981. The segregation potential of a freezing soil. *Canadian Geotechnical Journal*, 18: 482-491.

Konrad, J.M. and Morgenstern N.R. 1982. Effects of applied pressure on freezing soils, *Canadian Geotechnical Journal*, 19: 494-505.

Lewis, G.N. and Randall, M. 1961. *Thermodynamics*. 2nd edition, McGraw-Hill, New York.

Lovell, C. (1957) Temperature effects on phase composition and strength of partially frozen soil. U.S. Highway Research Board, *Bulletin No. 168*: 74-95.

Mageau D.W. and Morgenstern, N.R. 1979. Observations on moisture migration in frozen soils. *Canadian Geotechnical Journal*, 17: 54-60.

Mackay, J. R. (1974) Reticulate ice veins in permafrost, Northern Canada. *Canadian Geotechnical Journal* 11: 230-237.

Miller, R.D. 1972. Freezing and heaving of saturated and unsaturated soils. U.S. Highway Research Record, Report No. 393: 1-11.

Nakawo, M. and Sinha, N.K. 1981. Growth rate and salinity profile of first-year sea ice in the high Arctic. *Journal of Glaciology*, 27: 315-330.

Nersesova, Z. and Tsytoich, N.A. 1963. Unfrozen water in frozen soils. In *Proceedings of the 1<sup>st</sup> International Conference on Permafrost*, Purdue University, Lafayette, Ind. 230-234.

Nidowicz, B. and Shur, Y. L. 1998. Russian and North American approaches to pile design in relation to frost action. *Seventh international conference on Permafrost*, Yellowknife, NWT, Canada. *Collection Nordicana*, 57:803-809.

Oliphant, J.L., Tice, A.R. and Nakano, Y. 1983. Water migration due to a temperature gradient in frozen soil. In *Proceedings of the 4<sup>th</sup> International Conference on Permafrost*, Fairbanks, AK, USA: 951-956

Penner, E. 1972. Influence of freezing rate on frost heaving. U.S. Highway Research Record, Report No. 393: 56-64.

Popov, A. I. 1967. Permafrost phenomena in the earth's crust. *Cryolithology*. (In Russian). Moscow University Press, Moscow, U.S.S.R.

Rempel, A. M., Wettlaufer, J. S. and Worster, M. G. 2004. Premelting dynamics in a continuum model of frost heave. *The Journal of Fluid Mechanics*, 498: 227-244.

Sayles, F. N. and Iskandar, I. K., 1998. Ground freezing for containment of hazardous waste. International Containment Technology workshop, Baltimore, MD, United States, Aug. 28-31, 1995.

Sego, D C; Hofmann, B A; Robertson, P K; and Wride, C E (Fear, C E). 1998. Undisturbed sampling of loose sand using in-situ ground freezing. Proceedings of the international workshop on Physics and mechanics of soil liquefaction [modified], Baltimore, MD, United States, Sept. 10-11, 1998, 179-191.

Taber, S. 1929. Frost heaving. *Journal of Geology*, 37: 428-461.

Taber, S. 1930. The mechanics of frost heaving. *Journal of Geology*, 38: 303-317.

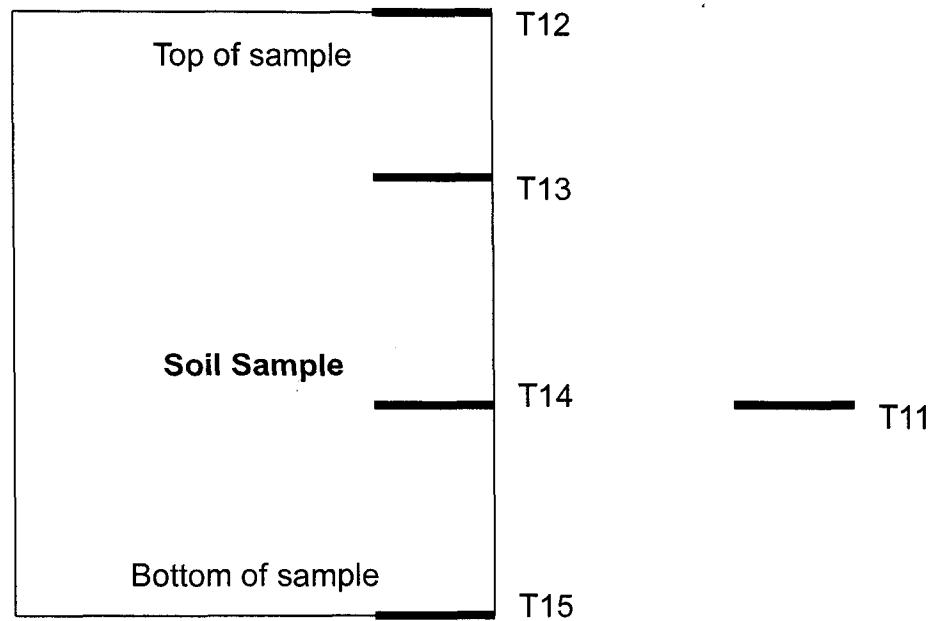
Vershinin, P.V., Deriagin, B.V., and Kirilenko, N.V., 1960. The non-freezing water in soil. U.S. Army Corps of Engineers, Arctic Construction and Frost Effects Laboratory, Translation No 30: 1-10.

Zhang, X., Zheng, and D., Feng, Y., 1993. Random characteristics of frost heave and application to the design of anti-frost lift reliability of grouting pile at building site. Sixth international conference on Permafrost, Beijing, China, Proceedings, July 5-9, 1993, 1:789-792.

## **APPENDIX A**

### **TEMPERATURE WITH TIME WITHIN EACH TEST**

Figure A.1 Location of each thermistor



Note: 1. Distance is 40mm between T12 and T13, 42mm between T13 and T14, 40 mm between T14 and T15.

2. T11 is for measuring air temperature in the cold room.

3. Room temperature control poor for tests #5, #6, #11, #12.

Figure A.2 Temperature with time during test #1

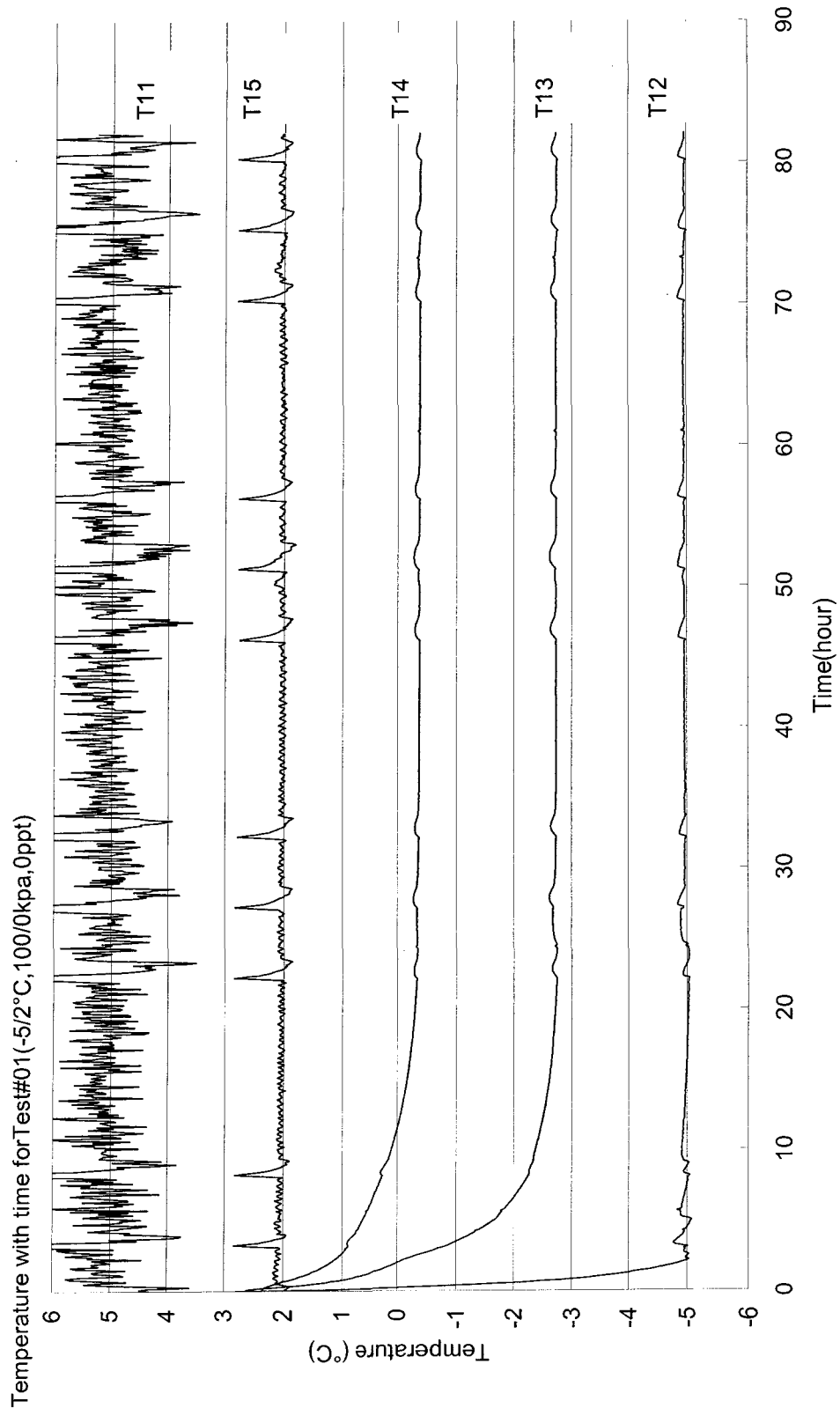


Figure A.3 Temperature with time during test #2

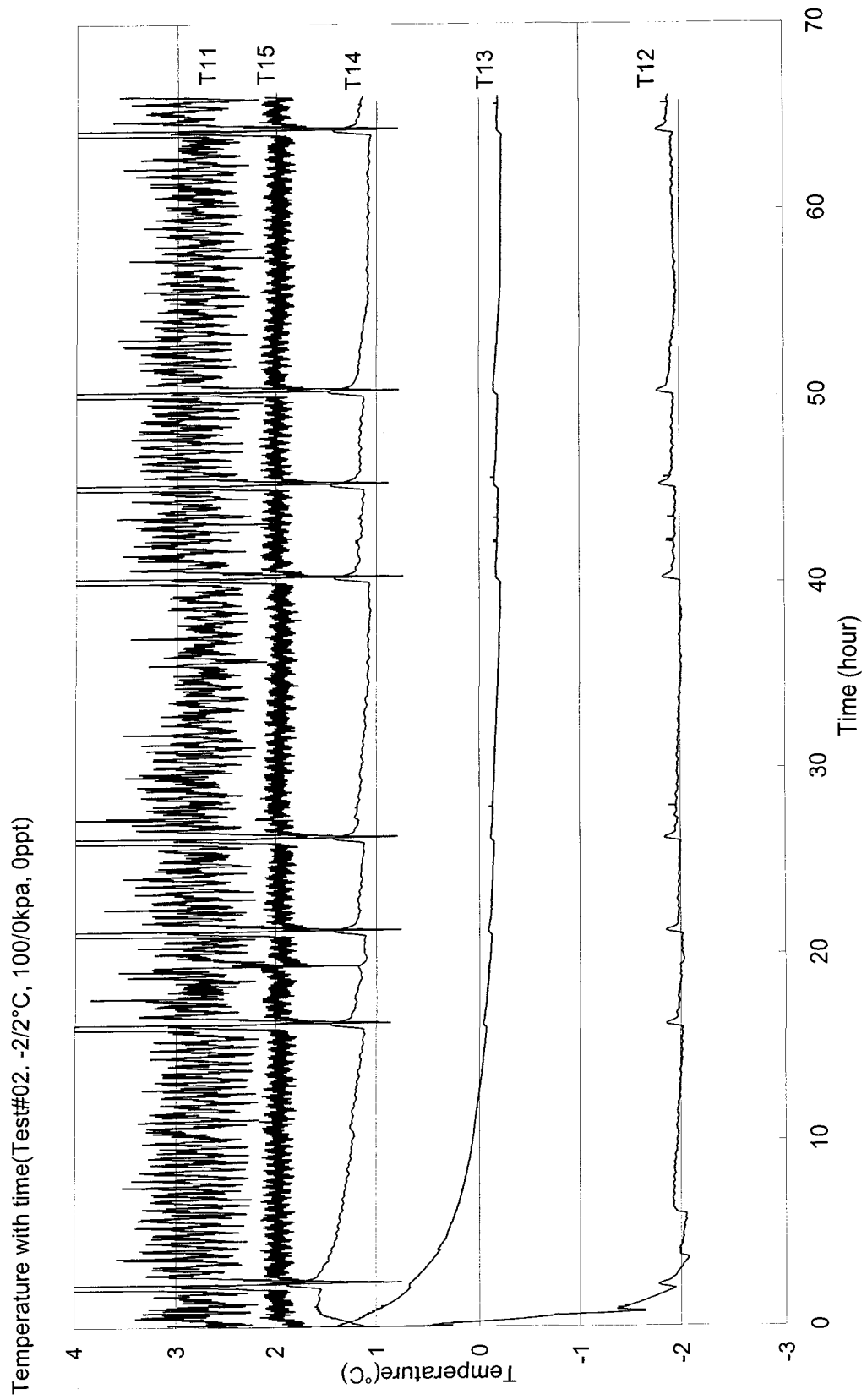


Figure A.4 Temperature with time during test #3

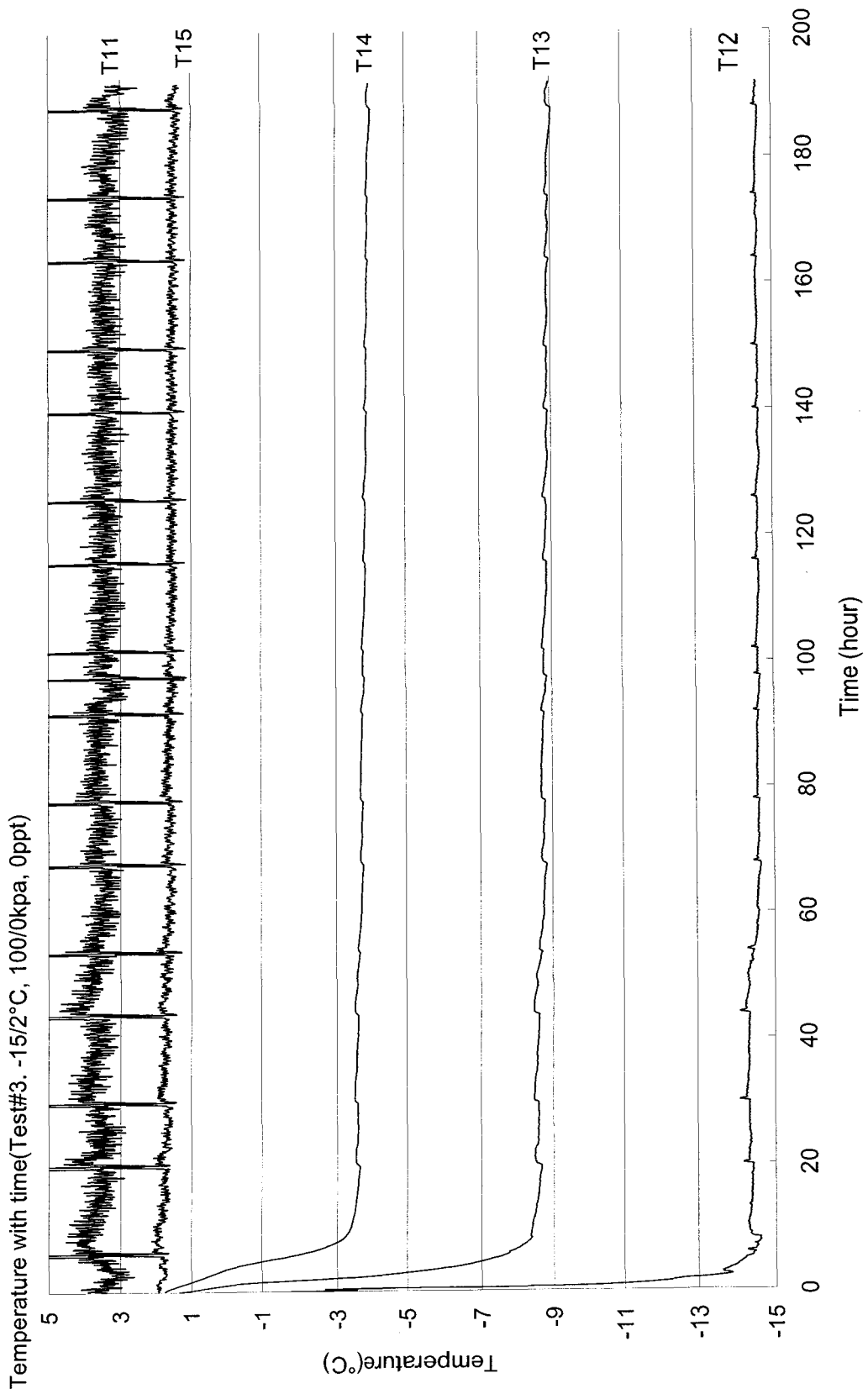


Figure A.5 Temperature with time during test #4

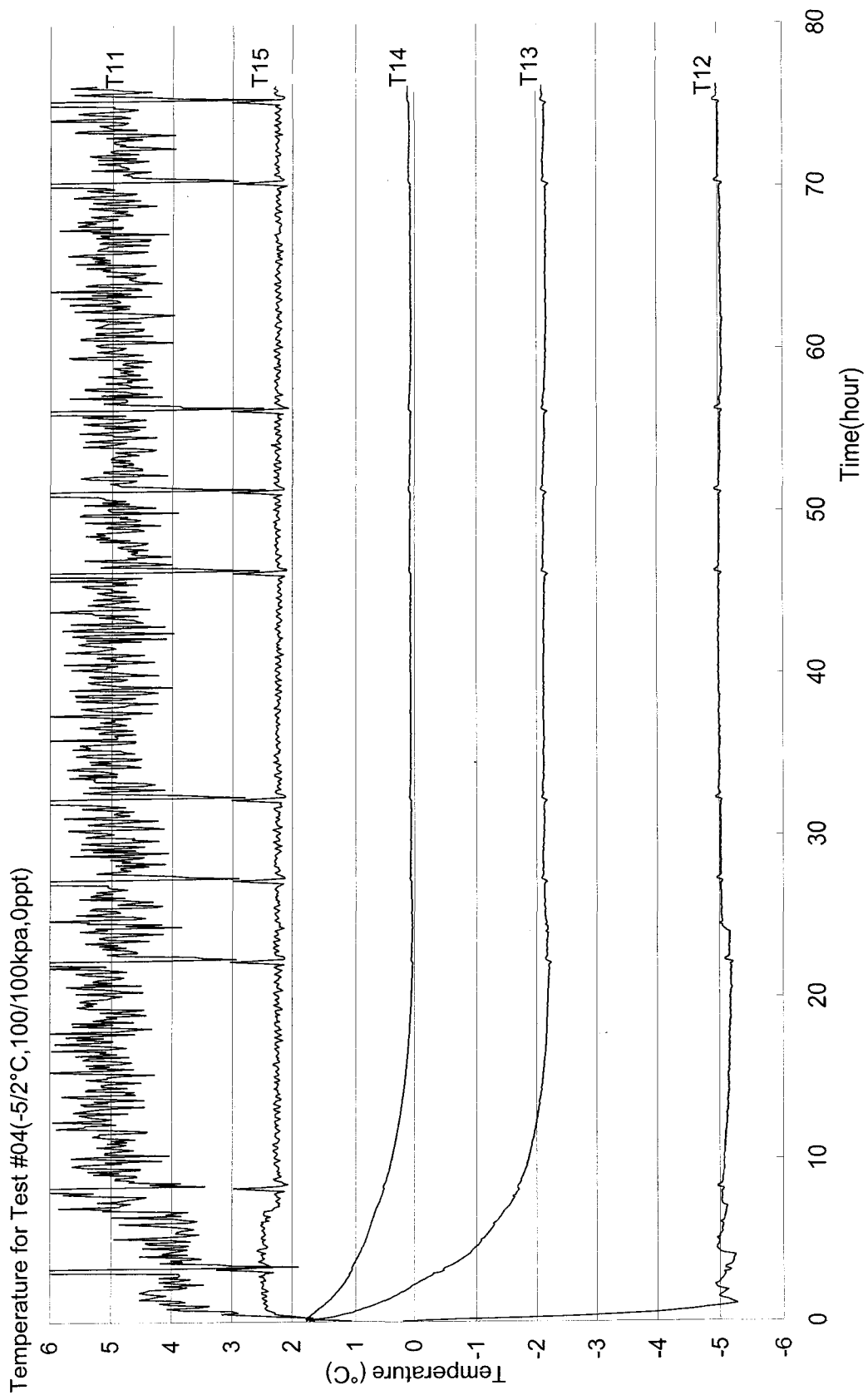


Figure A.6 Temperature with time during test #5

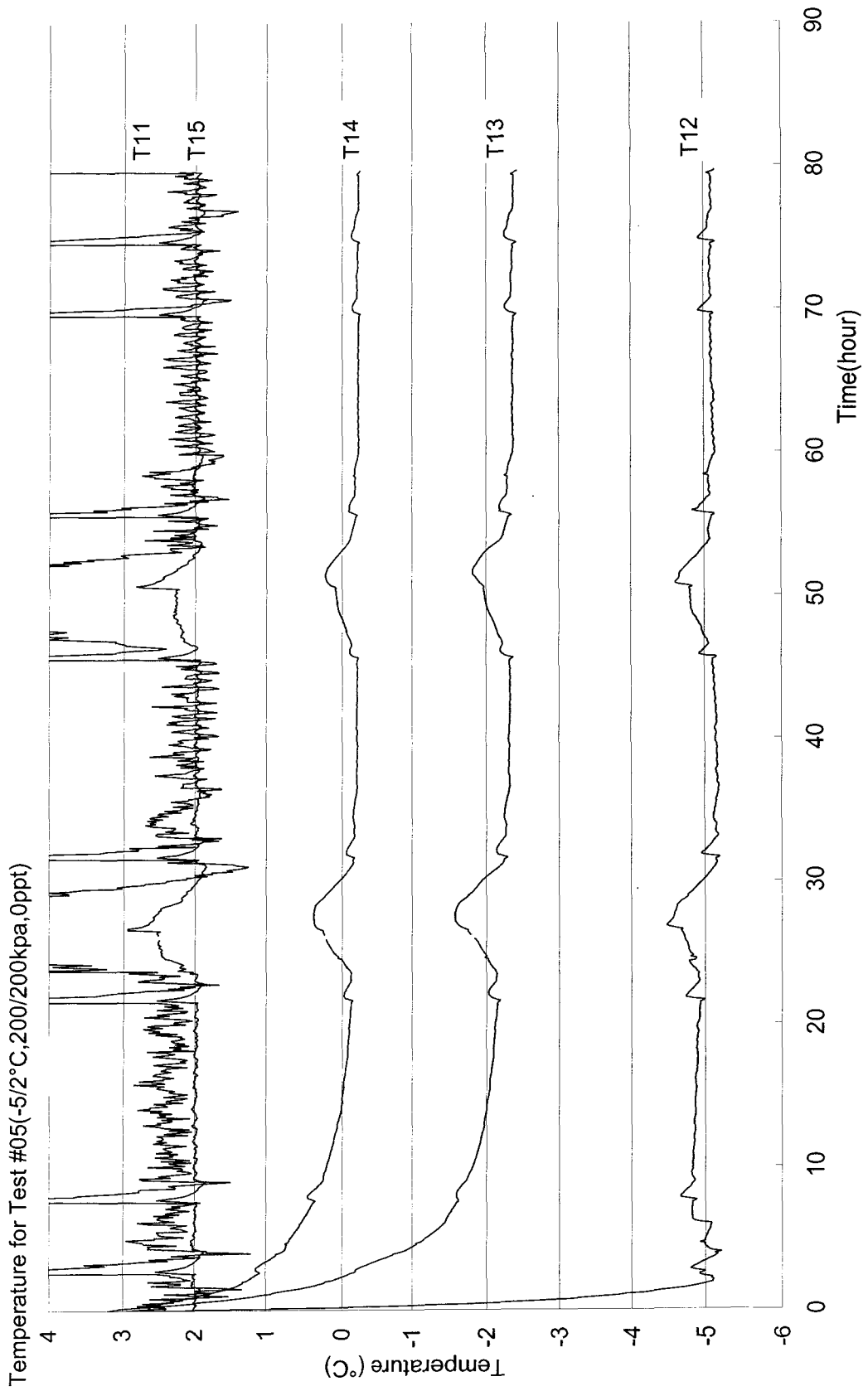


Figure A.7 Temperature with time during test #6

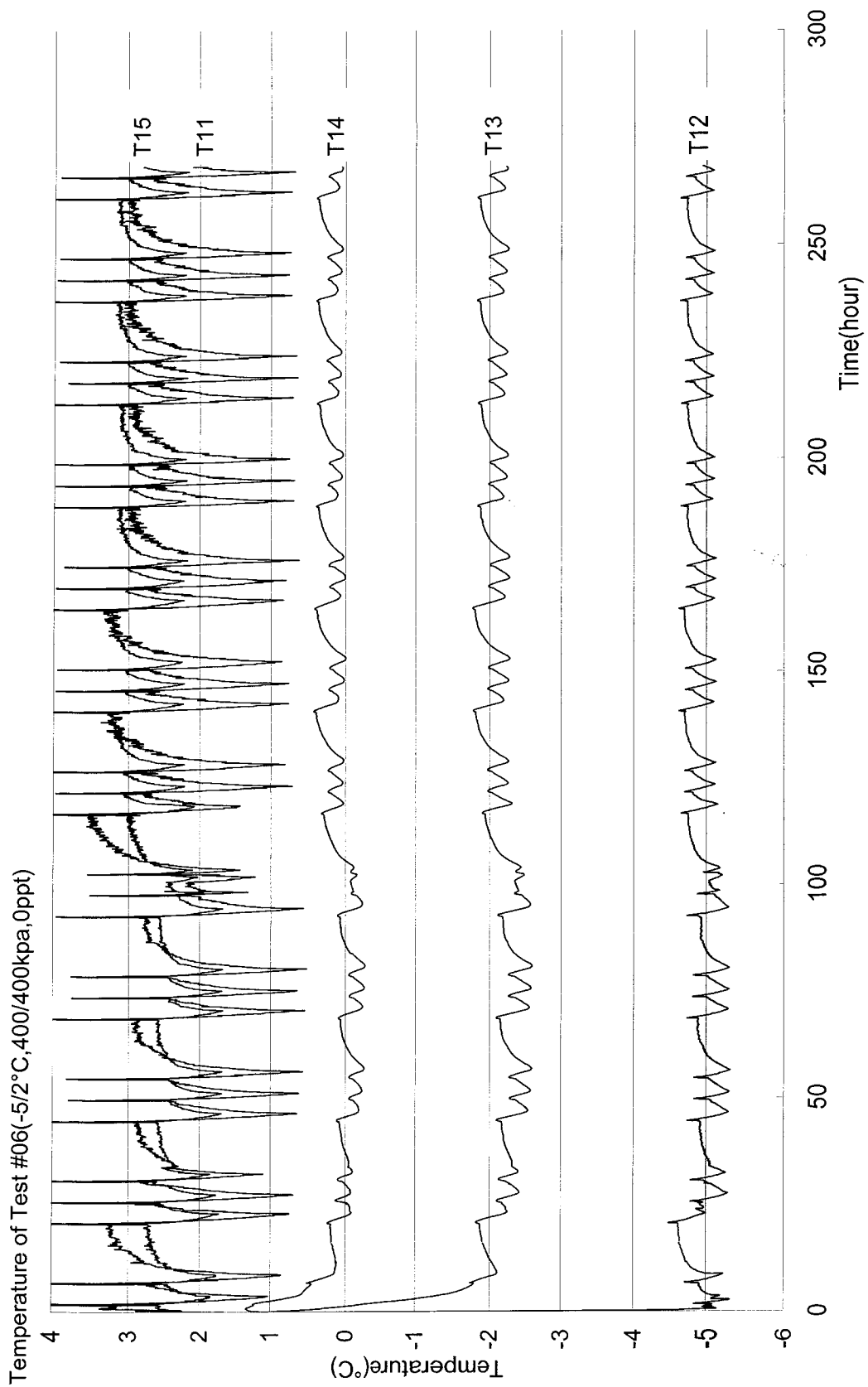
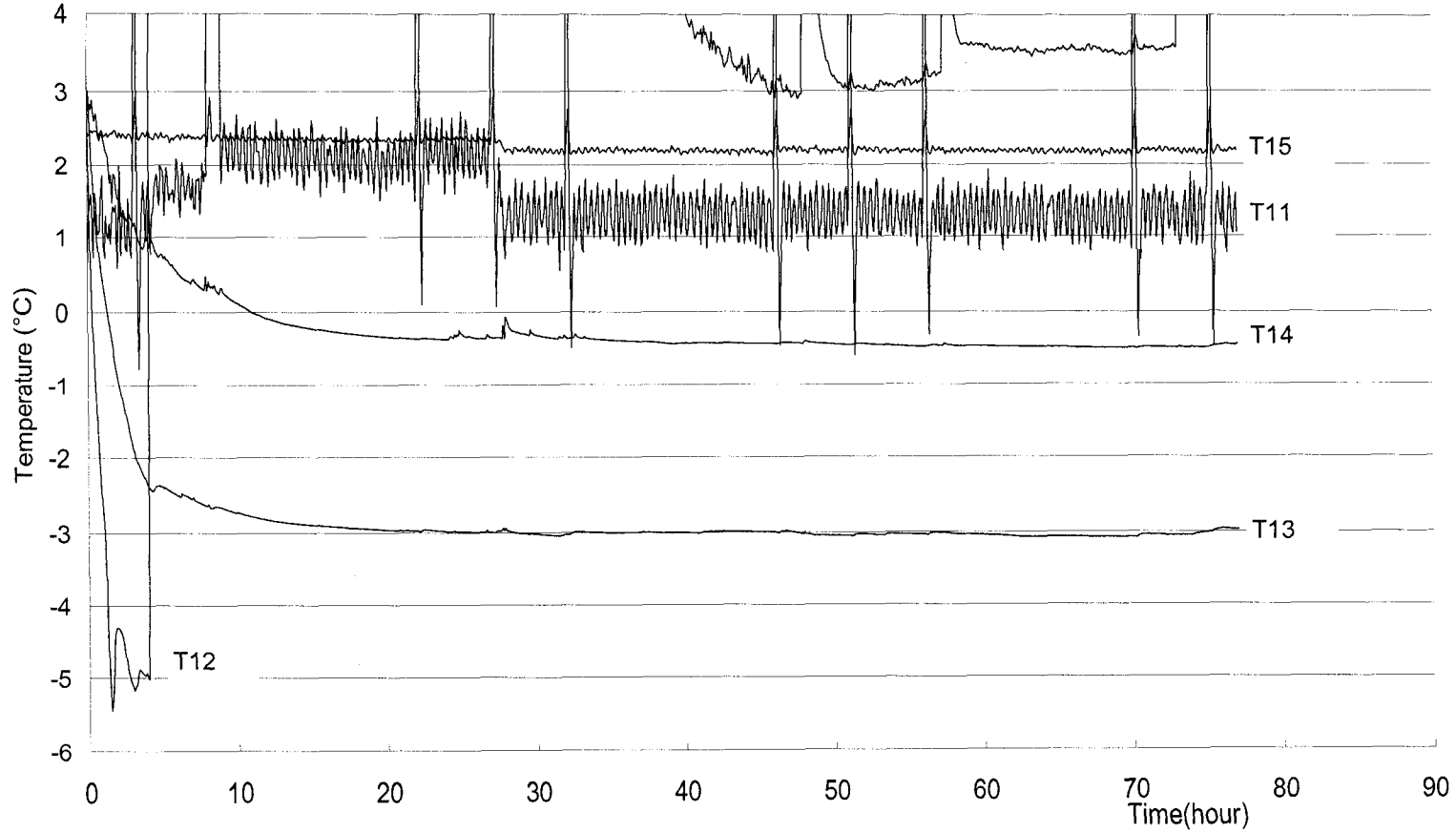


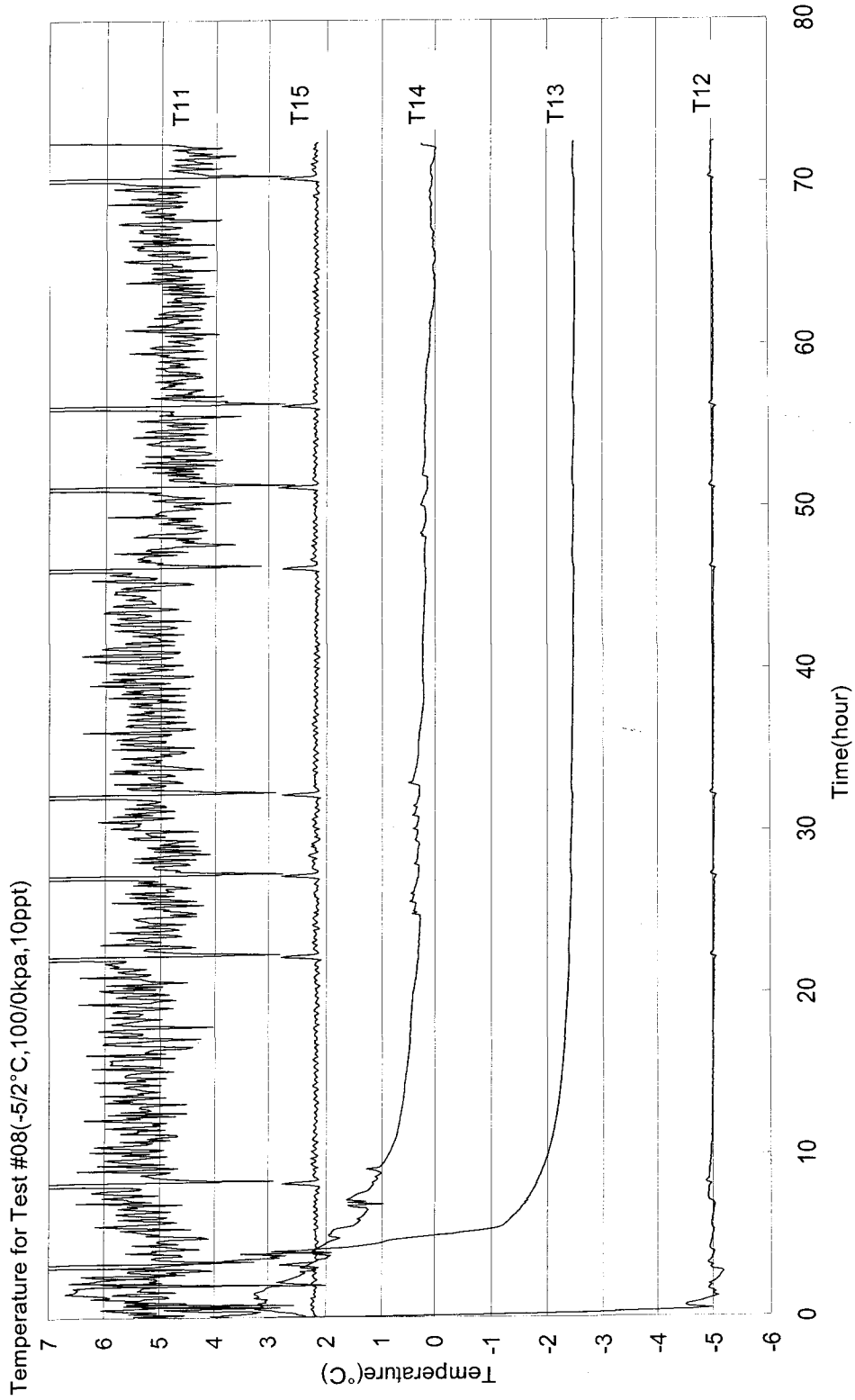
Figure A.8 Temperature with time during test #7

Temperature for Test #07(-5/2°C,100/0kpa,5ppt)



129 Note: Thermistor T12 damaged after the freezing start. The temperature of the top plate was controlled by the cold bath.

Figure A.9 Temperature with time during test #8



130 Note: Thermistor T13 damaged after the freezing start.

Figure A.10 Temperature with time during test #9

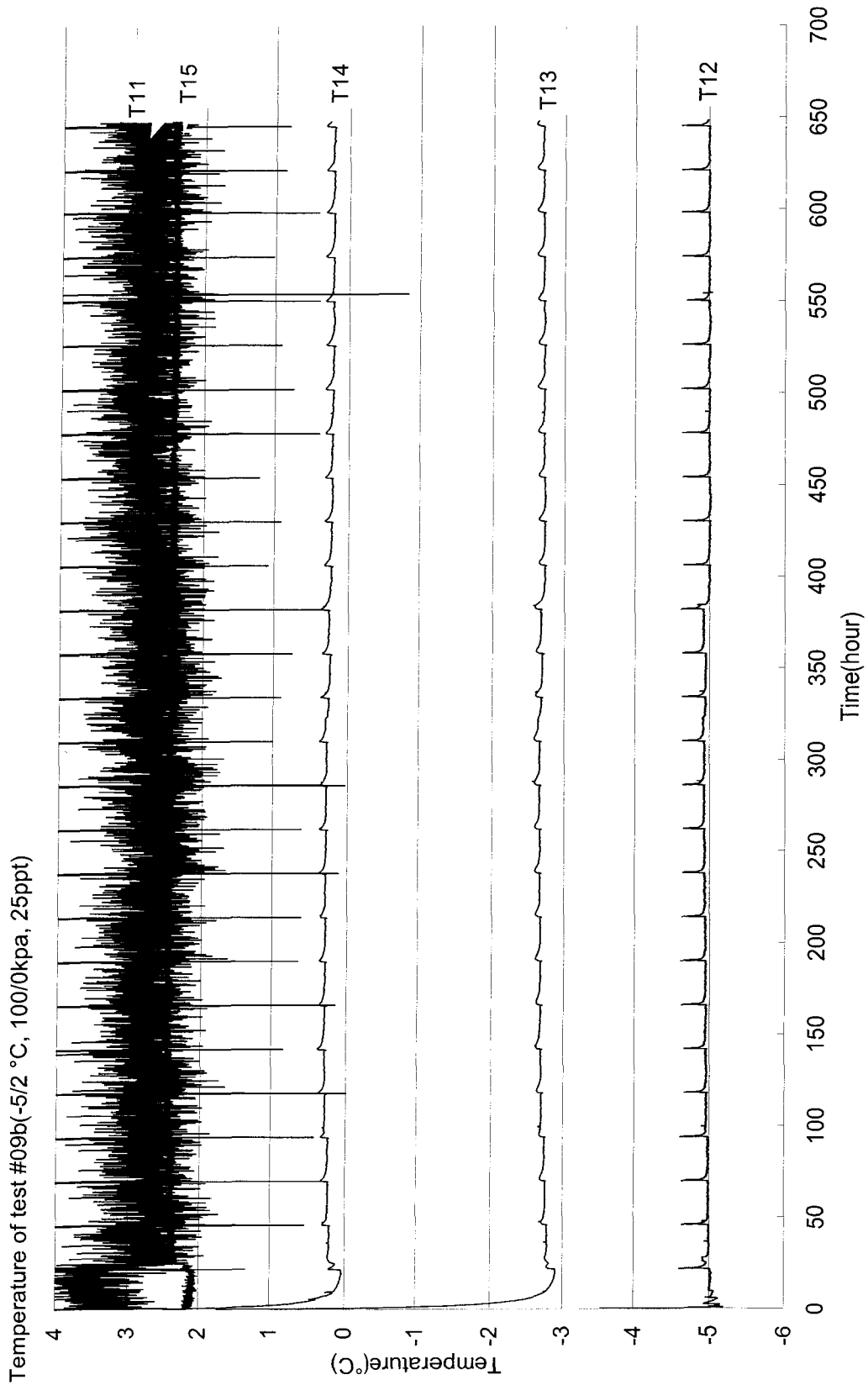
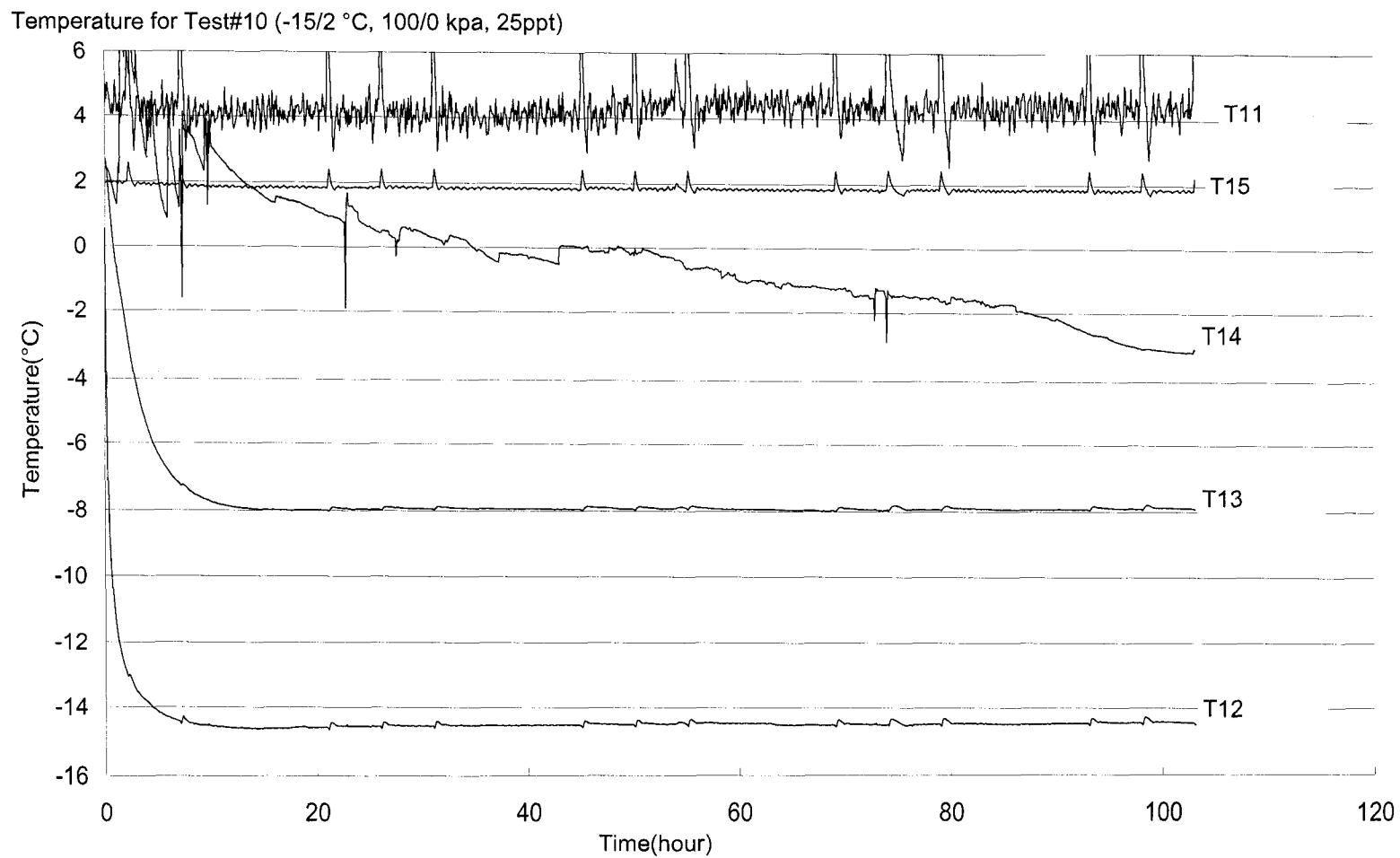


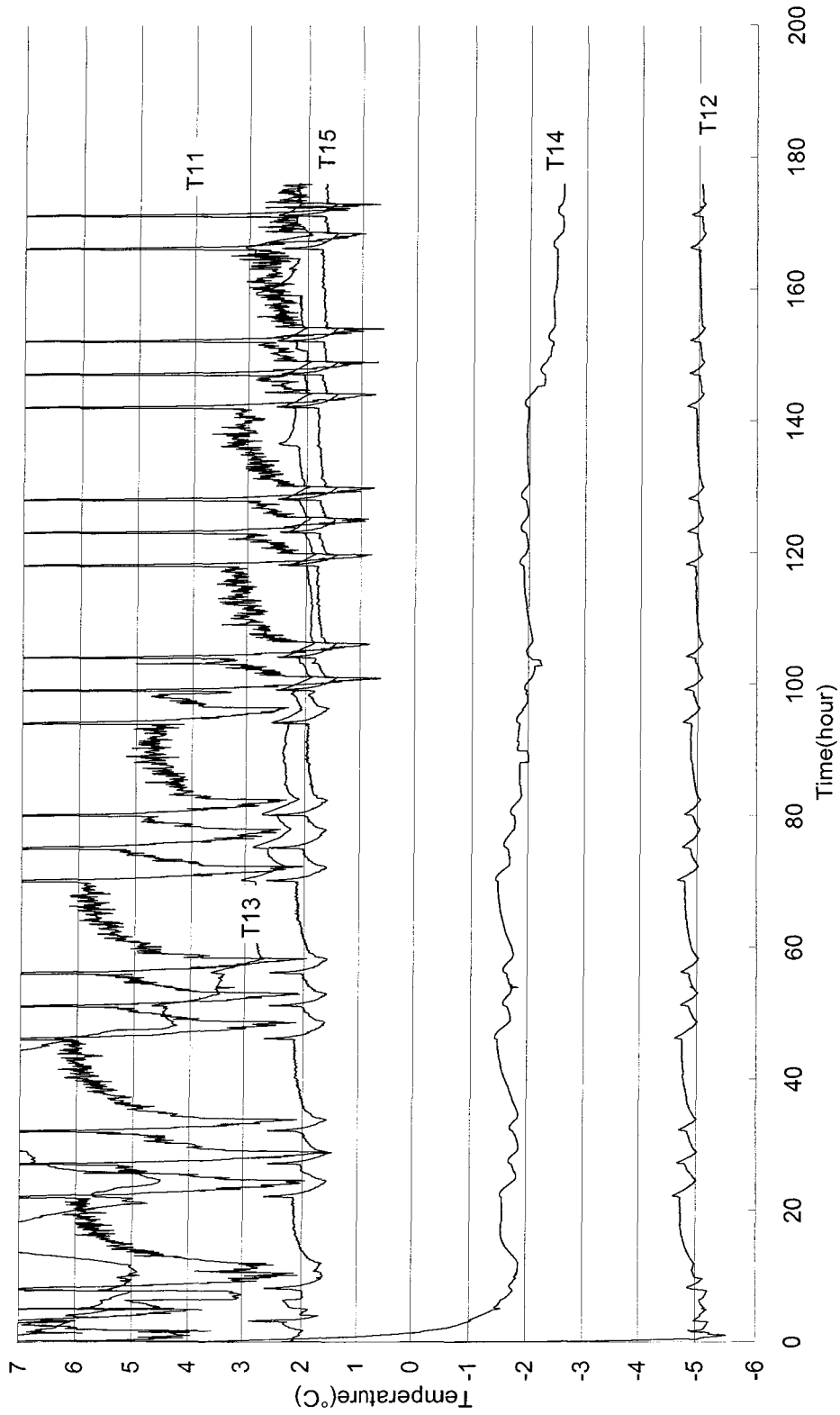
Figure A.11 Temperature with time during test #10



132 Note: Thermistor T14 damaged after the freezing start.

Figure A.12 Temperature with time during test #11

Temperature for Test #11 (-5/2°C, 200/200kpa, 25ppt)



Note: Thermistor T13 damaged after the freezing start.

Figure A.13 Temperature with time during test #12

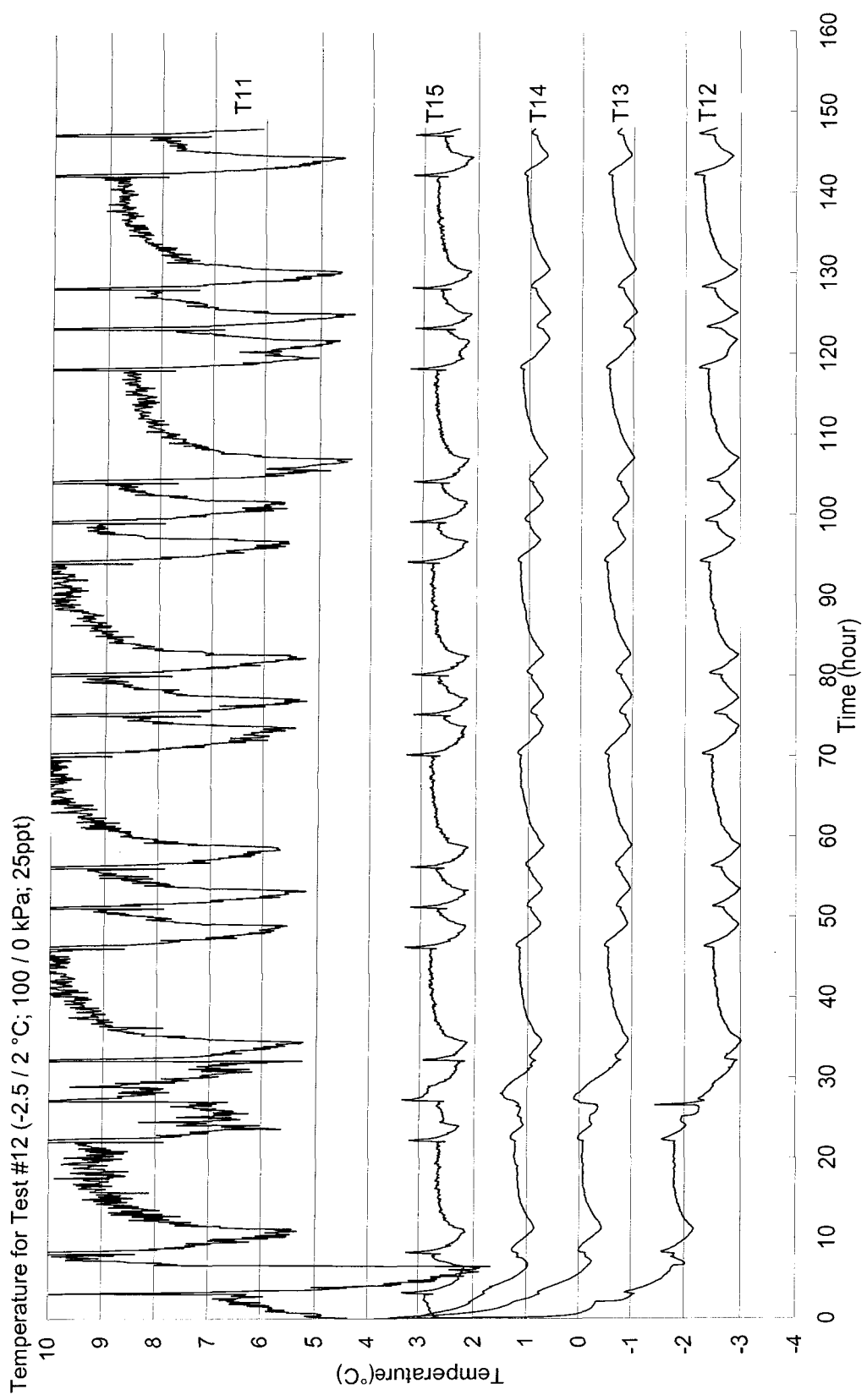


Figure A.14 Temperature profile at steady state in all tests

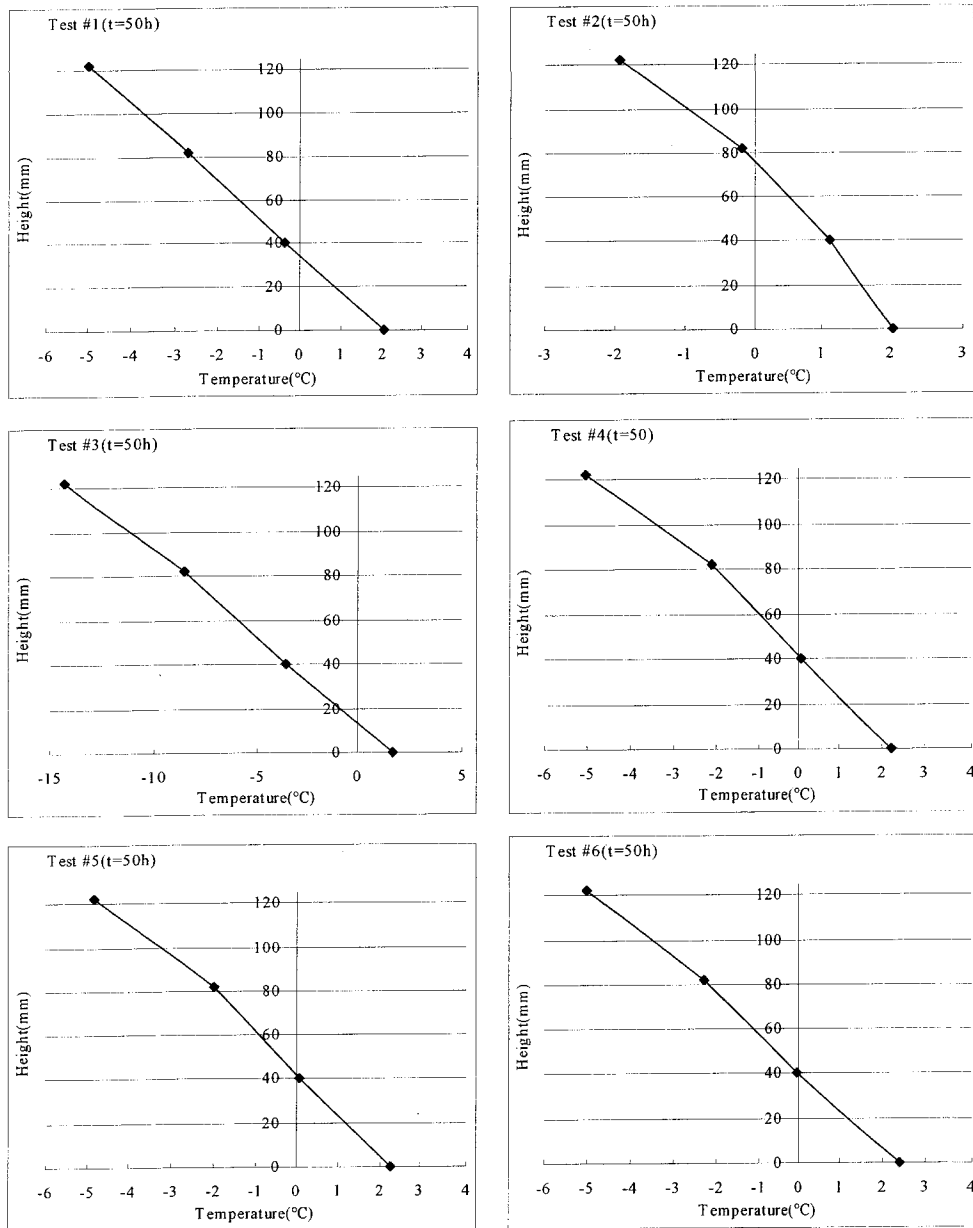
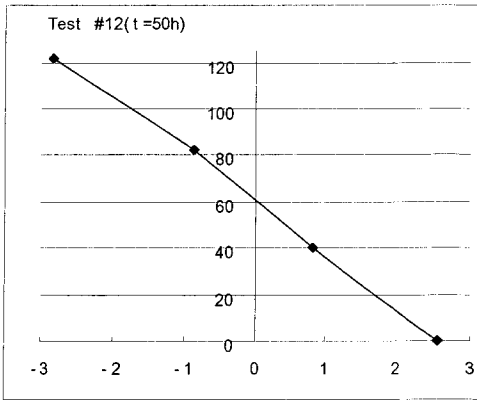
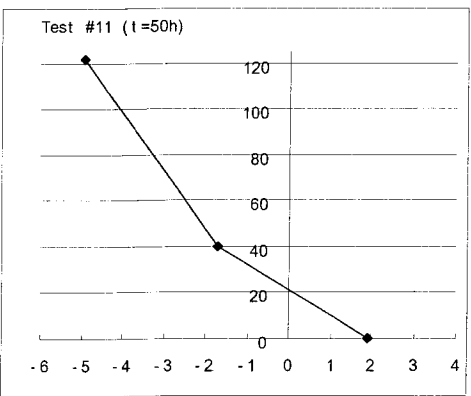
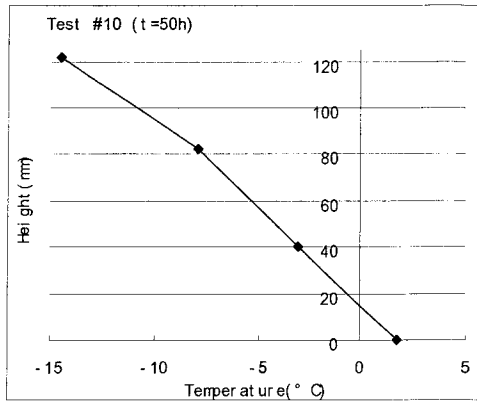
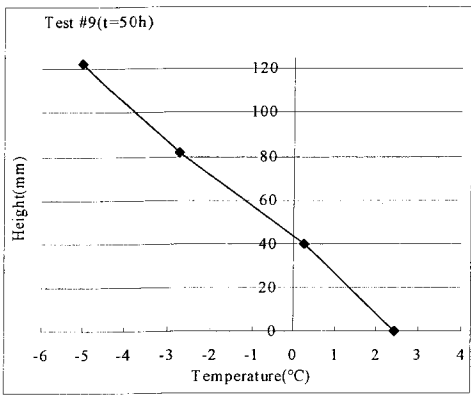
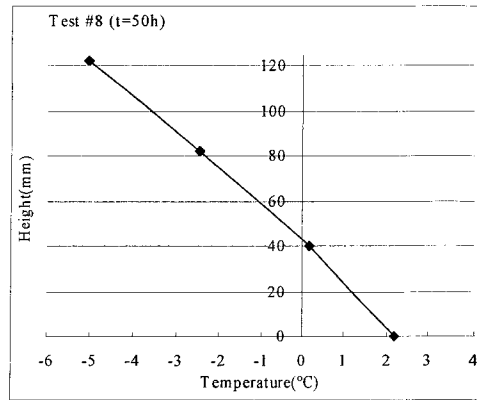
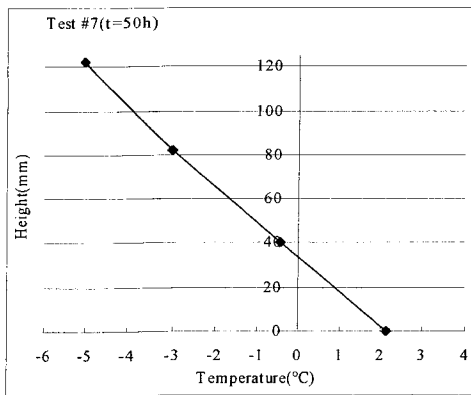


Figure A.14 (Continued)



## **APPENDIX B**

### **MOISTURE CONTENT AND SALINITY DATA OF EACH TEST**

Note: the Height is measured from the base of the samples in all tests.

Table B.1.a Moisture content before and after consolidation for test #1

	Sample 1	Sample 2	Sample 3	Average
Tare (g)	0.95	0.97	0.96	
Wet + Tare (g)	37.28	40.69	37.22	
Dry + Tare (g)	24.25	26.46	24.24	
Dry Soil (g)	23.30	25.49	23.28	
Water (g)	13.03	14.23	12.98	
MC (%) before consolidation	55.92	55.83	55.76	55.83
Height (mm) of sample before consolidation	-	-	-	182
Height (mm) of sample after consolidation	-	-	-	125
MC (%) after consolidation	-	-	-	26.53

Table B.1.b Moisture content at different elevation of sample after freezing for test #1.

Height (mm)	2.5	7.5	12.5	17.5	22.5	27.5	32.5	37.5	42.5	47.5	52.5	57.5
Tare (g)	0.99	0.98	0.92	1.01	0.99	1.00	0.95	0.93	0.94	0.93	0.95	0.95
Wet + Tare (g)	27.94	19.18	22.11	23.15	14.75	18.03	19.18	13.71	24.97	18.58	11.74	18.10
Dry + Tare (g)	23.24	16.01	18.43	19.33	12.44	15.13	16.08	11.52	17.72	14.44	9.30	14.24
Dry Soil (g)	22.25	15.03	17.51	18.32	11.45	14.13	15.13	10.59	16.78	13.51	8.35	13.29
Water (g)	4.70	3.17	3.68	3.82	2.31	2.90	3.10	2.19	7.25	4.14	2.44	3.86
MC (%)	21.12	21.09	21.02	20.85	20.17	20.52	20.49	20.68	43.21	30.64	29.22	29.04
Height (mm)	62.5	67.5	72.5	77.5	82.5	87.5	92.5	97.5	102.5	107.5	112.5	117.5
Tare (g)	0.94	0.94	0.94	0.93	0.94	0.93	0.95	0.94	0.94	0.95	0.95	0.95
Wet + Tare (g)	12.26	19.47	9.79	14.49	18.04	10.64	17.57	24.28	19.66	21.04	27.38	10.37
Dry + Tare (g)	9.76	15.35	7.81	11.46	14.23	8.48	13.88	19.26	15.52	16.63	21.54	8.29
Dry Soil (g)	8.82	14.41	6.87	10.53	13.29	7.55	12.93	18.32	14.58	15.68	20.59	7.34
Water (g)	2.50	4.12	1.98	3.03	3.81	2.16	3.69	5.02	4.14	4.41	5.84	2.08
MC (%)	28.34	28.59	28.82	28.77	28.67	28.61	28.54	27.40	28.40	28.13	28.36	28.34

Table B.2.a Moisture content before and after consolidation for test #2

	Sample 1	Sample 2	Sample 3	Average
Tare (g)	0.96	1.03	0.98	
Wet + Tare (g)	36.53	27.40	24.54	
Dry + Tare (g)	24.96	19.00	16.92	
Dry Soil (g)	24.00	17.97	15.94	
Water (g)	11.57	8.40	7.62	
MC (%) before consolidation	48.21	46.74	47.80	47.59
Height (mm) of sample before consolidation	-	-	-	173
Height (mm) of sample after consolidation	-	-	-	133
MC (%) after consolidation	-	-	-	27.86

Table B.2.b Moisture content at different elevation of sample after freezing for test #2.

Height (mm)	5	15	25	35	45	55	65	75	85	95	105	115
Tare (g)	1.00	1.01	0.96	1.04	1.00	1.01	0.97	0.95	0.95	0.95	0.94	0.96
Wet + Tare (g)	52.94	47.30	55.51	54.05	51.18	54.47	44.03	65.70	28.06	49.72	36.52	32.05
Dry + Tare (g)	41.91	37.14	43.61	42.76	40.82	43.75	35.64	51.32	17.74	36.81	28.18	24.99
Dry Soil (g)	40.91	36.13	42.65	41.72	39.82	42.74	34.67	50.37	16.79	35.86	27.24	24.03
Water (g)	11.03	10.16	11.90	11.29	10.36	10.72	8.39	14.38	10.32	12.91	8.34	7.06
MC (%)	26.96	28.12	27.90	27.06	26.02	25.08	24.20	28.55	61.47	36.00	30.62	29.38

Table B.3.a Moisture content before and after consolidation for test #3

	Sample 1	Sample 2	Sample 3	Average
Tare (g)	0.97	0.96	0.99	
Wet + Tare (g)	36.24	32.12	29.50	
Dry + Tare (g)	24.30	21.48	19.78	
Dry Soil (g)	23.33	20.52	18.79	
Water (g)	11.94	10.64	9.72	
MC (%)	51.18	51.85	51.73	51.59
Height (mm) of sample before consolidation	-	-	-	167
Height (mm) of sample after consolidation	-	-	-	121
MC (%) after consolidation	-	-	-	26.98

Table B.3.b Moisture content at different elevation of sample after freezing for test #3.

Height (mm)	5	15	25	35	45	55	65	75	85	95	105	115
Tare (g)	1.01	1.03	0.96	1.04	1.03	1.00	0.95	0.96	0.94	0.93	0.94	0.94
Wet + Tare (g)	15.82	15.44	16.22	15.97	19.36	21.11	18.60	25.34	23.88	23.43	14.56	23.12
Dry + Tare (g)	13.19	11.56	12.43	12.61	15.34	16.55	14.65	19.95	18.81	18.46	11.60	18.19
Dry Soil (g)	12.18	10.53	11.47	11.57	14.31	15.55	13.70	18.99	17.87	17.53	10.66	17.25
Water (g)	2.63	3.88	3.79	3.36	4.02	4.56	3.95	5.39	5.07	4.97	2.96	4.93
MC (%)	21.59	36.85	33.04	29.04	28.09	29.32	28.83	28.38	28.37	28.35	27.77	28.58

Table B.4.a Moisture content before and after consolidation for test #4

	Sample 1	Sample 2	Sample 3	Average
Tare (g)	0.98	0.94	0.95	
Wet + Tare (g)	29.52	31.03	28.54	
Dry + Tare (g)	18.99	19.94	18.36	
Dry Soil (g)	18.01	19.00	17.41	
Water (g)	10.53	11.09	10.18	
MC (%) before consolidation	58.47	58.37	58.47	58.44
Height (mm) of sample before consolidation	-	-	-	182
Height (mm) of sample after consolidation	-	-	-	121
MC (%) after consolidation	-	-	-	26.2

Table B.4.b Moisture content at different elevation of sample after freezing for test #4

Height (mm)	2.5	7.5	12.5	17.5	22.5	27.5	32.5	37.5	42.5	47.5	52.5	57.5
Tare (g)	1.00	0.98	0.94	1.01	0.98	1.00	0.94	0.92	0.93	0.91	0.93	0.94
Wet + Tare (g)	11.69	12.28	12.33	23.15	12.71	27.62	15.19	21.58	23.50	26.51	29.92	26.44
Dry + Tare (g)	9.89	10.40	10.47	19.51	10.88	23.28	12.84	18.09	16.48	20.44	23.24	20.56
Dry Soil (g)	8.89	9.42	9.53	18.50	9.90	22.28	11.90	17.17	15.55	19.53	22.31	19.62
Water (g)	1.80	1.88	1.86	3.64	1.83	4.34	2.35	3.49	7.02	6.07	6.68	5.88
MC (%)	20.25	19.96	19.52	19.68	18.48	19.48	19.75	20.33	45.14	31.08	29.94	29.97
Height (mm)	62.5	67.5	72.5	77.5	82.5	87.5	92.5	97.5	102.5	107.5	112.5	117.5
Tare (g)	0.93	0.94	0.93	0.95	0.95	0.95	0.98	0.95	0.96	0.94	0.94	0.94
Wet + Tare (g)	23.66	18.91	20.22	15.29	17.56	18.52	16.04	21.13	12.02	20.33	25.04	16.14
Dry + Tare (g)	18.44	14.84	15.83	12.08	13.84	14.60	12.79	16.79	9.59	16.25	19.96	12.57
Dry Soil (g)	17.51	13.90	14.90	11.13	12.89	13.65	11.81	15.84	8.63	15.31	19.02	11.63
Water (g)	5.22	4.07	4.39	3.21	3.72	3.92	3.25	4.34	2.43	4.08	5.08	3.57
MC (%)	29.81	29.28	29.46	28.84	28.86	28.72	27.52	27.40	28.16	26.65	26.71	30.70

Table B.5.a Moisture content before and after consolidation for test #5

	Sample 1	Sample 2	Sample 3	Average
Tare (g)	0.97	0.95	0.97	
Wet + Tare (g)	54.58	32.61	46.52	
Dry + Tare (g)	36.75	22.09	31.37	
Dry Soil (g)	35.78	21.14	30.40	
Water (g)	17.83	10.52	15.15	
MC (%) before consolidation	49.83	49.76	49.84	49.81
Height (mm) of sample before consolidation	-	-	-	180
Height (mm) of sample after consolidation	-	-	-	128
MC (%) after consolidation	-	-	-	24.52

Table B.5.b Moisture content at different elevation of sample after freezing for test #5.

Height (mm)	2.5	7.5	12.5	17.5	22.5	27.5	32.5	37.5	42.5	47.5	52.5	57.5
Tare (g)	1.00	1.01	0.93	1.03	1.00	1.03	0.96	0.96	0.95	0.96	0.95	0.97
Wet + Tare (g)	19.80	22.70	16.77	20.75	17.30	13.32	18.27	24.23	20.67	11.87	12.47	15.89
Dry + Tare (g)	16.56	19.04	14.23	17.50	14.64	11.33	15.46	20.37	17.16	8.05	9.87	12.56
Dry Soil (g)	15.56	18.03	13.30	16.47	13.64	10.30	14.50	19.41	16.21	7.09	8.92	11.59
Water (g)	3.24	3.66	2.54	3.25	2.66	1.99	2.81	3.86	3.51	3.82	2.60	3.33
MC (%)	20.82	20.30	19.10	19.73	19.50	19.32	19.38	19.89	21.65	53.88	29.15	28.73
Height (mm)	62.5	67.5	72.5	77.5	82.5	87.5	92.5	97.5	102.5	107.5	112.5	117.5
Tare (g)	0.94	0.97	0.97	0.95	0.95	0.95	0.94	0.97	0.95	0.93	0.95	0.96
Wet + Tare (g)	20.81	17.47	14.47	19.60	22.24	16.37	20.8	15.65	18.42	21.59	32.14	26.06
Dry + Tare (g)	16.56	14.06	11.75	15.83	17.98	13.33	16.91	12.79	15.06	17.62	26.18	21.30
Dry Soil (g)	15.62	13.09	10.78	14.88	17.03	12.38	15.97	11.82	14.11	16.69	25.23	20.34
Water (g)	4.25	3.41	2.72	3.77	4.26	3.04	3.89	2.86	3.36	3.97	5.96	4.76
MC (%)	27.21	26.05	25.23	25.34	25.01	24.56	24.36	24.20	23.81	23.79	23.62	23.40

Table B.6.a Moisture content before and after consolidation for test #6

	Sample 1	Sample 2	Sample 3	Average
Tare (g)	0.96	0.93	0.95	
Wet + Tare (g)	51.28	52.95	45.05	
Dry + Tare (g)	34.76	35.81	30.54	
Dry Soil (g)	33.80	34.88	29.59	
Water (g)	16.52	17.14	14.51	
MC (%) before consolidation	48.88	49.14	49.04	49.02
Height (mm) of sample before consolidation	-	-	-	183
Height (mm) of sample after consolidation	-	-	-	125
MC (%) after consolidation	-	-	-	21.52

Table B.6.b Moisture content at different elevation of sample after freezing for test #6.

Height (mm)	2.5	7.5	12.5	17.5	22.5	27.5	32.5	37.5	42.5	47.5	52.5	57.5
Tare (g)	0.98	1.00	0.94	1.02	1.00	1.03	0.97	0.96	0.98	0.94	0.95	0.97
Wet + Tare (g)	24.66	24.07	20.11	15.87	18.25	18.50	25.23	24.83	29.49	25.91	17.43	20.09
Dry + Tare (g)	20.72	20.24	16.99	13.48	15.44	15.68	21.34	21.03	25.08	20.38	14.15	16.24
Dry Soil (g)	19.74	19.24	16.05	12.46	14.44	14.65	20.37	20.07	24.10	19.44	13.20	15.27
Water (g)	3.94	3.83	3.12	2.39	2.81	2.82	3.89	3.80	4.41	5.53	3.28	3.85
MC (%)	19.96	19.91	19.44	19.18	19.46	19.25	19.10	18.93	18.30	28.45	24.85	25.21
Height (mm)	62.5	67.5	72.5	77.5	82.5	87.5	92.5	97.5	102.5	107.5	112.5	117.5
Tare (g)	0.95	0.95	0.96	0.95	0.96	0.97	0.97	0.96	0.98	0.97	0.97	0.99
Wet + Tare (g)	17.44	20.71	22.54	19.40	23.50	21.93	19.72	25.4	20.26	28.34	27.81	26.43
Dry + Tare (g)	14.25	17.02	18.51	16.01	19.38	18.15	16.37	21.07	16.86	23.56	23.15	21.62
Dry Soil (g)	13.30	16.07	17.55	15.06	18.42	17.18	15.40	20.11	15.88	22.59	22.18	20.63
Water (g)	3.19	3.69	4.03	3.39	4.12	3.78	3.35	4.33	3.40	4.78	4.66	4.81
MC (%)	23.98	22.96	22.96	22.51	22.37	22.00	21.75	21.53	21.41	21.16	21.01	23.32

Table B.7.a Moisture content and salinity before and after consolidation for test #7

	Sample 1	Sample 2	Sample 3	Average
Tare (g)	0.94	0.93	0.94	-
Wet + Tare (g)	32.15	32.68	29.31	-
Dry + Tare (g)	21.38	21.96	19.52	-
Dry Soil (g)	20.44	21.03	18.58	-
Water (g)	10.77	10.72	9.79	-
MC (%)	52.69	50.97	52.69	52.12
Tare (g)	11.43	11.41	11.25	-
Dry + Tare (g)	24.95	21.49	21.95	-
Wet + Tare (g)	75.26	75.22	74.78	-
Salinity(measured) (g/L)t	0.73	0.47	0.60	-
Dry Soil (g)	13.52	10.08	10.70	-
WaterM/Waterl	7.06	10.46	9.37	-
Salinity(calculated) (g/L)	5.74	5.66	6.31	5.90
Height (mm) of sample before consolidation	-	-	-	186
Height (mm) of sample after consolidation	-	-	-	131
MC (%) after consolidation	-	-	-	52.12

Table B.7.b Moisture content and salinity at different elevation of sample after freezing for test #7

Height (mm)	2.5	7.5	12.5	17.5	22.5	27.5	32.5	37.5	42.5	47.5	52.5	57.5
Tare (g)	0.99	1.00	0.94	0.95	0.99	0.96	0.95	0.96	0.95	0.96	0.95	0.95
Wet + Tare (g)	21.00	20.76	21.49	17.91	18.73	11.51	17.52	15.37	18.96	19.04	15.45	10.26
Dry + Tare (g)	17.31	17.09	17.70	14.79	15.56	9.58	14.53	12.81	15.71	15.88	11.14	7.75
Dry Soil (g)	16.32	16.09	16.76	13.84	14.57	8.62	13.58	11.85	14.76	14.92	10.19	6.80
Water (g)	3.69	3.67	3.79	3.12	3.17	1.93	2.99	2.56	3.25	3.16	4.31	2.51
MC (%)	22.61	22.81	22.61	22.54	21.76	22.39	22.02	21.60	22.02	21.18	42.30	36.91
Tare (g)	11.54	11.38	11.50	11.38	11.52	11.41	11.39	11.52	11.53	11.39	11.57	11.48
Dry + Tare (g)	20.41	19.57	19.76	18.63	18.79	20.01	20.79	17.95	20.79	21.16	19.38	17.97
Wet + Tare (g)	73.74	73.60	72.93	73.91	73.68	74.36	74.21	72.70	74.00	74.50	74.28	73.39
Salinity(measured) (g/L)	0.200	0.182	0.185	0.149	0.142	0.183	0.217	0.127	0.253	0.286	0.187	0.141
Dry Soil (g)	8.87	8.19	8.26	7.25	7.27	8.60	9.40	6.43	9.26	9.77	7.81	6.49
WaterM/Waterl	26.59	28.92	28.47	33.82	34.70	28.23	25.81	39.41	26.10	25.78	16.62	23.13
Salinity (calculated) (g/L)	7.68	7.83	7.79	8.03	7.99	7.67	7.90	8.48	8.94	9.70	4.58	5.30

Table B.7.b Moisture content and salinity at different elevation of sample after freezing for test #7 (continued)

Height (mm)	62.5	67.5	72.5	77.5	82.5	87.5	92.5	97.5	102.5	107.5	112.5	117.5
Tare (g)	0.95	0.94	0.94	0.94	0.96	0.94	0.95	0.94	0.94	0.94	0.95	0.93
Wet + Tare (g)	14.74	16.90	18.67	16.84	18.96	13.36	15.40	19.35	15.12	13.86	16.38	25.66
Dry + Tare (g)	11.45	13.30	14.71	13.36	15.18	10.72	12.29	15.49	12.20	11.19	13.15	20.44
Dry Soil (g)	10.50	12.36	13.77	12.42	14.22	9.78	11.34	14.55	11.26	10.25	12.20	19.51
Water (g)	3.29	3.60	3.96	3.48	3.78	2.64	3.11	3.86	2.92	2.67	3.23	5.22
MC (%)	31.33	29.13	28.76	28.02	26.58	26.99	27.43	26.53	25.93	26.05	26.48	26.76
Tare (g)	11.52	11.54	11.39	11.41	11.45	11.50	11.33	11.63	11.36	11.56	11.37	11.39
Dry + Tare (g)	21.26	21.80	21.89	20.90	21.41	21.16	22.09	21.74	21.38	21.55	22.04	19.19
Wet + Tare (g)	76.08	76.54	76.34	76.45	74.29	75.28	75.78	76.73	76.35	76.82	75.45	73.08
Salinity(measured) (g/L)	0.254	0.295	0.287	0.257	0.295	0.259	0.292	0.249	0.257	0.258	0.289	0.234
Dry Soil (g)	9.74	10.26	10.50	9.49	9.96	9.66	10.76	10.11	10.02	9.99	10.67	7.80
WaterM/Waterl	17.96	18.32	18.03	20.89	19.97	20.75	18.19	20.50	21.16	21.24	18.91	25.82
Salinity (calculated) (g/L)	6.17	7.06	6.80	7.24	7.69	7.24	6.95	6.94	7.34	7.39	7.17	8.35

Table B.8.a Moisture content and salinity before and after consolidation for test #8

	Sample 1	Sample 2	Sample 3	Average
Tare (g)	0.94	0.95	0.95	-
Wet + Tare (g)	42.06	44.83	45.58	-
Dry + Tare (g)	27.35	29.08	29.56	-
Dry Soil (g)	26.41	28.13	28.61	-
Water (g)	14.71	15.75	16.02	-
MC (%)	55.70	55.99	55.99	55.89
Tare (g)	11.54	11.41	11.58	-
Dry + Tare (g)	30.81	31.51	25.23	-
Wet + Tare (g)	78.48	80.03	76.25	-
Salinity(measured) (g/L)t	2.08	2.05	1.56	-
Dry Soil (g)	19.27	20.10	13.65	-
WaterM/Waterl	4.44	4.31	6.68	-
Salinity(calculated) (g/L)	9.85	9.43	11.20	10.16
Height (mm) of sample before consolidation	-	-	-	185
Height (mm) of sample after consolidation	-	-	-	129
MC (%) after consolidation	-	-	-	27.55

Table B.8.b Moisture content and salinity at different elevation of sample after freezing for test #8

Height (mm)	2.5	7.5	12.5	17.5	22.5	27.5	32.5	37.5	42.5	47.5	52.5	57.5
Tare (g)	1.00	0.99	0.95	1.02	0.98	1.03	0.94	0.95	0.95	0.94	0.95	0.94
Wet + Tare (g)	21.21	13.88	13.89	20.75	13.54	20.78	25.50	23.93	23.84	30.81	15.49	25.75
Dry + Tare (g)	16.93	11.12	11.15	16.56	10.93	16.79	20.48	19.27	19.39	24.94	11.49	19.30
Dry Soil (g)	15.93	10.13	10.20	15.54	9.95	15.76	19.54	18.32	18.44	24.00	10.54	18.36
Water (g)	4.28	2.76	2.74	4.19	2.61	3.99	5.02	4.66	4.45	5.87	4.00	6.45
MC (%)	26.87	27.25	26.86	26.96	26.23	25.32	25.69	25.44	24.13	24.46	37.95	35.13
Tare (g)	11.51	11.36	11.48	11.36	11.67	11.43	11.53	11.57	11.51	11.38	11.59	11.47
Dry + Tare (g)	27.43	21.49	21.58	26.72	21.42	25.16	30.64	29.11	26.76	26.69	22.14	26.32
Wet + Tare (g)	76.44	71.51	72.20	75.74	66.77	73.36	76.09	75.12	73.54	75.21	73.43	74.11
Salinity(measured) (g/L)	0.95	0.57	0.55	0.86	0.57	0.75	1.11	1.01	0.87	0.91	0.61	0.98
Dry Soil (g)	15.92	10.13	10.10	15.36	9.75	13.73	19.11	17.54	15.25	15.31	10.55	14.85
WaterM/Waterl	11.46	18.12	18.66	11.84	17.73	13.87	9.26	10.31	12.71	12.96	12.81	9.16
Salinity (calculated) (g/L)	11.94	11.73	11.59	11.20	11.42	11.56	11.19	11.39	12.12	12.93	8.78	9.84

Table B.8.b Moisture content and salinity at different elevation of sample after freezing for test #8 (continued)

Height (mm)	62.5	67.5	72.5	77.5	82.5	87.5	92.5	97.5	102.5	107.5	112.5	117.5
Tare (g)	0.93	0.94	0.95	0.94	0.95	0.95	0.96	0.95	0.93	0.96	0.95	0.95
Wet + Tare (g)	26.62	20.99	16.24	25.59	13.62	22.50	14.71	21.97	12.78	18.29	12.31	15.55
Dry + Tare (g)	20.29	16.20	12.68	19.87	10.66	17.41	11.56	17.25	10.07	14.46	9.90	12.29
Dry Soil (g)	19.36	15.26	11.73	18.93	9.71	16.46	10.60	16.30	9.14	13.50	8.95	11.34
Water (g)	6.33	4.79	3.56	5.72	2.96	5.09	3.15	4.72	2.71	3.83	2.41	3.26
MC (%)	32.70	31.39	30.35	30.22	30.48	30.92	29.72	28.96	29.65	28.37	26.93	28.75
Tare (g)	11.52	11.57	11.38	11.38	11.49	11.53	11.28	11.60	11.34	11.54	11.39	11.40
Dry + Tare (g)	25.27	26.28	22.28	25.90	21.00	24.67	21.86	24.88	20.45	24.86	20.27	22.76
Wet + Tare (g)	72.28	75.74	75.15	73.89	72.03	72.79	70.65	73.83	72.00	73.31	69.65	74.60
Salinity(measured) (g/L)	0.92	0.94	0.69	0.97	0.57	0.85	0.68	0.86	0.54	0.90	0.57	0.75
Dry Soil (g)	13.75	14.71	10.90	14.52	9.51	13.14	10.58	13.28	9.11	13.32	8.88	11.36
WaterM/Waterl	10.46	10.71	15.98	10.94	17.60	11.84	15.52	12.73	19.08	12.82	20.65	15.87
Salinity (calculated) (g/L)	10.51	11.04	12.29	11.65	11.43	11.04	11.77	12.06	11.74	12.66	13.39	13.27

Table B.9.a Moisture content and salinity before and after consolidation for test #9

	Sample 1	Sample 2	Sample 3	Average
Tare (g)	0.94	0.93	0.92	-
Wet + Tare (g)	57.45	48.95	55.66	-
Dry + Tare (g)	37.35	31.93	36.22	-
Dry Soil (g)	36.41	31.00	35.30	-
Water (g)	20.10	17.02	19.44	-
MC (%)	55.20	54.90	55.07	55.06
Tare (g)	11.55	11.39	11.56	-
Dry + Tare (g)	32.95	34.02	33.88	-
Wet + Tare (g)	79.78	80.44	78.68	-
Salinity(measured) (g/L)t	5.81	6.16	6.36	-
Dry Soil (g)	21.40	22.63	22.32	-
WaterM/Waterl	3.96	3.74	3.64	-
Salinity(calculated) (g/L)	25.55	25.61	25.83	25.66
Height (mm) of sample before consolidation	-	-	-	183
Height (mm) of sample after consolidation	-	-	-	129
MC (%) after consolidation	-	-	-	27.68

Table B.9.b Moisture content and salinity at different elevation of sample after freezing for test #9

Height (mm)	2.5	7.5	12.5	17.5	22.5	27.5	32.5	37.5	42.5	47.5	52.5	57.5
Tare (g)	1.01	1.02	0.95	1.04	1.02	1.03	0.96	0.96	0.97	0.97	0.96	0.96
Wet + Tare (g)	63.64	62.64	70.64	68.98	81.32	67.48	77.94	63.45	105.11	66.33	71.40	89.93
Dry + Tare (g)	50.35	49.52	55.68	54.36	64.13	53.28	61.61	50.22	83.10	52.61	56.61	71.45
Dry Soil (g)	49.34	48.50	54.73	53.32	63.11	52.25	60.65	49.26	82.13	51.64	55.65	70.49
Water (g)	13.29	13.12	14.96	14.62	17.19	14.20	16.33	13.23	22.01	13.72	14.79	18.48
MC (%)	26.94	27.05	27.33	27.42	27.24	27.18	26.92	26.86	26.80	26.57	26.58	26.22
Tare (g)	11.56	11.38	11.49	11.37	11.49	11.40	11.39	11.53	11.54	11.39	11.58	11.49
Dry + Tare (g)	33.10	33.78	35.87	36.80	34.49	34.65	36.90	39.17	36.70	38.31	35.74	36.53
Wet + Tare (g)	79.92	79.56	80.58	81.98	81.18	80.24	81.56	82.45	79.50	81.45	78.88	79.29
Salinity(measured) (g/L)	2.97	3.32	3.60	3.84	3.30	3.43	3.53	4.15	3.63	4.22	3.98	4.05
Dry Soil (g)	21.54	22.40	24.38	25.43	23.00	23.25	25.51	27.64	25.16	26.92	24.16	25.04
WaterM/Waterl	8.07	7.56	6.71	6.48	7.45	7.22	6.50	5.83	6.35	6.03	6.72	6.51
Salinity (calculated) (g/L)	25.24	26.72	25.92	26.85	26.18	26.44	24.59	26.27	24.75	27.67	28.94	28.59

Table B.9.b Moisture content and salinity at different elevation of sample after freezing for test #9 (continued)

Height (mm)	62.5	67.5	72.5	77.5	82.5	87.5	92.5	97.5	102.5	107.5	112.5	117.5
Tare (g)	0.94	0.96	0.95	0.95	0.96	0.96	0.99	0.96	0.97	0.98	0.98	0.98
Wet + Tare (g)	120.30	146.67	51.23	51.09	62.45	62.45	68.71	75.45	82.42	71.84	79.4	72.09
Dry + Tare (g)	95.82	118.20	39.05	36.98	44.65	44.65	49.67	55.74	61.81	54.33	60.15	54.84
Dry Soil (g)	94.88	117.24	38.10	36.03	43.69	43.69	48.68	54.78	60.84	53.35	59.17	53.86
Water (g)	24.48	28.47	12.18	14.11	17.80	17.80	19.04	19.71	20.61	17.51	19.25	17.25
MC (%)	25.80	24.28	31.97	39.16	40.74	40.74	39.11	35.98	33.88	32.82	32.53	32.03
Tare (g)	11.54	11.57	11.42	11.44	11.53	11.55	11.36	11.65	11.37	11.56	11.40	11.38
Dry + Tare (g)	38.51	38.00	35.64	35.17	35.92	36.92	36.48	37.52	34.36	34.23	37.14	31.44
Wet + Tare (g)	82.01	82.73	81.74	80.05	80.31	79.22	80.60	83.61	80.56	81.47	81.15	74.92
Salinity(measured) (g/L)	4.50	3.77	2.85	3.32	3.37	4.04	3.58	4.01	2.97	4.05	4.80	4.48
Dry Soil (g)	26.97	26.43	24.22	23.73	24.39	25.37	25.12	25.87	22.99	22.67	25.74	20.06
WaterM/Waterl	6.25	6.97	5.95	4.83	4.47	4.09	4.49	4.95	5.93	6.35	5.26	6.77
Salinity (calculated) (g/L)	30.72	28.31	17.79	17.08	16.06	17.91	17.24	21.50	18.55	27.87	27.67	33.10

Table B.10.a Moisture content and salinity before and after consolidation for test #10

	Sample 1	Sample 2	Sample 3	Average
Tare (g)	0.95	0.96	0.96	-
Wet + Tare (g)	38.66	34.88	42.03	-
Dry + Tare (g)	25.04	22.64	27.18	-
Dry Soil (g)	24.09	21.68	26.22	-
Water (g)	13.62	12.24	14.85	-
MC (%)	56.54	56.46	56.64	56.54
Tare (g)	11.51	11.38	11.55	-
Dry + Tare (g)	22.26	23.39	28.98	-
Wet + Tare (g)	72.40	70.31	75.51	-
Salinity(measured) (g/L)t	2.75	3.10	4.70	-
Dry Soil (g)	10.75	12.01	17.43	-
WaterM/Waterl	8.25	6.92	4.71	-
Salinity(calculated) (g/L)	23.68	22.69	24.27	23.55
Height (mm) of sample before consolidation	-	-	-	184
Height (mm) of sample after consolidation	-	-	-	127
MC (%) after consolidation	-	-	-	27.34

Table B.10.b Moisture content and salinity at different elevation of sample after freezing for test #10

Height (mm)	2.5	7.5	12.5	17.5	22.5	27.5	32.5	37.5	42.5	47.5	52.5	57.5
Tare (g)	1.01	1.01	0.97	1.03	1.00	1.02	0.96	0.95	0.94	0.95	0.95	0.97
Wet + Tare (g)	32.27	32.09	36.13	24.96	22.40	22.63	21.69	28.56	17.60	18.34	25.86	14.76
Dry + Tare (g)	26.50	26.40	29.70	20.49	18.11	17.98	16.87	22.23	13.82	14.39	20.26	11.65
Dry Soil (g)	25.49	25.39	28.73	19.46	17.11	16.96	15.91	21.28	12.88	13.44	19.31	10.68
Water (g)	5.77	5.69	6.43	4.47	4.29	4.65	4.82	6.33	3.78	3.95	5.60	3.11
MC (%)	22.64	22.41	22.38	22.97	25.07	27.42	30.30	29.75	29.35	29.39	29.00	29.12
Tare (g)	11.54	11.38	11.48	11.39	11.50	11.42	11.39	11.54	11.55	11.38	11.56	11.46
Dry + Tare (g)	28.49	27.01	30.76	24.13	28.58	28.36	27.28	27.58	24.05	24.82	26.76	22.11
Wet + Tare (g)	83.08	70.62	73.87	71.03	73.26	75.24	71.97	74.00	71.68	73.71	73.94	72.42
Salinity(measured) (g/L)	1.76	2.03	2.53	1.56	2.02	1.98	2.24	2.43	1.89	1.99	2.27	1.54
Dry Soil (g)	16.95	15.63	19.28	12.74	17.08	16.94	15.89	16.04	12.50	13.44	15.20	10.65
WaterM/Waterl	14.23	12.45	9.99	16.03	10.43	10.09	9.28	9.73	12.98	12.38	10.70	16.22
Salinity (calculated) (g/L)	26.83	26.98	26.85	26.88	22.50	21.34	22.14	25.13	26.24	26.30	25.86	26.87

Table B.10.b Moisture content and salinity at different elevation of sample after freezing for test #10 (continued)

Height (mm)	62.5	67.5	72.5	77.5	82.5	87.5	92.5	97.5	102.5	107.5	112.5	117.5
Tare (g)	0.96	0.95	0.94	0.93	0.95	0.95	0.95	0.94	0.95	0.96	0.96	0.94
Wet + Tare (g)	22.19	21.67	16.48	22.14	18.31	25.23	20.23	23.19	20.3	31.52	30.75	19.86
Dry + Tare (g)	17.46	17.07	13.03	17.49	14.51	19.95	16.04	18.41	16.12	24.91	24.31	15.53
Dry Soil (g)	16.50	16.12	12.09	16.56	13.56	19.00	15.09	17.47	15.17	23.95	23.35	14.59
Water (g)	4.73	4.60	3.45	4.65	3.80	5.28	4.19	4.78	4.18	6.61	6.44	4.33
MC (%)	28.67	28.54	28.54	28.08	28.02	27.79	27.77	27.36	27.55	27.60	27.58	29.68
Tare (g)	11.53	11.53	11.41	11.42	11.50	11.54	11.32	11.62	11.36	11.55	11.40	11.38
Dry + Tare (g)	28.06	27.67	22.47	27.92	25.04	27.82	26.79	25.73	26.5	30.48	28.59	25.85
Wet + Tare (g)	73.22	74.86	74.39	72.82	72.00	74.82	73.58	73.64	73.39	76.70	74.83	73.44
Salinity(measured) (g/L)	2.62	2.44	1.53	2.56	2.02	2.30	2.26	1.98	2.19	2.77	2.61	2.30
Dry Soil (g)	16.53	16.14	11.06	16.50	13.54	16.28	15.47	14.11	15.14	18.93	17.19	14.47
WaterM/Waterl	9.53	10.25	16.45	9.69	12.38	10.39	10.89	12.41	11.24	8.85	9.75	11.08
Salinity (calculated) (g/L)	26.50	26.57	27.08	26.35	26.69	25.43	26.21	26.24	26.23	25.99	27.02	27.13

Table B.11.a Moisture content and salinity before and after consolidation for test #11

	Sample 1	Sample 2	Sample 3	Average
Tare (g)	0.96	0.96	0.97	-
Wet + Tare (g)	47.15	45.77	51.82	-
Dry + Tare (g)	31.38	30.47	34.49	-
Dry Soil (g)	30.42	29.51	33.52	-
Water (g)	15.77	15.30	17.33	-
MC (%)	51.84	51.85	51.70	51.80
Tare (g)	11.53	11.40	11.54	-
Dry + Tare (g)	29.09	32.14	35.81	-
Wet + Tare (g)	74.72	77.10	79.87	-
Salinity(measured) (g/L)t	4.49	5.04	6.50	-
Dry Soil (g)	17.56	20.74	24.27	-
WaterM/Waterl	5.01	4.18	3.51	-
Salinity(calculated) (g/L)	24.58	23.19	25.46	24.41
Height (mm) of sample before consolidation	-	-	-	176
Height (mm) of sample after consolidation	-	-	-	123
MC (%) after consolidation	-	-	-	24.83

Table B.11.b Moisture content and salinity at different elevation of sample after freezing for test #11

Height (mm)	2.5	7.5	12.5	17.5	22.5	27.5	32.5	37.5	42.5	47.5	52.5	57.5
Tare (g)	1.02	1.01	0.94	1.04	1.02	1.03	0.98	0.98	0.97	0.96	0.96	0.97
Wet + Tare (g)	21.44	14.76	25.16	22.80	21.14	20.80	21.03	23.66	23.92	20.73	24.58	22.70
Dry + Tare (g)	17.53	12.11	20.50	18.64	17.33	17.12	17.26	19.45	19.64	17.08	20.24	18.78
Dry Soil (g)	16.51	11.10	19.56	17.60	16.31	16.09	16.28	18.47	18.67	16.12	19.28	17.81
Water (g)	3.91	2.65	4.66	4.16	3.81	3.68	3.77	4.21	4.28	3.65	4.34	3.92
MC (%)	23.68	23.87	23.82	23.64	23.36	22.87	23.16	22.79	22.92	22.64	22.51	22.01
Tare (g)	11.55	11.37	11.49	11.36	11.51	11.41	11.36	11.55	11.52	11.37	11.59	11.51
Dry + Tare (g)	28.09	22.49	31.05	28.98	27.83	27.51	27.67	30.02	30.21	27.53	30.85	29.30
Wet + Tare (g)	78.26	73.02	79.31	77.86	77.40	77.19	78.51	78.72	78.15	78.25	79.36	78.89
Salinity(measured) (g/L)	1.88	1.30	2.29	2.07	1.89	1.85	1.81	2.11	2.17	1.77	2.23	2.07
Dry Soil (g)	16.54	11.12	19.56	17.62	16.32	16.10	16.31	18.47	18.69	16.16	19.26	17.79
WaterM/Waterl	12.81	19.03	10.36	11.74	13.00	13.49	13.46	11.57	11.19	13.86	11.19	12.66
Salinity (calculated) (g/L)	25.75	26.77	25.24	25.92	26.28	26.70	26.08	26.03	25.87	26.28	26.57	27.97

Table B.11.b Moisture content and salinity at different elevation of sample after freezing for test #11 (continued)

Height (mm)	62.5	67.5	72.5	77.5	82.5	87.5	92.5	97.5	102.5	107.5	112.5	117.5
Tare (g)	0.95	0.96	0.97	0.96	0.94	0.97	0.98	0.97	0.96	0.99	0.98	1.00
Wet + Tare (g)	18.11	32.28	22.70	21.40	22.41	21.34	17.78	19.66	20.88	27.66	26.6	25.76
Dry + Tare (g)	15.01	26.39	17.99	16.98	17.79	17.06	14.23	15.74	16.73	22.17	21.38	20.72
Dry Soil (g)	14.06	25.43	17.02	16.02	16.85	16.09	13.25	14.77	15.77	21.18	20.40	19.72
Water (g)	3.10	5.89	4.71	4.42	4.62	4.28	3.55	3.92	4.15	5.49	5.22	5.04
MC (%)	22.05	23.16	27.67	27.59	27.42	26.60	26.79	26.54	26.32	25.92	25.59	25.56
Tare (g)	11.55	11.56	11.43	11.44	11.52	11.55	11.35	11.62	11.36	11.54	11.39	11.38
Dry + Tare (g)	25.57	34.59	28.41	27.47	28.36	27.61	24.58	26.32	27.11	32.74	31.79	31.08
Wet + Tare (g)	77.06	81.47	76.62	76.89	79.67	77.05	76.08	77.30	77.84	82.01	78.91	82.19
Salinity(measured) (g/L)	1.60	2.60	1.96	1.92	2.01	2.06	1.69	1.87	2.05	2.85	2.89	2.68
Dry Soil (g)	14.02	23.03	16.98	16.03	16.84	16.06	13.23	14.70	15.75	21.20	20.40	19.70
WaterM/Waterl	16.66	8.79	10.26	11.17	11.11	11.57	14.53	13.07	12.24	8.97	9.03	10.15
Salinity (calculated) (g/L)	28.63	24.26	21.48	22.93	23.85	25.44	26.33	26.13	26.77	27.08	27.64	28.87

Table B.12.a Moisture content and salinity before and after consolidation for test #12

	Sample 1	Sample 2	Sample 3	Average
Tare (g)	0.97	0.96	0.97	-
Wet + Tare (g)	43.87	36.45	48.73	-
Dry + Tare (g)	28.40	23.73	31.63	-
Dry Soil (g)	27.43	22.77	30.66	-
Water (g)	15.47	12.72	17.10	-
MC (%)	56.40	55.86	55.77	56.01
Tare (g)	11.55	11.39	11.55	-
Dry + Tare (g)	27.67	29.10	30.46	-
Wet + Tare (g)	71.13	76.11	73.12	-
Salinity(measured) (g/L)t	4.72	4.60	5.65	-
Dry Soil (g)	16.12	17.71	18.91	-
WaterM/Waterl	4.78	4.75	4.04	-
Salinity(calculated) (g/L)	24.72	23.91	25.31	24.65
Height (mm) of sample before consolidation	-	-	-	175
Height (mm) of sample after consolidation	-	-	-	122
MC (%) after consolidation	-	-	-	27.62

Table B.12.b Moisture content and salinity at different elevation of sample after freezing for test #12

Height (mm)	2.5	7.5	12.5	17.5	22.5	27.5	32.5	37.5	42.5	47.5	52.5	57.5
Tare (g)	1.00	1.00	0.96	1.01	1.00	1.02	0.97	0.96	0.97	0.96	0.99	0.98
Wet + Tare (g)	28.17	24.59	22.93	32.36	31.11	25.94	31.76	41.09	47.05	35.49	44.05	31.77
Dry + Tare (g)	22.32	19.47	18.15	25.46	24.54	20.52	25.06	32.40	37.08	28.05	34.77	25.19
Dry Soil (g)	21.32	18.47	17.19	24.45	23.54	19.50	24.09	31.44	36.11	27.09	33.78	24.21
Water (g)	5.85	5.12	4.78	6.90	6.57	5.42	6.70	8.69	9.97	7.44	9.28	6.58
MC (%)	27.44	27.72	27.81	28.22	27.91	27.79	27.81	27.64	27.61	27.46	27.47	27.18
Tare (g)	11.56	11.38	11.48	11.32	11.50	11.57	11.38	11.53	11.54	11.38	11.42	11.49
Dry + Tare (g)	27.46	29.81	28.64	35.76	29.39	31.08	27.45	30.41	34.88	31.53	37.33	28.55
Wet + Tare (g)	74.60	74.59	75.28	78.77	74.26	75.87	73.84	73.32	78.77	77.58	79.43	74.61
Salinity(measured) (g/L)	2.20	2.73	2.45	3.68	2.61	2.90	2.30	2.91	3.41	2.89	3.69	2.43
Dry Soil (g)	15.90	18.43	17.16	24.44	17.89	19.51	16.07	18.88	23.34	20.15	25.91	17.06
WaterM/Waterl	10.80	8.77	9.77	6.24	8.99	8.26	10.38	8.22	6.81	8.32	5.91	9.93
Salinity (calculated) (g/L)	24.07	24.96	24.63	24.67	24.33	25.16	24.34	25.14	24.80	25.25	23.47	24.80

Table B.12.b Moisture content and salinity at different elevation of sample after freezing for test #12 (continued)

Height (mm)	62.5	67.5	72.5	77.5	82.5	87.5	92.5	97.5	102.5	107.5	112.5	117.5
Tare (g)	0.95	0.95	0.96	0.97	0.96	0.96	0.98	0.97	0.95	0.96	0.96	0.96
Wet + Tare (g)	30.96	29.15	32.65	25.76	22.56	24.47	26.24	19.74	33	26.14	30.79	36.8
Dry + Tare (g)	24.53	23.13	25.92	20.51	18.02	19.63	21.13	15.93	25.21	19.87	23.42	28.27
Dry Soil (g)	23.58	22.18	24.96	19.54	17.06	18.67	20.15	14.96	24.26	18.91	22.46	27.31
Water (g)	6.43	6.02	6.73	5.25	4.54	4.84	5.11	3.81	7.79	6.27	7.37	8.53
MC (%)	27.27	27.14	26.96	26.87	26.61	25.92	25.36	25.47	32.11	33.16	32.81	31.23
Tare (g)	11.53	11.54	11.42	11.42	11.52	11.54	11.34	11.61	11.37	11.55	11.39	11.38
Dry + Tare (g)	35.08	33.70	36.36	30.97	26.57	30.24	31.48	26.55	30.91	30.07	32.89	29.59
Wet + Tare (g)	76.09	78.58	82.16	79.11	75.72	81.77	77.21	74.43	76.50	78.21	75.24	75.68
Salinity(measured) (g/L)	3.57	3.17	3.50	2.69	2.44	2.40	2.80	1.96	2.57	2.70	3.75	2.87
Dry Soil (g)	23.55	22.16	24.94	19.55	15.05	18.70	20.14	14.94	19.54	18.52	21.50	18.21
WaterM/Waterl	6.39	7.46	6.81	9.16	12.27	10.63	8.95	12.58	7.27	7.84	6.00	8.10
Salinity (calculated) (g/L)	24.45	25.08	25.52	25.67	30.78	26.17	26.22	24.51	19.33	22.05	24.24	24.40